# Crystallization and structural characterization of protein complexes involved in the energy metabolism of *Yarrowia lipolytica*

**Dissertation**

zur Erlangung des Doktorgrades
der Naturwissenschaften

vorgelegt beim Fachbereich Biochemie, Chemie und Pharmazie
der Goethe-Universität
in Frankfurt am Main

von

Blanka Ksymena Wrzesniewska

aus Opole (Polen)

Frankfurt am Main 2009

(D30)

Vom Fachbereich Biochemie, Chemie und Pharmazie der Goethe-Universität als Dissertation angenommen.

| | |
|---|---|
| Dekan: | Prof. Dr. Dieter Steinhilber |
| Gutachter: | Prof. Dr. Bernd Ludwig |
| | Prof. Dr. Ulrich Brandt |

Datum der Disputation: 27.04.2009

Die vorliegende Arbeit wurde in der Zeit von September 2004 bis September 2008 im Gustav-Embden Zentrum der Biologischen Chemie, Molekulare Bioenergetik, des Universitätsklinikums der Goethe-Universität in Frankfurt am Main unter Anleitung von Prof. Dr. Ulrich Brandt durchgeführt.

## Acknowledgements

I would like to sincerely thank Prof. Ulrich Brandt who offered me a warm welcome in the Molecular Bioenergetics group, provided with financial support and necessary research facilities in his lab. For his excellent scientific supervision, advice, continuous support and passion for science, I am greatly thankful.

I am grateful to Prof. Bernd Ludwig for taking the responsibility of external supervision.

I would like to thank Dr. Volker Zickermann for outstanding scientific guidance, valuable suggestions and many fruitful discussions, as well as for critical reading of the manuscript.

I thank Prof. Carola Hunte for support in crystallography and fruitful cooperation.

I would also like to thank
Prof. Hermann Schägger for scientific discussions and helpful suggestions.
Dr. Stefan Kerscher for scientific support in the molecular biology field.
Dr. Ilka Wittig for introduction to cell culture techniques as well as mass spectrometry.
Maja Tocilescu for a helpful hand, lots of stimulating discussions and for being a dear friend.
Karin Siegmund and Andrea Duchene for excellent technical assistance, encouragement and lots of heart.
Dr. Klaus Zwicker for valuable suggestions and kindness.
Esther Nübel for 'all that jazz…'
Lucie Sokolova for performing the LILBID experiments.
Dipl.-Ing. Gudrun Beyer for valuable hints in the molecular biology field.
Nicola Crosetto for introduction to SPR techniques.
Andrea Böttcher for support in IT-related issues.

I am very thankful to all group members for creating a nice working environment.

Last, but not least, I would like to thank Kris, without whom I wouldn't have been, where I am now.
Finally, I am grateful to my family Mom, Dad, Anetka, Mariusz, Michal, Marta, Sandra, Iwona, Zbyszek who always believed in me.

Mojej rodzinie, Krzysiowi

# Crystallization and structural characterization of protein complexes involved in the energy metabolism of *Yarrowia lipolytica*

## Part I

Fab co-complexes of proton pumping
NADH:ubiquinone oxidoreductase (complex I)

## Part II

UDP-glucose pyrophosphorylase

# Part I-General introduction

NADH:ubiquinone oxidoreductase (complex I)

Antibody mediated crystallization of membrane proteins

# 1 COMPLEX I – MYSTERIOUS MOLECULAR MACHINERY

NADH:ubiquinone oxidoreductase (complex I, EC 1.6.5.3) is the largest, most complicated but least understood member of the respiratory chain [1]. Although, the bovine enzyme was first purified more than 50 years ago [2], the knowledge on its mechanism and structure still remains limited. Electron microscopic studies of complex I from different sources typically showed an L-shaped molecule, with a peripheral arm protruding into the mitochondrial matrix and a perpendicular membrane arm embedded in a lipid bilayer [3-7]. As the electron entry site of mitochondrial electron transfer chain, complex I plays a critical role in molecular bio-energetics (Figure 1.1). The enzyme couples the transfer of two electrons from NADH to ubiquinone to the translocation of four protons across the inner mitochondrial membrane and the plasma membrane of many bacteria. This generates the major portion of the proton motive force required for the ATP synthesis by complex V. Complex I has been shown to be a component of multi-complex assemblies called respirasomes [8] the formation of which is important for stability of the enzyme [9;10] . Disorders of mitochondrial NADH:ubiquinone oxidoreductase were identified in many neurodegenerative diseases, such as encephalomyopathies or Leigh syndrome, as well as in the process of aging [11-13]. Together with cytochrome $bc_1$ complex, complex I is the main site of the reactive oxygen species (ROS) production in oxidative phosphorylation [14].

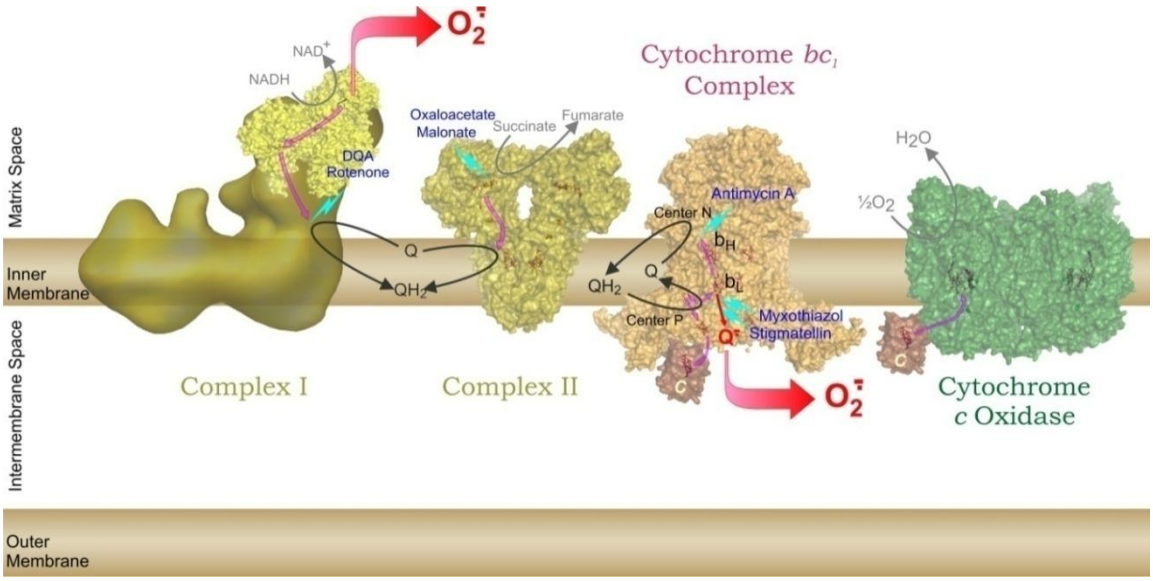


**Figure 1.1: Mitochondrial electron transfer chain.**

Complex I is the only member of the respiratory chain for which no detailed structure is available. The sites of reactive oxygen species production are shown by red arrows. Reprinted from [14]

## *1.1 SUBUNIT COMPOSITION OF COMPLEX I*

Eukaryotic complex I is composed of more than 40 subunits, resulting in a molecular mass of almost 1 MDa [15-18]. Among them, 14 central subunits are conserved in eukaryotes and prokaryotes and represent a minimal set required for functionality of the enzyme [19]. The central subunits comprise all redox centers known for complex I: flavine mononucleotide (FMN) and up to nine iron-sulfur clusters (Fe-S) [20;21]. The central subunits can be divided into two classes. The first class is represented by seven highly hydrophobic polypeptides (ND1 to ND6 and ND4L) encoded in most eukaryotes by the mitochondrial DNA and located in the membrane arm of the protein. These subunits are postulated to be involved in proton translocation. About 60 transmembrane helices have been predicted for the central hydrophobic subunits. Additionally, alkaline phosphatase fusions indicated that some of the previously predicted transmembrane helices form extended extramembraneous domains [22;23]. The remaining seven central subunits are hydrophilic proteins and contain distinct binding motifs for all redox centers and NADH. The additional, so called accessory subunits are characteristic only for the eukaryotes, but their role in energy conversion is unclear. Several accessory subunits located in the membrane arm were classified as single transmembrane domain subunits (STMD). These are small proteins containing a single transmembrane helix and highly hydrophobic domains with charged residues facing both sides of the membrane [17;18]. Bovine complex I was predicted to contain fourteen STMD subunits [24]. It was postulated that the STMD proteins mediate assembly of the mitochondrially encoded subunits and stabilize the membrane portion of complex I [18].

Purified bovine enzyme was shown to dissociate into subcomplexes upon treatment with detergents and chaotropes like perchlorate [24-26]. The soluble, catalytically active flavoprotein subcomplex (FP) comprises the FMN molecule, the NADH binding site, one [2Fe-2S] and one [4Fe-4S] cluster (Figure 1.2) [27-29]. The iron-protein (IP) is composed of the 75-kDa, 49-kDa, 30-kDa, TYKY and PSST subunits [30]. The last subcomplex is known as hydrophobic protein (HP) and was first characterized in [18]. Using the non-denaturing detergent lauryldimethylamine oxide (LDAO), followed by ion-exchange chromatography, the bovine complex I was resolved into subcomplexes Iα and Iβ (Figure 1.2) [25;31]. Iβ represents the major portion of the membrane part of complex I. Upon prolonged incubation in LDAO, fraction Iα releases the predominantly hydrophilic subcomplex Iλ [16]. The described subcomplexes were used for identification and assignment of the particular subunits to different parts of complex I by means of Edman degradation, gel electrophoresis and mass spectrome-

try [32]. For excellent reviews on mitochondrial complex I see [1] and Zickermann et al (submitted).

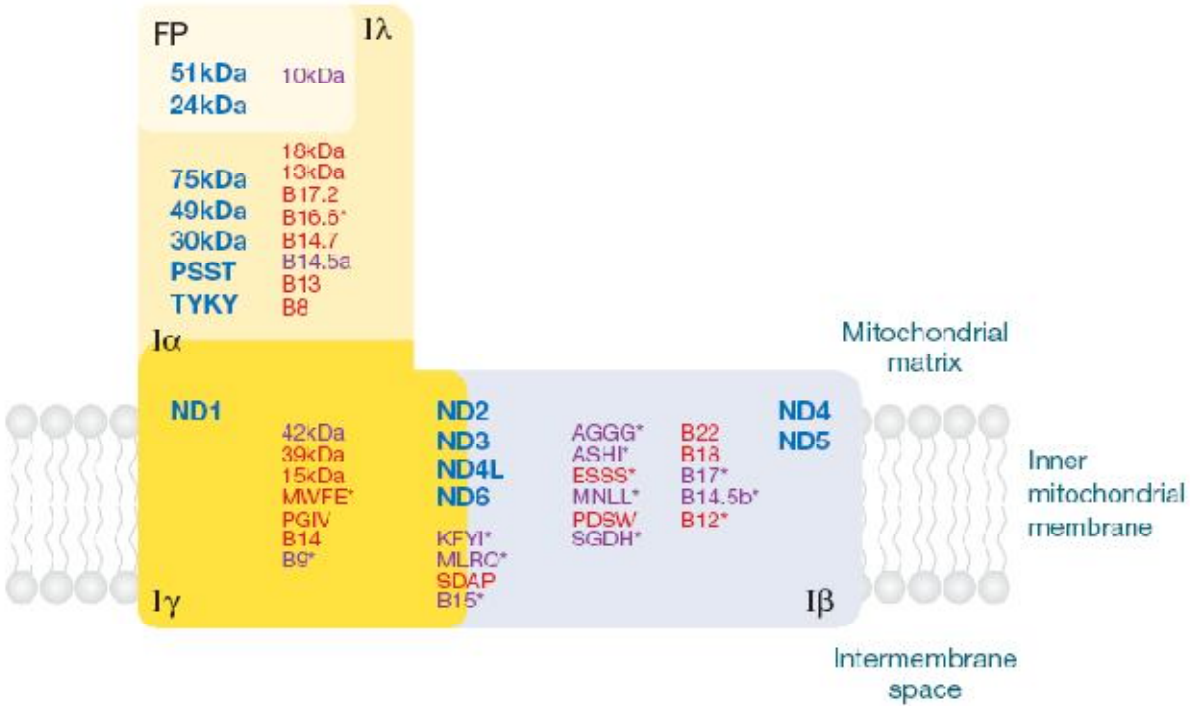


**Figure 1.2: Subcomplexes and subunits of bovine heart mitochondria.**

Flavoprotein (FP) is a component of the Iλ subcomplex (light yellow). Iλ and Iγ (yellow) together form Iα. Iβ (grey blue) represents the major portion of the membrane arm of complex I. Central subunits are printed in blue, accessory subunits common to all eukaryotes – in red, and subunits characteristic for metazoa – in purple. Asterisk indicates subunits, for which a single transmembrane domain was predicted. Figure reprinted from [1].

## *1.2 FUNCTIONAL MODULES OF COMPLEX I*

Extensive phylogenetic studies of the complex I central subunits revealed unambiguous relationships with different types of hydrogenases [33;34] and three functional modules of complex I were defined: the N module, comprising the electron entry site, the Q module or electron output module and the P module, responsible for proton translocation across the inner mitochondrial membrane.

The N module comprises the 75-kDa, 51-kDa and 24-kDa subunits and is related to the α and γ subunits of $NAD^+$-reducing hydrogenases, as the one found in *Alcaligenes eutrophus* [35]. The electrons are transferred from NADH via FMN to a wire of iron-sulfur clusters. FMN is non-covalently bound to the 51 kDa subunit, which possesses an NADH-binding motif and a characteristic βαβ-nucleotide fold on its N terminus [12]. Additionally, the N module contains a set of eight iron–sulfur clusters bound by distinct binding motifs. In some bacteria, includ-

ing *Escherichia coli*, an additional tetranuclear cluster, bound to [CxxCxxxC-$(x)_{27}$-C] motif was observed [36]. All the Fe-S clusters are present in the recently released X-ray structure of the peripheral arm of complex I from *Thermus thermophilus* [37]. Nevertheless, the assignment of the electron paramagnetic resonance (EPR) signals to particular clusters is the subject of a current debate [38;39].

The Q module mediates the transfer of electrons from the N module, via three further iron-sulfur clusters to ubiquinone or menaquinone in case of some bacteria. The 49-kDa, 30-kDa, PSST and TYKY subunits are the building blocks of the Q module. The 49-kDa subunit and the PSST subunit display homology, respectively, to the large and small subunits of water-soluble [NiFe] hydrogenases [40;41]. In *E. coli*, the 30-kDa subunit is fused to the 49-kDa subunit [42]. Subunit TYKY comprises binding motifs [CxxCxxCxxxCP-$(x)_{27}$-CxxCxxCxxxCP] for two further tetranuclear iron-sulfur clusters. Cluster N2, which is associated with the PSST subunit [43;44] has the highest redox potential that is pH dependent [20;45]. N2 is believed to be the direct electron donor to ubiquinone [46].

The P module is composed of seven, mitochondrially encoded and membrane-embedded subunits, ND1, ND2, ND3, ND4, ND4L, ND5 and ND6. Homology studies have shown that the ND2/ND4/ND5 family of subunits have evolved from the *mrp* (multiple resistance and pH adaptation) type $Na^+/H^+$ antiporters known for *Bacillus subtilis* and other bacteria [19;22]. MrpA and MrpD represent proteins that are important for $Na^+$ resistance and homeostasis, and function as $Na^+/H^+$ antiporters. Remarkably, subunit ND4L displays homology to the MrpC protein of the *mrpA-G* operon [47]. These antiporters are commonly found in bacteria. It is likely that the ion translocation functions of the *mrp* proteins were retained by homologous complex I subunits embedded in the membrane. The topology of the proton pumping elements is still for the most part unclear. A review prepared by Zickermann et al., (submitted) summarizes the current knowledge on the architecture of complex I peripheral and membrane arm.

## *1.3 STRUCTURE OF COMPLEX I*

Until recently, the structural information on complex I was exclusively obtained by electron microscopic single particle analysis and two-dimensional crystallography. Enzyme purified from *Bos taurus*, *Yarrowia lipolytica*, *Neurospora crassa*, *Arabidopsis thaliana* and *E. coli* showed typically an L-shaped structure, with the peripheral arm extending into the mitochondrial matrix or the bacterial cytoplasm, and membrane arm embedded in the lipid bilayer [3-7]. A high resolution X-ray structure of the hydrophilic domain of complex I from *Th. ther-*

*mophilus* was presented by Sazanov and Hinchliffe [37]. The partial structure (PDB 2fug) contains eight subunits Nqo1-6, Nqo9, and Nqo15, as well as nine iron-sulfur clusters, together with N7, which is found only in some bacteria (Figure 1.3).

An extensive electron microscopic study of *Y. lipolytica* complex I provided a new, detailed model of the eukaryotic enzyme [6]. EM reconstructions of the yeast enzyme subcomplex, lacking the 51-kDa and the 24-kDa subunits, allowed unambiguous localization of these two central subunits within the N module [48]. The published bacterial X-ray partial structure was fitted into the 3D reconstruction of the holoenzyme. Out of six possible fits discussed in the study, fit 1, placing the N2 cluster roughly 60 Å above the membrane represents the most probable arrangement. This challenges the orientation of the peripheral arm with respect to the membrane as suggested by Sazanov et al., [37;49] (Figure 1.3). Moreover, fit 1 is in good agreement with the antibody binding experiments, which locate the 49-kDa subunit away from the membrane [50;51]. The proposed architecture of the eukaryotic enzyme raises fundamental questions concerning the energy coupling: How is the electron transfer related to the proton translocation and how are the electrons transferred to the hydrophobic ubiquinone?

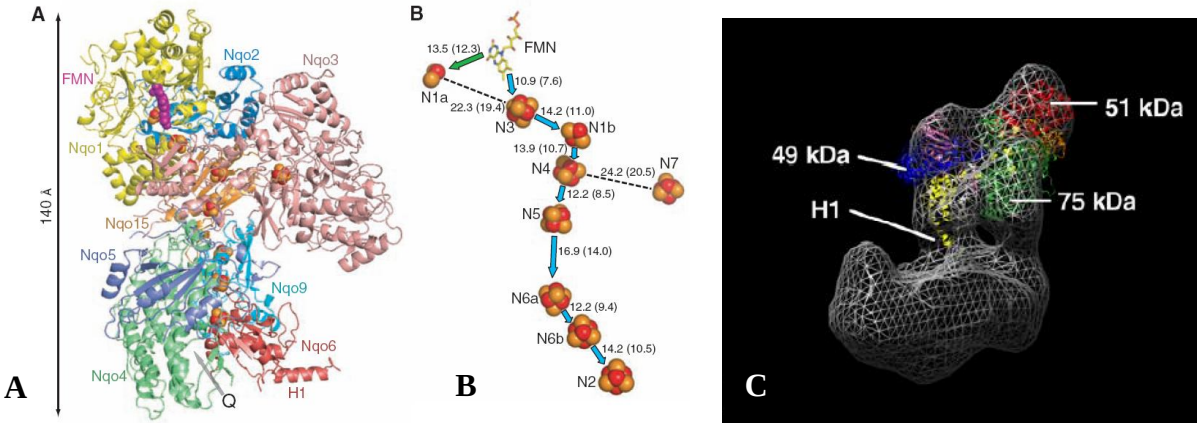


**Figure 1.3: Structure of the hydrophilic domain of complex I from *Th. thermophilus* and electron microscopic reconstruction of *Y. lipolytica* enzyme.**

A: X-ray structure of the peripheral domain from *Th. thermophilus* [37]. The subunit Nqo4 (49-kDa) reaches the membrane arm and the H1 helix extends in the direction of the membrane distal part of the enzyme. B: Arrangement of iron-sulfur clusters in the peripheral arm [37]. C: Fitting of the bacterial X-ray model (A) into 3D reconstruction of complex I from *Y. lipolytica* [48]. H1 is the helix of the PSST subunit, which extends towards the membrane arm.

## *1.4 ENERGY COUPLING HYPOTHESIS*

Quite contrary to the other complexes of the respiratory chain, all the known complex I redox groups are enclosed within the membrane extrinsic arm. This implies that all the redox chemistry takes place in the peripheral arm, while the proton translocation is limited to the membrane arm. How the energy is transferred over a distance of more than hundred Ångstroms, is still uncertain, but recent EM data of *Y. lipolytica* complex I shed light on a possible mechanism of energy coupling. The EM representations show the peripheral arm attached to the membrane arm via a 'double stalk', with a cavity in between (Figure 1.3 C) [6]. It was postulated, that the first stalk (common stalk) corresponds to the connection seen also for the bacterial enzyme and is composed of central subunit domains, while the second stalk is formed by accessory subunit domains, possibly including the 39-kDa subunit [17]. Fitting of the *Th. thermophilus* structure into the 3D reconstruction of *Y. lipolytica* enzyme positions the PSST subunit and at the same time, the quinone binding pocket around 60 Å above the membrane. In this fit, only the H1 helix of the PSST subunit extends towards the membrane arm and fills up one of the stalks. It was speculated, that the 34 N-terminal amino acids of the 49-kDa subunit and 32 N-terminal amino acids of the PSST subunits, which are disordered in the published structure [37], might take part in the formation of the common stalk. It is likely that additional contributions come from the ND1 subunit, for which a pronounced portion of extramembraneous domain was predicted [23]. Analogously, subunits ND2 and ND3, which are predicted to have large extramembraneous domains may provide enough protein mass to build the common stalk. The presence of an amphipathic junction between the peripheral and membrane arm offers a plausible pathway for the hydrophobic quinone to leave the membrane and to come in contact with cluster N2 Alternatively, large scale conformational changes, which would bring cluster N2 in the proximity of the membrane for reduction of quinone were discussed [52].

The ambiguities about the orientation of the peripheral arm and the lack of structural information on the membrane arm render elucidation of the energy coupling mechanism very difficult. A high resolution X-ray structure of the holocomplex will be required for understanding of the relationship between the redox chemistry entailed in the peripheral arm and the proton translocation taking place in the membrane arm of the NADH:ubiquinone oxidoreductase.

# 2 CRYSTALLIZATION OF MEMBRANE PROTEINS

Integral membrane proteins mediate the functional properties of biological membranes, serving as the energy transducers, channels and receptors, which are essential components of numerous fundamental cellular processes. Moreover, integral membrane proteins are targets of a large number of drugs. Comprehensive knowledge of membrane protein structures is essential for understanding their function, but also for the development of modern medicine through rational drug design. The first high resolution structure of a membrane protein, the photosynthetic reaction centre from *Rhodopseudomonas virdis* was published in 1985 [53]. According to data of the Protein Data Bank, there are more than 49000 protein structures known up to date, out of which only 171 represent structures of integral membrane proteins (http://blanco.biomol.uci.edu/Membrane_Proteins_xtal.html). Taking into account, that between twenty and thirty-five percent of the genome encoded proteins are integral membrane proteins, the overwhelming imbalance in the statistics of solved protein structures is remarkable. The major obstacle in the 3-D crystallization of membrane proteins is posed by the amphipathic nature of their surface. In vivo, the membrane proteins are embedded in a dynamic lipid bilayer, where the hydrophobic areas of the proteins are in contact with the acyl chains of the phospholipids, whereas the polar surfaces face the polar head groups of the lipids and the aqueous phase. Detergent molecules, which mimic the nature of the biological membranes, are used to solubilize the membrane proteins in their native conformation from the lipid bilayers. Each detergent is characterized by the so called critical micelle concentration (CMC). At concentrations below the CMC, the detergent molecules are present in the solution as monomers and form a monolayer at the water-air boundary. At concentrations higher than CMC, the detergents spontaneously form micelles, with the hydrophobic tails oriented towards the centre (Figure 2.1). Driven by the hydrophobic effect detergents cover the hydrophobic surfaces of proteins in a belt-like manner, shielding them from the aqueous environment [54;55]. The water soluble protein detergent co-complex (PDC) is the starting material for further purification and crystallization and the solubilization process represents a crucial step in the purification procedure of membrane proteins.

## *2.1 SELECTION OF A SUITABLE DETERGENT*

Selection of a suitable detergent is essential for successful crystallization of membrane proteins. Detergents, fall into three main groups, with respect to the type of the head group they

possess: ionic, nonionic and zwitterionic. Using mild detergents, such as polyoxyethylenes or N-dodecyl-β-maltoside, the membrane proteins can be isolated from the lipid bilayers in their native conformation. In contrast, surfactants with charged polar head groups, like sodium-dodecylsulfate, readily denature proteins [56]. Detergents display a complicated phase behavior, which includes separation into detergent-rich and detergent-poor phases in some regions of their temperature/composition diagrams [57]. This phenomenon is called the 'cloud point' and is indicated by turbidity, of a previously clear, homogenous detergent solution, caused by temperature differences [55]. In fact, crystallization often takes place at the cloud point. The boundary between the detergent phase and the two immiscible aqueous phases is known as a consolute boundary and depends on the detergent type, salt, temperature and precipitant [58].
The length of the detergent acyl-chain plays an important role in the crystallization of membrane proteins. An interesting example was provided by the case of the yeast cytochrome $bc_1$ complex, which crystallized in the presence of undecyl-maltopyranoside, whereas dodecyl-maltopyranoside did not yield any crystals [59;60]. According to Martin Caffrey's Membrane Protein Data Bank (http://www.mpdb.ul.ie), a great majority (around 75%) of membrane protein structures solved by X-ray diffraction up to date, originated from crystals grown in the presence of N-octyl-ß-D-glucopyranoside (OG), the alkyl chain of which is one of the shortest among all detergents. This implies that detergents forming small micelles that do not interfere with crystal packing are most suitable for crystallization of polytopic membrane proteins. However, attractive interactions between polar head groups of the detergent micelles could be vital for crystal lattice stability. The properties of the hydrophilic heads showed also to be meaningful for the success of membrane protein crystallization. In the case of the two subunit cytochrome *c* oxidase from *Paracoccus denitrificans,* change from N-dodecyl-β-maltoside to 6-cyclohexyl-hexyl-β-maltoside (Cymal-6) or undecyl-maltopyranoside resulted in a significantly improved diffraction limit of the crystals (from 8 Å to 2.5 Å) [61]. Exchange of the detergent used in the solubilization procedure during the purification steps, seems to be a valuable technique supporting crystallization of membrane proteins. Moreover, the use of secondary detergents as additives in crystallization setups might be beneficial for crystal quality.

## *2.2 TYPES OF MEMBRANE PROTEIN CRYSTALS*

There are three categories of membrane protein crystals (Figure 2.1). The first category is represented by 2D crystals, which are basically membrane proteins reconstituted into lipid bilayers. These crystals are amenable to structural studies by electron crystallography and atomic force microscopy [62]. X-ray structural analysis at high resolution requires well-

ordered 3D crystals. Three dimensional crystals fall into two groups: type I and type II crystals. Type I crystals are basically stacked 2D crystals, where the hydrophobic and polar interactions are important in the two dimensions, whereas only the hydrophilic attractive interactions stabilize the third dimension [56]. Lipid cubic phase has proven to be a useful method for generation of type I crystals. The three dimensional continuous lipid phase serves as a solvent matrix for membrane proteins, which allows direct contacts between hydrophobic surfaces of the molecules.

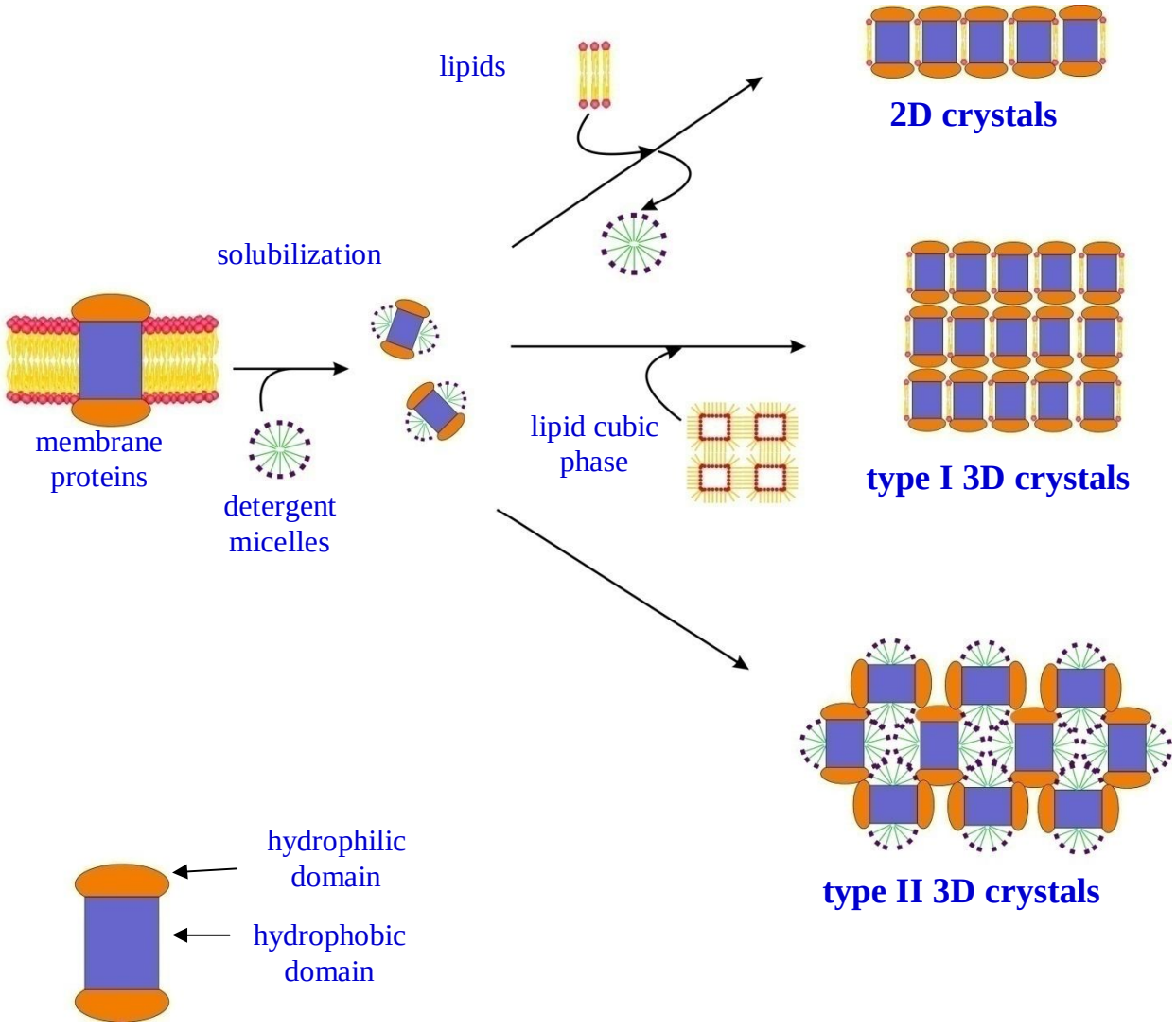


**Figure 2.1: Solubilization of the membrane proteins by means of detergents.**

There are three types of membrane protein crystal, 2D crystals, type I 3D crystals and type II 3D crystals. The last type is best suited for structural analysis of membrane proteins. Modified after Michel [56].

The method has been most successful for structural analysis of the related proteins, bacteriorhodopsin [63], halorhodopsin [64], sensory-rhodopsin II [65;66] as well as the human adrenoreceptor $\beta_2$AR [67].

Type II crystals are the most common category of membrane protein crystals. Solubilized in detergents, the membrane proteins acquire characteristics of soluble proteins, rendering crystallization procedures similar to that employed for soluble proteins. The crystal contacts are exclusively built via polar interactions of the protein surfaces extending from the detergent micelles (Figure 2.1). Although attractive interactions between polar head groups of neighboring detergent micelles may stabilize the crystal lattice, these interactions do not provide robust crystal contacts. Lack of sufficient hydrophilic surfaces poses a major obstacle in crystallizing integral membrane proteins. In the case of many ion channels or transporters, most of the protein is represented by helices buried in the membrane, whereas only short loops exposed to the polar phase make up for the hydrophilic surface. Enlargement of the hydrophilic surfaces by attachment of polar domains represents a promising technique to generate well-ordered type II crystals. An attractive approach was proposed by Ostermeier et al., where Fv antibody fragments were used as specifically binding polar domains in the crystallization of bacterial cytochrome c oxidase (COX) [68]. Since then, the method attracted the attention of membrane protein crystallographers and was successfully employed in the structure determination of several integral membrane proteins.

## *2.3 ANTIBODY FRAGMENTS FOR CO-CRYSTALLIZATION WITH MEMBRANE PROTEINS*

Complete antibodies are not suitable for co-crystallization experiments due to their internal flexibility of the hinge region and their bivalent character (Figure 2.2 A, B). Employment of the fragments of monoclonal antibodies, such as Fab or Fv, obviates these problems and serves as a promising tool in generation of high quality type II crystals. All the antibody fragments used in reported successful co-crystallization trials originated from antibodies obtained using standard hybridoma technology [69]. To be suitable for co-crystallization, the IgG fragments must fulfill the following requirements: (1) binding the antigen in its native conformation, (2) having a high binding constant and (3) forming a stable and rigid co-complex with the antigen. Apart from participation in the formation of crystal contacts, immunoglobulin fragments may stabilize a particular conformation of the protein of interest and facilitate crystallization. There is no rule as to whether Fab or Fv fragments would be more

suitable for successful crystallization with a particular target molecule. The best idea is thus probably to try both. In general, the antibody fragment (extended hydrophilic domain) must reach out of the detergent micelle in order to contribute to the formation of rigid crystal contacts. The difference in size of Fab (~ 50 kDa) and Fv (~ 25 kDa) fragments may therefore be critical for successful crystallization. As the immunoglobulin domain fold is highly conserved, the Fab fragments can be employed for determination of the phases during structural characterization. In contrast to Fv fragments, which are small compact domains, Fab fragments however display certain flexibility, referred to as the 'elbow motion' (Figure 2.2B), which can be detrimental for crystallization. The most important aspects related to the immunoglobulin fragments are described shortly below.

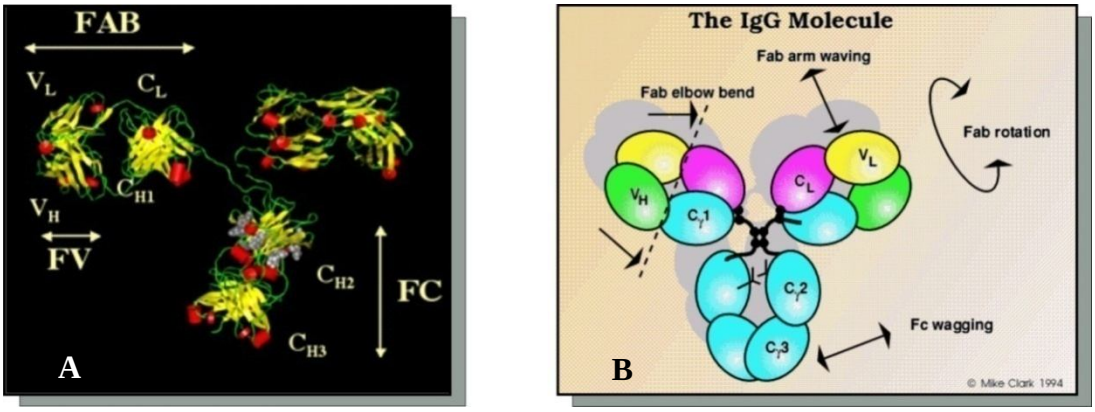


**Figure 2.2: Native antibody structure.**

A: Structure of a native antibody with its basic modules: Fv, Fab and Fc parts. B: diagram summarizing modes of flexibility of an IgG molecule. These figures were taken from Dr. Mike Clark's resources (http://www.path.cam.ac.uk/~mrc7/mikeimages.html).

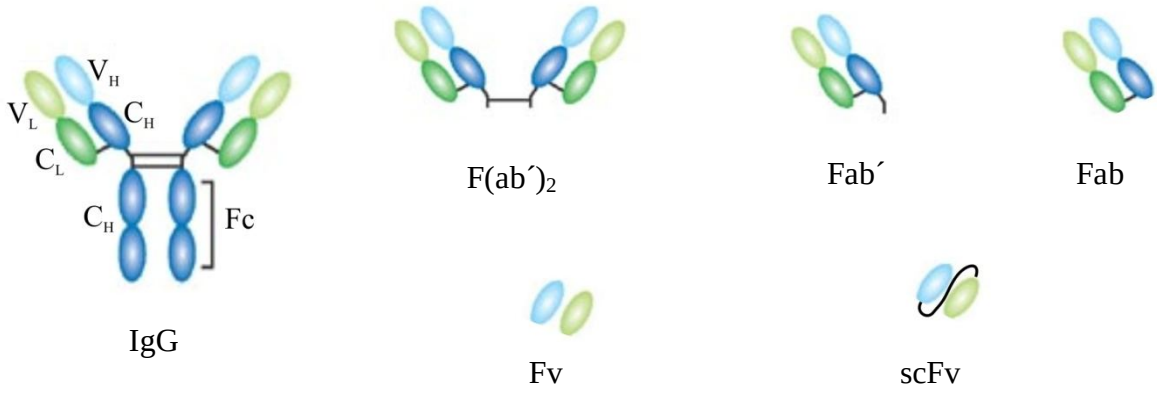


**Figure 2.3: Antibody fragments.**

The intact antibody and its basic fragments are depicted. There are two forms of Fab fragment (antibody binding fragment): Fab and Fab', where the Fab´ represents the Fab with an additional small polypeptide portion of the

heavy chain constant domain. scFv (single chain variable fragment) is composed of the variable domains of each of the light and heavy chains, linked by a polypeptide linker. Figure from [70].

### *2.3.1 Fab and Fv fragments*

Fab fragments contain the antigen binding region and represent a fully functional part of an immunoglobulin. The ~ 50 kDa molecule is composed of one constant and one variable domain of each of the heavy and the light chain (Figure 2.2, Figure 2.3). Fab fragments can be generated proteolytically by digestion of an intact antibody with cysteine proteases such as papain or ficin. The intact antibodies are produced in cell culture of murine hybridoma cell lines or obtained by ascites production. The monoclonal antibodies are subsequently purified by Protein A/G affinity chromatography. Pure Mabs (monoclonal antibodies) are then fragmented by proteases in the presence of cysteine. Papain was originally isolated from *Carica papaya* and is a nonspecific thiol-endopeptidase containing a sulfhydryl group in its active site that must be in the reduced state for the activity of the enzyme. When incubated with papain in the presence of cysteine, intact immunoglobulins are split at the hinge region, generating three fragments of similar size: two identical Fab fragments and one Fc (crystallizable fragment) fragment. The Fc fragments can be separated from the papain digestion mixture by Protein G/A affinity chromatography. Ficin also belongs to the cysteine proteases and is isolated from fig latex. Depending on the concentration of the reducing agent required for its activity, ficin will generate $F(ab')_2$, in the presence of 1 mM cysteine, or Fab fragments in the presence of 10 mM cysteine. Care needs to be taken in order to obtain a homogenous Fab preparation. The presence of heterogeneous fragments like Fab´ still containing small parts of the hinge region constant domain and in some cases glycosylated regions, may prevent co-crystallization. Digestion with papain may cause damage of the antigen binding sites of the Fab fragments, rendering them nonfunctional [71].

Fv fragments (variable fragments) are soluble, globular, monovalent domains of roughly 25 kDa and represent the smallest portion of an antibody retaining antigen binding ability (Figure 2.2 A, Figure 2.3). The fragments are composed of the variable domains of the light and heavy chain. Well established genetic engineering protocols allow the preparation of pure and homogenous fragments of recombinant antibodies. Two forms of Fv fragments can be produced: Fv and scFv (single chain Fv). In case of the single chain Fv fragments, the light and heavy chain domains are linked by a short peptide linker, usually poly-serine or poly-glycin (Figure 2.3). scFv fragments have multiple applications, such as in immunochemistry, flow cytometry and medicine [72]. Historically, scFv fragments were introduced to facilitate phage display, where it is more suitable to express single peptide domains [73]. Phage display libra-

ries and ribosome display systems offer a convenient approach for the generation of Fab and Fv/scFv fragments against membrane proteins in their native conformation without need for immunization [74;75]. The first method involves cloning of an antibody fragment into the phage genome as fusion with one of the phage coat proteins. Multiple rounds of panning (affinity selection process) are carried out to enrich appropriate binder phages, consequently identified by screening after each round of selection [76]. In ribosome display, the peptide of interest and its mRNA are covalently bound and associated with the ribosome. Affinity selection of the binder proteins is performed using a protein – ribosome – mRNA – complex (PRM complex) [77].

Recombinant Fv and Fab fragments can be generated by cloning of the encoding genes from the hybridoma cell lines and subsequent expression in various systems [78-80]. A very well characterized *E. coli* expression system, introduced by Kleymann et al., [79] was employed for the generation of the Fv fragments used in the co-crystallization of the yeast cytochrome $bc_1$ complex (QCR) from *Saccharomyces cerevisiae* [60] and the cytochrome *c* oxidase from *P. denitrificans* [68]. The Fv fragments are produced in an oxidizing periplasm ensuring appropriate arrangement of the disulphide bonds. Nevertheless, the comparatively small volume of the periplasm is a limiting factor for the production of antibody fragments in high yields. A potentially interesting approach was described by Venturi *et al.*, who used an *E.coli* strain with an impaired reducing system. This enabled high yield (10-30 mg/L of bacterial culture) production of Fab fragments in an oxidizing cytoplasm [81].

Cell-free expression systems represent an alternative method for antibody fragment production. Successful expression of Fab and Fv/scFv fragments were reported using *E. coli* based *in vitro* coupled transcription/translation systems [82-84]. Employment of reduced and oxidized glutathione, protein disulphideisomerase (PDI) and molecular chaperones enhanced the protein solubility and increased antigen binding activity of the produced antibody fragments. The advantages of the cell-free expression over expression in microbial cells could be (1) possibility of simultaneous transcription and translation of two genes and (2) avoiding formation of inclusion bodies.

## *2.4 CRYSTALLIZATION OF MEMBRANE PROTEINS WITH ANTIBODY FRAGMENTS*

Extension of the polar surface of polytopic membrane proteins can be achieved by attachment of antibody fragments. The first successful antibody fragment-mediated crystallization of a membrane protein was reported for the cytochrome *c* oxidase from *P. denitrificans*, where the Fv fragments were attached to a four-subunit complex (Figure 2.4 C). The Fv fragments participated in all crystal contacts and the structure was determined to a resolution of 2.8 Å [68]. Since, the protein-protein contacts along the c-axis were limited, the diffraction pattern was anisotropic and the crystals not easily reproducible. Using the same approach, the authors crystallized a subcomplex of the two functionally most important subunits of COX. The crystal lattice was formed by interactions between cytoplasmic and periplasmic surfaces of the neighboring COX molecules, in addition to Fv mediated contacts.

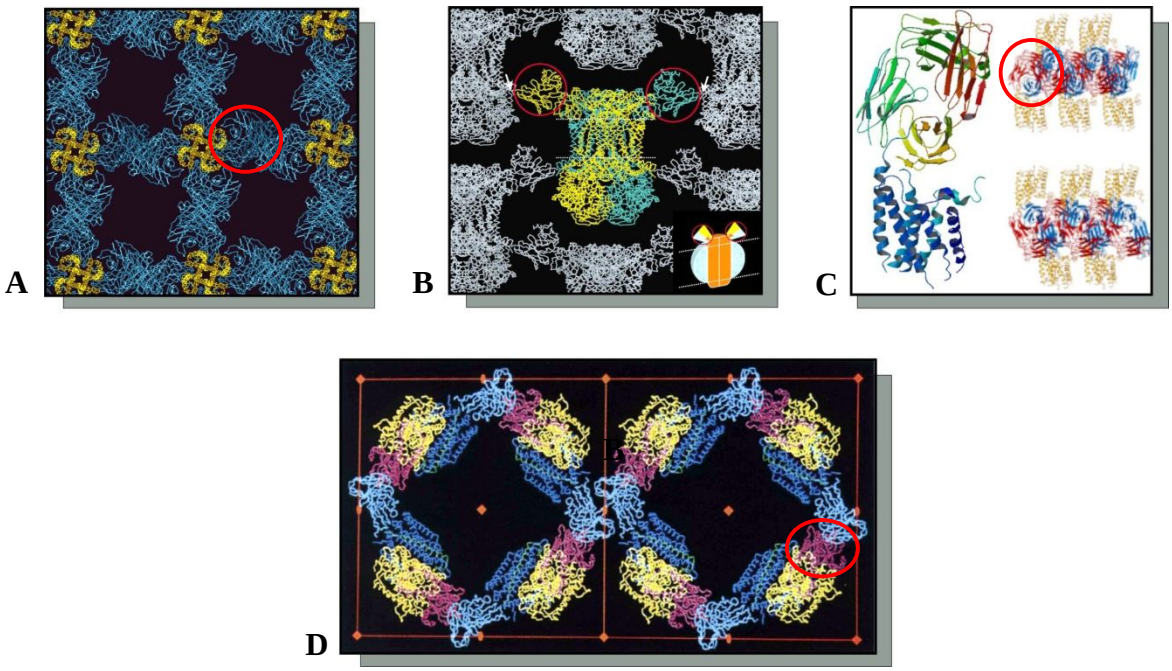


**Figure 2.4: High resolution structures of membrane proteins complexed with antibody fragments (shown in red circles).**

A: Fab-mediated crystallization of the KcsA $K^+$ channel. Crystal packing; Fab fragments are depicted in blue, whereas the KcsA $K^+$ is shown in yellow. PDB code: 1k4c [85]. B: Fv co-complex of yeast cytochrome $bc_1$ complex (QCR); the Fv fragment (in red circle) binds to the extrinsic domain of the Rieske protein. PDB code: 1ezv [60]. C: Fab complex of human adrenoreceptor $\beta_2$AR. Left: asymmetric unit representation; right: packing of the $\beta_2$AR-Fab in crystals formed in DMPC bicelles ($\beta_2$AR in gold, Fab heavy chain in blue, Fab light chain in red). PDB code: 2r4s [67]. D: Bacterial cytochrome *c* oxidase, four subunit crystallization, with Fv fragments (magenta) as crystallization enhancers. PDB code: 1qle [68].

The co-complex structure was determined at 2.7 Å [61]. In this example, the Fv fragments played a double role. Apart from, enhancing the crystallization, the strep-tag fused to the antibody fragments, was used to purify the COX-Fv co-complex by means of a streptavidin affinity chromatography [79]. The structure of the Fv fragment used in the crystallization of COX was determined at 1.28 Å resolution. Comparison of the free and antigen-bound Fv did not show significant structural differences [86].

Another successful Fv-mediated crystallization of a membrane protein was recorded for the yeast cytochrome $bc_1$ complex (QCR) from *S. cerevisiae* [60]. The antibody fragment originated from a conformational antibody binding to the extrinsic domain of the Rieske protein (Figure 2.4 B). The structure of the co-complex was solved to 2.3 Å resolution. The cytochrome $bc_1$ complex possesses two relatively large hydrophilic surfaces, one facing the intermembrane space (~ 46 kDa), the other protruding into the matrix (~ 86 kDa). Interestingly, yeast QCR crystals, suitable for X-ray structural study were obtained only for the protein co-complexed with Fv fragments. Purification via streptavidin affinity chromatography, similar to the one applied for bacterial COX, was not possible for the yeast QCR-Fv co-complex. The Rieske protein is attached to the periphery of the transmembrane part of the QCR by a single helix. Binding of the co-complex to a streptavidin column via Rieske-bound Fv fragment caused disintegration of QCR [87]. Yeast QCR-Fv co-complex was also crystallized with its substrate cytochrome *c* bound. Confirming activity measurements structural analysis revealed that, the antibody fragments did not interfere with substrate binding [87;88]

The potassium channel KcsA was the first example of successful crystallization of an integral membrane protein with Fab fragments [85]. The proteolytic Fab fragment originated from an antibody recognizing the native homotetrameric form of the channel and was bound to the $K^+$ channel on the extracellular surface. Furthermore, the bound Fab fragments did not hinder ion binding by leaving the passageway outside the pore wide open. The crystal contacts were exclusively mediated by the Fab fragments, which created a spacious crystal lattice, leaving room for large decyl-maltoside micelles (Figure 2.4 A). The extra polar surface provided by the Fab fragments, was of a deciding value for the crystal quality. The co-complex crystals diffracted X-ray to a significantly better resolution (below 2 Å) when compared to the single subunit structure of the KcsA $K^+$ solved without antibody fragments, where the crystals diffracted X-rays to a resolution of 3.2 Å [89]. Employment of the Fab fragments was also beneficial for the crystallographic analysis. The phases were determined by molecular replacement using a previously published Fab structure as the search model. Thus, Fab fragment-mediated

crystallization offers an interesting approach for the structural investigation of channels and other membrane protein, which do not possess significant large hydrophilic surfaces.

The complex of human adrenoreceptor $\beta_2$AR is the second known case of Fab co-complex crystallization [67]. Inherent structural flexibility associated with the basal activity of the G-protein-coupled receptors (GPCRs) has hindered their structural analysis. Proteolytic antibody fragments were generated to ensure conformational stability. The deglycosylated complex bound to an inverse agonist carazolol was crystallized in DMPC bicelles (10% w/v DMPC:CHAPSO in 10 mM HEPES, pH 7.5, 100 mM NaCl). The Fab fragment was bound to the third intracellular loop, which is involved in activation of the G protein as well as in selectivity of the GPCR-G protein interactions. The antibody fragment did not affect the activity of the receptor nor influenced the native structure. The structure was determined at 3.4 Å/3.7 Å resolution.

## *2.5 ENLARGEMENT OF THE POLAR SURFACE – ALTERNATIVE TO THE ANTIBODY FRAGMENTS*

Essentially, every soluble protein that specifically binds to the target protein may be considered as a candidate for co-crystallization attempts. Engineered protein scaffolds were proposed as an alternative for the antibody fragments [90;91]. Employing the phage display technique, the protein scaffolds could be applied to select for suitable binding partners. So far no examples of co-crystallization with membrane proteins were reported.

Fusion partners employed for expansion of polar surfaces of membrane proteins represents a potentially promising approach. However, the fusion proteins are attached to the target protein via a linker. Flexibility introduced by the linker region may be detrimental for crystallization. In the crystallization of membrane-bound cytochrome $bo_3$ ubiquinol oxidase from *E. coli*, protein Z was fused to the subunit IV at the C-terminus [92;93]. The resultant fusion protein crystallized in conditions similar to the native counterpart, but the crystals were even less ordered and it was not possible to employ molecular replacement as a structural method. In order to avoid flexibility, the fusion protein – cytochrome $b_{562}$ – was inserted into one of the inner cytoplasmic loops (between two transmembrane helices) of *E. coli* lactose permease [94]. Crystallization of the 'red permease' resulted in 2D crystals, which diffracted X-rays to a resolution of 20 Å [95].

# Part I-Results

Crystallization of complex I/Fab co-complexes

# 3 GENERATION OF ANTIBODY FAB FRAGMENTS

## *3.1 PRODUCTION AND PURIFICATION OF MONOCLONAL ANTIBODIES*

The monoclonal antibodies used in this work were produced using the hybridoma cell culture technique as described in 13.2. The clones 1F5 and 44G10 were more sensitive to decreasing concentration of fetal calf serum in the growth medium in comparison to the antibody 31A8. These cell lines were cultivated in 1-2 % growth enhancing factor during the last stages of the antibody production. The cell culture supernatant was purified using Protein G affinity chromatography (13.3). Neutralization with 1M TrisCl, pH 9.0 buffer assured non-denaturing condition after the low pH elution. The peak fractions were analyzed on SDS-PAGE as shown in Figure 3.1. Fractions represented by the most prominent IgG bands were pooled and concentrated.

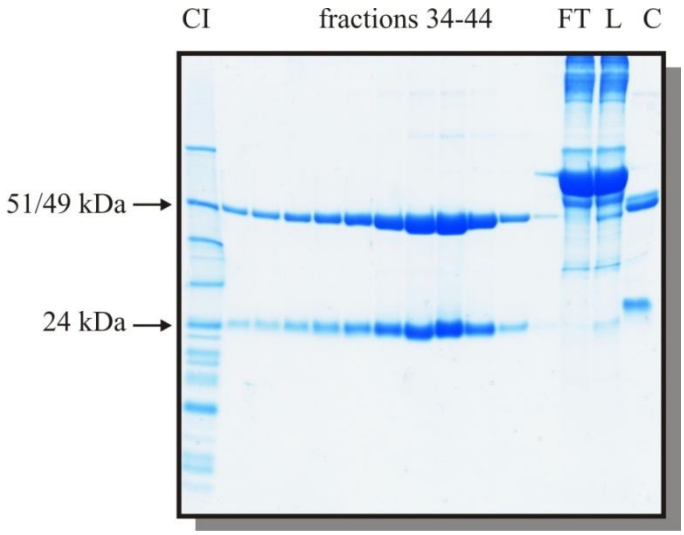


**Figure 3.1: Purification of antibody 31A8. Fractions eluted from Protein G column.**

10% SDS-PAGE under reducing conditions. CI: complex I; fractions 34-44: peak fractions; FT: flow through; L: load on the column; C: control, purified 37F3.

The functionality of the purified monoclonal antibodies was analyzed by binding of complete IgG to complex I (CI), in a 1: 1 molar ratio. The resultant mixture was applied to an analytical gel filtration column (TSK g4000swxl, 7.8 mm x 30 cm). The elution profile revealed the presence of four different species (Figure 3.2 A), representing CI at different IgG saturation levels (peaks 1-3) and antibody excess (peak 4). Peak 1 most probably resulted from formation of a ternary complex, where one antibody molecule bound two CI molecules. Peak 2 cor-

responded to CI/IgG co-complexes, with one IgG molecule per complex I. Peak 3 was at the same elution volume as for the un-complexed enzyme (green trace, Figure 3.2 A) and most likely represented complex I without attached antibodies. The presence of antibody revealed by Western blotting in fraction 9 (peak 3) could be explained by a partial overlap with peak 2. The unbound antibody molecules contributed to peak 4, as revealed by SDS-PAGE and Western blot. A Western blot of the peak fractions showed that the antibodies bound tightly to complex I (Figure 3.2 B, right panel). The binding of the immunoglobulins 1F5 and 44G10 to the native complex I was analyzed in an experiment similar to the one described for 31A8 and in each case the results were comparable (data not shown).

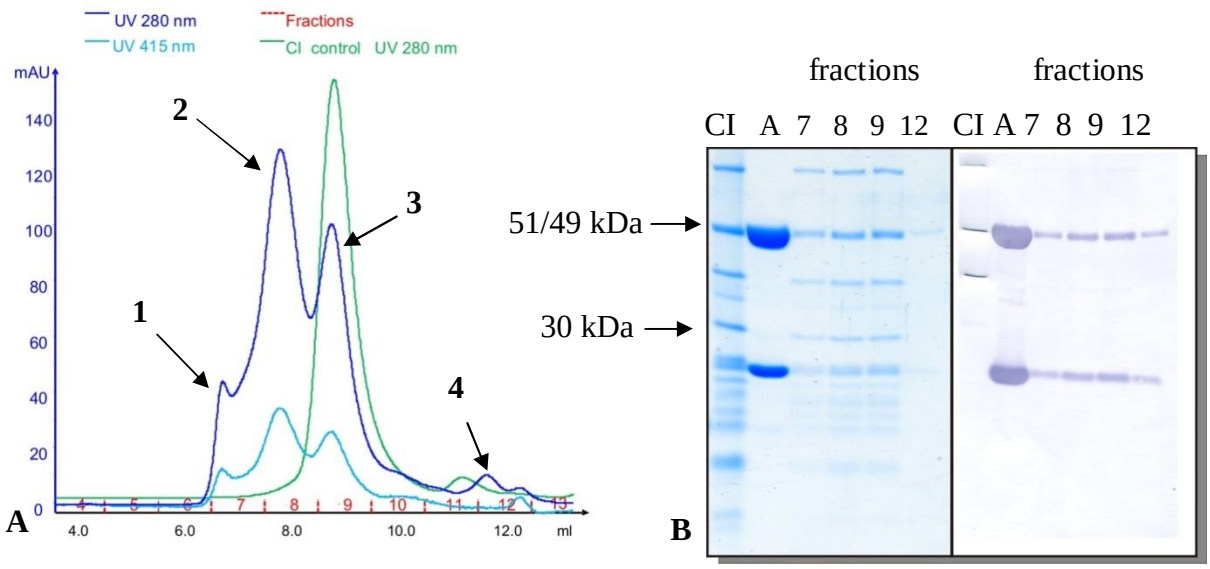


**Figure 3.2: Binding of complete IgG 31A8 to purified complex I.**

A: Gel filtration profile. The dark blue trace represents run of CI with bound intact antibody 31A8. The green profile corresponds to CI without antibody. B; left panel: 10% SDS gel, right panel: developed Western blot membrane. Fractions were prepared under reducing conditions. CI: complex I; A: IgG 31A8; 7-9, 12: peak fractions. The CI subunits (75- kDa, 51/49-kDa and 39-kDa) were marked for comparison on the Western blot membrane. The bands were stained in a chromogenic reaction with NBT and represent pseudo positive signals in Western blot (Figure 3.2 B, lane 'CI').

The 1F5 antibody showed only limited solubility at low temperatures. As the affinity purification step was carried out at 4°C, the antibody precipitated in the collection tubes. The precipitate disappeared without additional treatment upon sample transfer to temperatures above 18°C. Antibodies are very robust proteins and re-nature easily from mild denaturing conditions. Also in this case the 1F5 antibodies remained intact upon precipitation. The precipitated and subsequently re-dissolved samples were analyzed using SDS-PAGE (Figure 3.3). The bands in the region of 100 kDa presumably represent not fully reduced sample. The precipi-

tated samples (F) and the precipitate itself (PR) were shown to bind to complex I in a manner similar to the control (C) and un-precipitated fractions (P) (data not shown). In a concentrated sample the whitish precipitate would re-appear upon transfer to low temperatures.

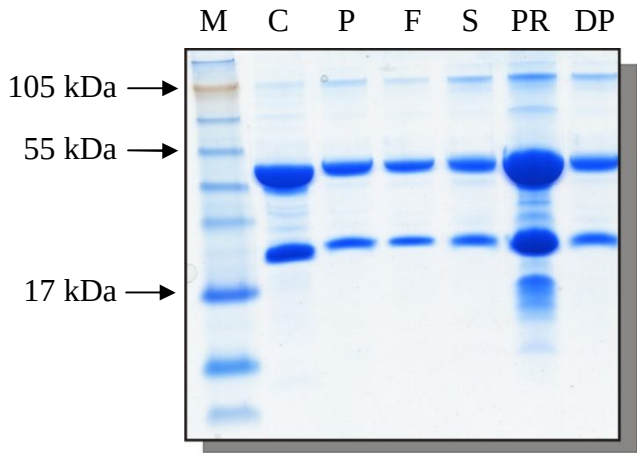


**Figure 3.3: 1F5 precipitation at low temperatures.**

10% SDS-PAGE under reducing conditions. M: molecular mass marker (SeeBlue® Plus2, Invitrogen); C: control, purified 31A8; P: pooled fractions 35-44, without 38 and 39; F: fractions 38 and 39; S: supernatant of the centrifuged fractions 38 and 39; PR: precipitate of the centrifuged fractions 38 and 39; DP: room temperature dissolved fractions 38 and 39**.**

Typical yields of the purification procedure are summarized in Table 3.1. The purified antibodies were frozen in 0.1 M PBS, pH 7.0 buffer and stored in liquid nitrogen. The storage conditions did not affect the functionality of the antibodies as verified by ELISA tests and binding experiments, similar to those described before (data not shown).

| Clone | Yield/ L of cell culture |
|---|---|
| | mg |
| 31A8 | 55 |
| 1F5 | 35 |
| 44G10 | 30 |

Table 3.1: Average yield of the purified monoclonal antibodies.

## *3.2 GENERATION OF PROTEOLYTIC ANTIBODY FRAGMENTS*

Production of pure and functional Fab fragments was an essential part of this project. Since, the fragmentation result depended strongly on the immunoglobulin type and may even be clone specific, several techniques were employed in order to find an optimal procedure which would give reproducible and reliable result. The following section is focused on fragmentation of the monoclonal antibodies. Initially the Fab fragments were not separated from Fc parts, which have the same molecular mass (~50 kDa). It is worth mentioning at this point that a fraction of the IgG molecules, Fab fragments, and most probably the Fc fragments fall apart into light and heavy chain or two heavy chains (respectively) on SDS-PAGE, even under non-reducing conditions (R. MacKinnon, personal communication). As a result a pure Fab sample may be represented by two bands on an SDS gel: a ~ 48 kDa band corresponding to whole Fab, and a 24 kDa band, representing the portion where the inter chain disulphide bonds were broken (Figure 3.4). This phenomenon is not a sign of general antibody instability, since the gel filtration experiment showed that the Fab fragments remained intact under native conditions and small molecular weight fragments were not observed (see below). In some cases, under SDS conditions, the intra chain disulphide bonds are broken, but the chains are not fully unfolded leaving some non-covalent interactions intact. The SDS-PAGE migrations of these fragments are different to those where the domains are fully unfolded (H. Schägger, unpublished). Because of that, additional bands may occur.

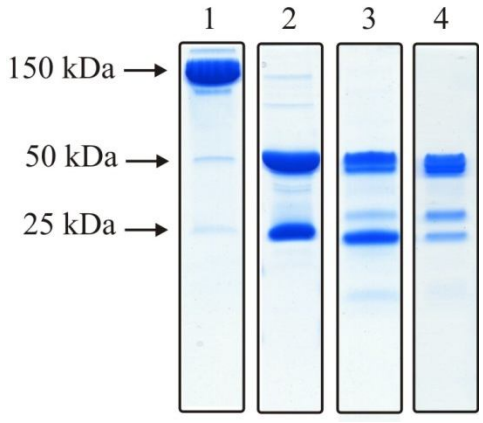


**Figure 3.4: Migration of IgG and IgG fragments in SDS-PAGE.**

10% SDS-PAGE. 1: IgG 1F5 non-reduced; 2: IgG 1F5 reduced with mercaptoethanol; 3: immobilized papain digestion mixture under non-reducing conditions; 4: purified Fab 1F5 under non-reducing conditions.

Crystalline papain, immobilized papain, immobilized ficin and trypsin were employed for generation of the antibody Fab fragments. The trypsin digestion protocol was not reproducible and is not presented in the following section. The serine proteases were activated with 10 mM cysteine. Inactivation of the crystalline papain was carried out using alkylating agents, like N-ethylmaleimide or 2-iodoacetamide. Use of the immobilized forms obviated the need to inactivate the enzymes and separation was simply done by centrifugation. Immobilized papain was chosen for standard preparation of Fab fragments due to straight forward protocol and reproducibly of the results.

Purification of the proteolytic fragments was performed initially by ion-exchange chromatography. It was not possible to resolve the papain digestion mixture by cation exchange chromatography. The fragments purified by anion exchange chromatography were most probably the Fc fragments. Use of unpurified IgG digest was not optimal, since presence of large amounts of undigested or partially digested antibody fragments posed a critical problem for further crystallization trials. Double gel filtration chromatography ensured elimination of high molecular weight species (un- and partially digested immunoglobulins), but did not remove the Fc parts. The most optimal method of isolation of pure antibody Fab fragments from proteolytic digestion mixture was use of Protein G affinity chromatography followed by size exclusion chromatography. In the first step, the Fc and Fc-containing fragments were removed, while the second step resulted in preparation of homogeneous Fab fragments.

The following chapters describe the procedures of generation and purification of functional proteolytic Fab fragments in detail.

### *3.2.1 Crystalline papain*

Digestion of the purified antibody 31A8 was performed as described (13.5.1.2) and the amount of the protease was optimized. Use of papain at concentration lower than 2% (w/w) resulted in a low fragmentation yield (Figure 3.5). The high molecular weight fragments (un- or partially digested immunoglobulins) were less abundant for enzyme concentrations higher than 2%. Slight over digestion of the immunoglobulins was observed for 5% w/w ratio of papain to antibody. Use of 15% of papain resulted in a complete fragmentation of the antibodies, but at the same time the over digestion was most pronounced (lane 4, Figure 3.5). A 2% w/w papain to protein ratio was used in further experiments in order to avoid over digestion.

The digestion time was another important factor in the optimization procedure. The minimal time range required for an efficient fragmentation of the monoclonal antibodies was 2 hours (Figure 3.6).

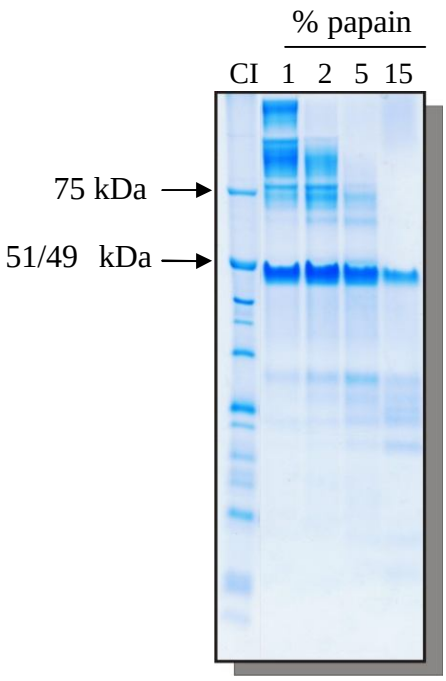


**Figure 3.5: Papain concentration for optimal IgG fragmentation.**

10 % SDS-PAGE, non-reducing conditions. CI: complex I used as a molecular weight marker; 1, 2, 5, 15: the values represent percent of w/w ratio of papain to IgG.

When using shorter reaction times, large proportions of undigested or partially digested antibody molecules were observed rendering the method unproductive. In a standard experiment papain was inactivated with 30 mM NEM after 3-4 hours. 2-iodoacetamide (50 mM) could alternatively be used as an alkylating agent without changing the fragmentation pattern (data not shown). Papain was activated by cysteine in the presence of EDTA. Purified monoclonal antibodies were incubated with 1% (w/w) papain activated with different concentrations of cysteine.

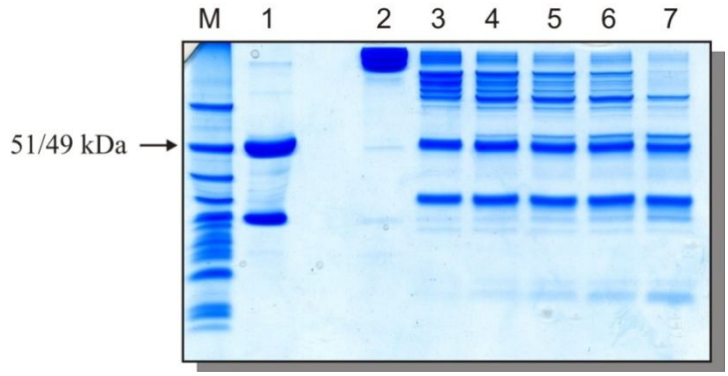


**Figure 3.6: Time course of the digestion of 31A8 IgG with crystalline papain.**

10% SDS-PAGE. M: complex I non-reduced; 1: IgG 31A8 reduced; 2: IgG 31A8 non-reduced (0 min); 3: 30 min; 4: 60 min; 5: 90 min; 6: 120 min; 7: 240 min. Samples 2-7 were not reduced.

The enzyme was inactivated according to a standard procedure after 120 minutes. Change of the cysteine concentration (5 - 10 mM) did not influence IgG fragmentation (data not shown). 10 mM cysteine was used in the standard fragmentation protocol for the crystalline papain activation. .

### *3.2.2 Immobilized ficin*

Fragmentation of antibodies with ficin was performed for two pH values, pH 6.0 and pH 7.0 following the manufacturer's suggestions. The reaction carried out at pH 7.0 (50 mM phosphate buffer) resulted in poor fragmentation. Most of the protein stayed intact after 4 hours of digestion (Figure 3.7 B, lane 3). It was not possible to resolve the resulting fragments using an anion exchange chromatography with the Mono Q column (GE Health Care; Figure 3.7 A). The sample eluted after one third of the gradient as a homogenous peak, representing mainly the undigested immunoglobulin molecules (Figure 3.7 B, lanes 3 and 4). When the immobilized ficin was activated with 10 mM cysteine in 0.1 M citrate buffer pH 6.0, the main products were 48 kDa fragments (Figure 3.8, B). The digestion mixture was purified using ion exchange chromatography (Figure 3.8 A). The peak number 1 (lane 1, Figure 3.8 B) presumably represents the undigested IgG molecules.

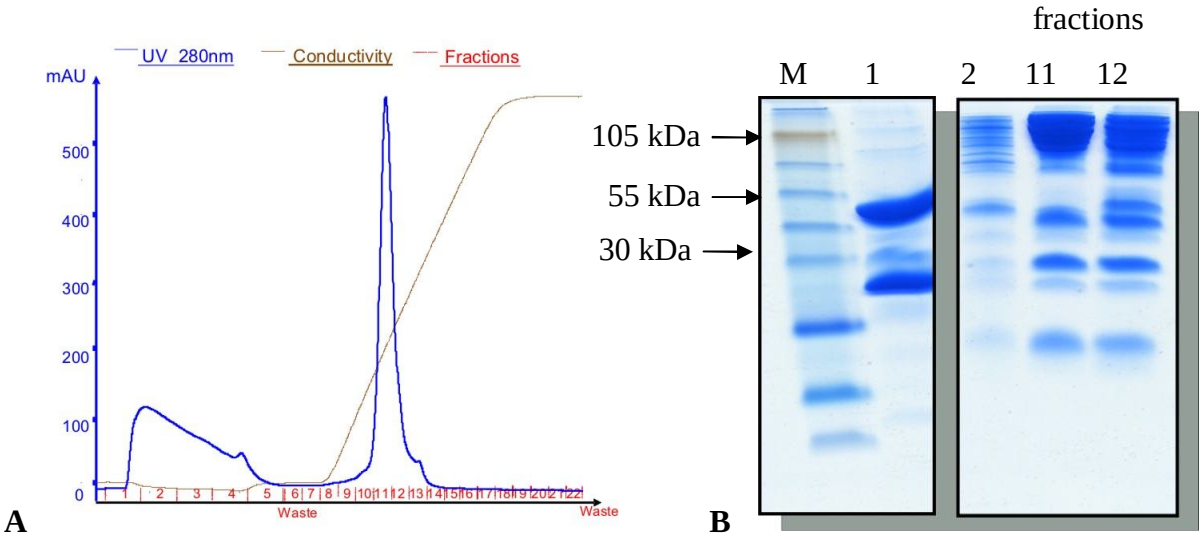


**Figure 3.7: IgG digestion with immobilized ficin at pH 7.0.**

A: Mono Q column elution profile. The chromatography was performed as described in13.5.2.1. B: 10% SDS-PAGE; M: molecular mass standard (SeeBlue®, Invitrogen); 1: ficin digest reduced; 2: load on Mono Q column; 3: peak fraction 11; 4: peak fraction 12.

The $(Fab')_2$ fragments and other partially digested antibody fragments contribute to the peak 2 (lane 2, Figure 3.8 B). Lane 3 corresponds to the third peak and is the fraction with the highest abundance of the 48 kDa fragments, most likely Fab and Fc fragments. Additionally, a band of around 54 kDa is present, which could account for a proteolytic fragment with altered SDS migration properties due to broken internal disulphide bonds (as described before). The fourth peak exclusively contained pure fragments of a mass of 48 kDa. The presence of the lower bands was discussed in the introduction to this section 3.2 (page 22).

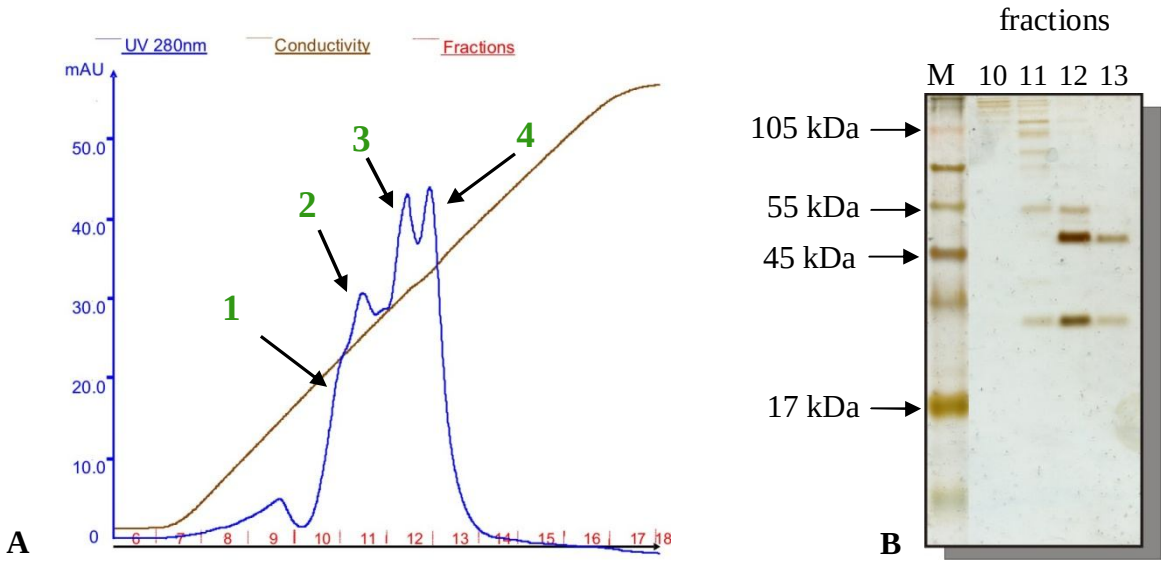


**Figure 3.8: IgG digestion with immobilized ficin at pH 6.0.**

A: elution profile from a Mono Q column. The chromatography was performed as described in 13.5.2.1. B: silver stained 10% SDS-PAGE, non-reducing conditions; M: molecular mass standard (SeeBlue®, Invitrogen); 10-13: corresponding peak fractions.

### *3.2.3 Immobilized papain*

The digestion was performed as described in 13.5.1.3. After 14 hours, most of the immunoglobulin sample was digested. The digestion mixture gave a positive signal in the native ELISA test (data not shown). In contrast to the two IgG digestion methods described above, the immobilized papain digestion (IPD) resulted in a slightly different digestion pattern. Instead of one, two bands are observed in the range of 50 kDa (Figure 3.9, lane 4). Both bands are recognized by anti-mouse IgG in western blot. One explanation would be the presence of another isoform of Fab like Fab', which is only 2 kDa larger. In order to distinguish between the two isoforms, a gel filtration step was employed in the purification procedure (described in greater detail below). Secondly, the double band may be the consequence of differential migration due to cleavage of intra-chain disulphide bonds. Use of the immobilized form of the enzyme

eliminated the need of inactivation of the protease, as well as facilitated the separation procedure. Thus, the immobilized papain method was chosen as a standard technique for further experiments.

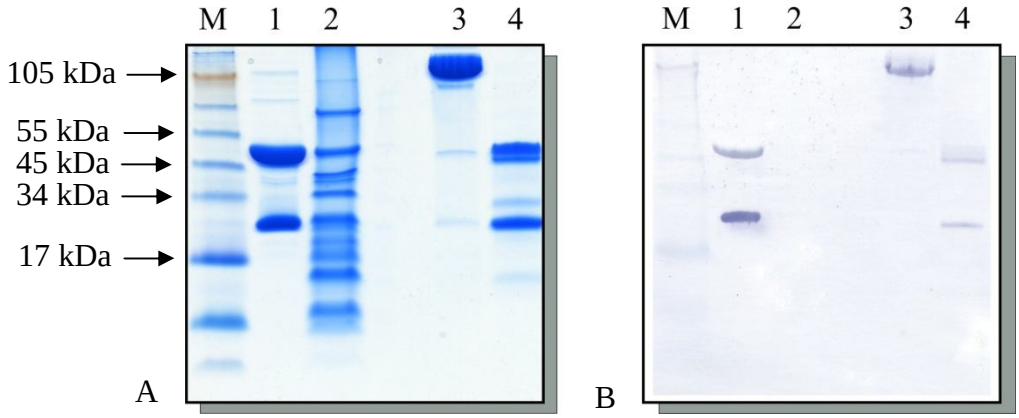


**Figure 3.9: Digestion of IgG 1F5 with immobilized papain.**

The enzyme: substrate ratio was1:160 w/w and the reaction time12 hrs. A. 10% SDS-PAGE, Coomassie stain. M: molecular mass standard (SeeBlue®, Invitrogen); 1: IgG 1F5 reduced; 2: complex I reduced; 3: IgG 1F5 non-reduced; 4: digestion mixture non-reduced. B: developed Western blot membrane. Legend as in A.

## *3.3 PURIFICATION OF FUNCTIONAL FAB FRAGMENTS*

### *3.3.1 Cation exchange*

The IPD (immobilized papain digestion) mixture of IgG 31A8 was purified using cation exchange chromatography (S Hyper D column, Bio Sepra) as described in 13.5.2.2. The resulting separation was poor and it was not possible to isolate pure IgG fragments (Figure 3.10 A and B).

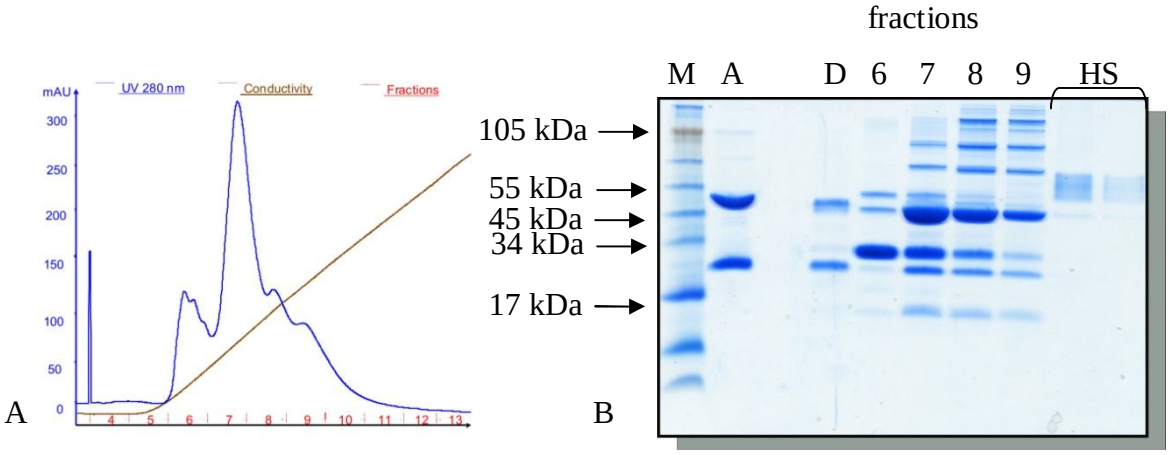


**Figure 3.10: Purification of immobilized papain digest of IgG 31A8 using cation exchange chromatography.**

A: S Hyper D column elution profile. B: 10% SDS-PAGE, Coomassie stain. M: molecular mass standard (See-Blue®, Invitrogen); A: IgG 31A8 reduced; D: digestion mixture (control); 6-9: peak fractions (see A); HS: high salt elution product.

### *3.3.2 Anion exchange*

The IPD mixture of 31A8 IgGs was purified by anion exchange chromatography (Mono Q column, GE Health Care) with good separation yields. The undigested and partially digested antibody fragments contributed to peak 1 in Figure 3.11A and represent the flow-through sample. The peak 2, which eluted in the middle of the salt gradient, could represent a mixture of the Fab and Fc parts. The corresponding fractions (11 and 12) were pooled and purified by size exclusion chromatography as described in 13.5.2.5. The elution profile was uniform (Figure 3.12A) and the sample was exclusively represented by a 50 kDa IgG fragment (Figure 3.12B, lanes 25-30). To check the functionality of the purified fragment, the concentrated sample (pooled fractions 25-28, Figure 3.12) was mixed with complex I and the mixture was applied to an analytical gel filtration column (TSK G3000swxl, TOSOHaas Science). The size exclusion chromatography profile was represented by two distinct peaks (Figure 3.13 A).

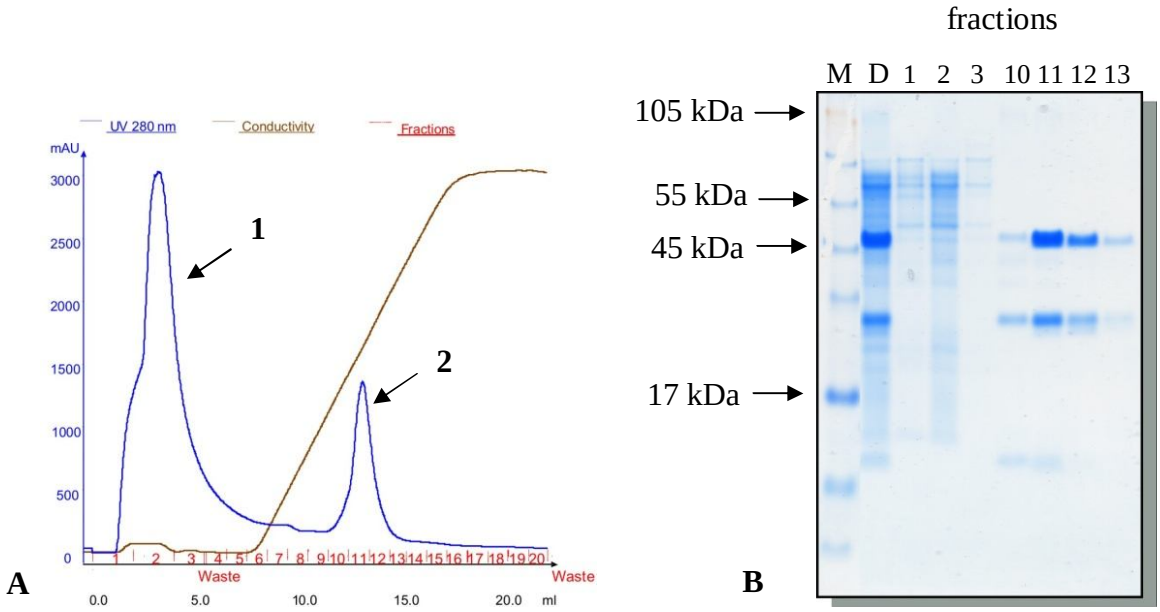


**Figure 3.11: Purification of the papain digestion mixture of antibody 31A8 by anion exchange chromatography.**

A: Anion exchange column elution profile. B: 10% SDS gel, non-reducing conditions. M: molecular mass standard (SeeBlue®, Invitrogen); D: papain digestion mixture of 31A8 IgG; 1-3: first three fractions eluted from the column (flowthrough portion); 10-13: fraction of the peak 2. The fractions were not concentrated.

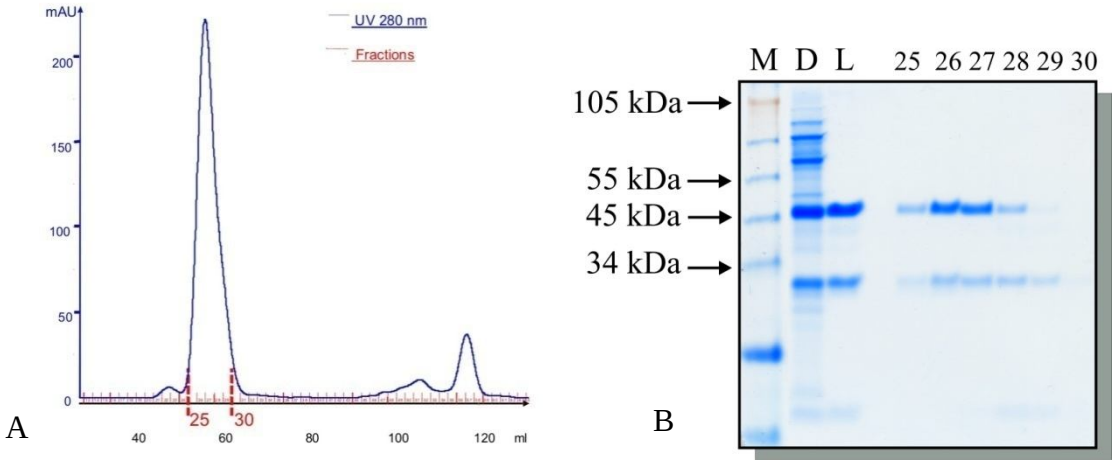


**Figure 3.12: Gel filtration of pooled fractions after ion exchange chromatography.**

A: gel filtration profile. B: 10% SDS PAGE, non-reducing conditions. M: molecular mass standard (SeeBlue®, Invitrogen); D: papain digestion mixture of 31A8; L: Mono Q fractions (11+12 Figure 3.11 A); 25-30: main peak fractions, see A.

The fractions were analyzed by SDS-PAGE under reducing and non-reducing conditions (Figure 3.13 B). Immunodetection with the use of the alkaline phosphatase conjugate assay showed that the purified antibody fragments did not bind to purified complex I. As proven by Western blot (Figure 3.13), peak 1 (Figure 3.13 A) represented by lane 3 on Figure 3.13 (B and C) corresponded to complex I alone.

All the unbound antibody fragments eluted as peak 2, and were detected with anti-mouse IgGs (Figure 3.13 C). In the left panel of the Figure 3.13 B, the antibody fragments were fully reduced and were detected in Western blot in the region of 25 kDa. The right panel shows fractions, which were not reduced with mercaptoethanol. The proteolytic fragments dissociated partially into light and heavy chain and for the fractions 9 and 12 (Figure 3.13 B, C) two bands were detected. The binding experiment showed that the prepared antibody fragments were not functional. The ability to interact with complex I was lost during the preparation procedure, since the intact immunoglobulins were shown to bind tightly to the purified complex I from *Y. lipolytica* (3.1). The same Fab production and purification procedure was applied in the case of the immunoglobulins 1F5 and 44G10. It was found that the purified antibody fragments did not bind complex I (data not shown). We concluded that the IgG antigen binding ability was lost after the anion exchange chromatography step (Mono Q column). Most probably the isolated fragment was the Fc part of the antibody.

More unlikely, the antigen binding region of the proteolytic fragments was disturbed during the ion exchange purification. As a consequence the Mono Q column purification step was excluded from the standard procedure of the Fab preparation.

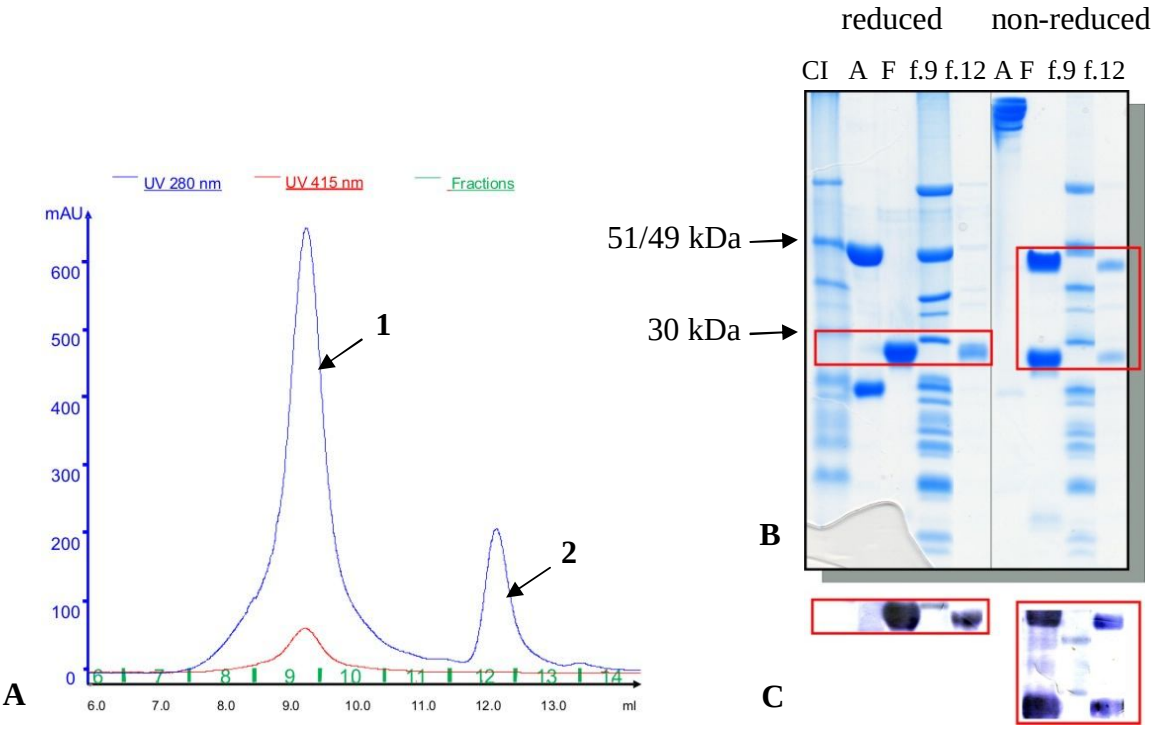


**Figure 3.13: Binding of 31A8 IgG fragments to complex I.**

A: Gel filtration profile. B: 10% SDS-PAGE. Left panel shows reduced fractions, right panel, shows the same, non-reduced fractions. Red boxes indicate the region shown in C. CI: complex I; A: IgG 31A8; F: pure antibody fragment 31A8; f.9: fraction 9; f.12: fraction 12. C: Western blot insets.

### *3.3.3 Immobilized papain digestion mixture as Fab source*

Since it was not possible to isolate functional Fab fragments using ion exchange chromatography, the immobilized papain digestion (IPD) mixture was used as a Fab source. The antibody fragments were prepared as described in 13.5.1.3. The IPD mix was added to complex I and the sample was purified using size exclusion chromatography only. The resulting elution profile displayed a shoulder on the left side of the main peak, which indicated the presence of some high molecular mass impurities (Figure 3.14 A).

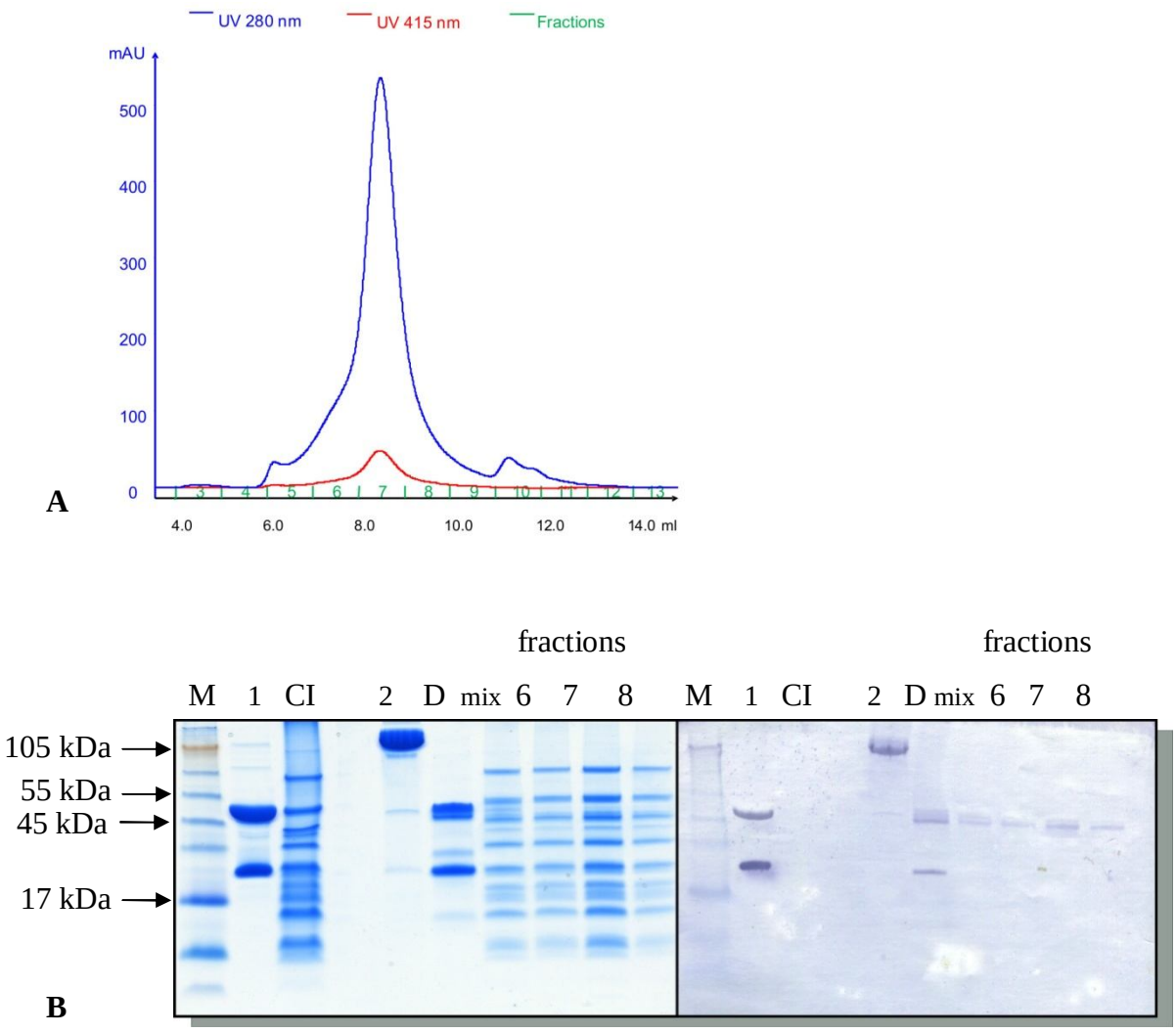


**Figure 3.14: Binding of immobilized papain digest (IPD) 1F5 to complex I.**

A: Gel filtration profile of complex I/IPD mixture of 1F5. B: left panel: 10% SDS-PAGE, Coomassie stained; right panel: developed Western membrane. Antibody fragments were detected using goat anti-mouse, alkaline phosphatase conjugate antibodies in dilution 1:5000. M: molecular mass standard (SeeBlue®, Invitrogen); 1: 1F5 antibody reduced; CI: complex I; 2: 1F5 antibody non-reduced; D: immobilized papain digestion mixture; mix: complex I mixed with the digest D in two fold molar excess of Fabs; 6-8: peak fractions 6-8.

Although the antibody fragments were detected by Western blot in the peak fractions, the Coomassie stained polyacrylamide gel revealed only minor bands in the region around 50 kDa (Figure 3.14 B, lanes: mix and fractions 6-8). The underrepresentation of the bands may mirror sub-stochiometric binding of the antibody fragments to complex I The use of the immobilized papain digestion mixture without purification has its limitation due to possible presence of un- und partially digested antibody fragments. Moreover, presence of the Fc fragments may lead to incorrect calculation of the amount of Fab fragments needed to saturate complex I in a 1:1 ratio.

### *3.3.4 Isolation of pure Fab fragments from the immobilized papain digestion mixture*

#### 3.3.4.1 Double gel filtration

Sample homogeneity and purity is critical for successful protein crystallization. In order to eliminate the co-complexes of complex I and un- and partially digested antibodies, a new purification strategy was designed. The IPD mixture was purified via double gel filtration chromatography using a HiLoad Superdex 16/60 prepgrade 75 column (GE Healthcare). The column resolution (3,000 – 70,000 Da) allowed good separation of the proteolytic fragments according to an SDS gel (Figure 3.15 B).

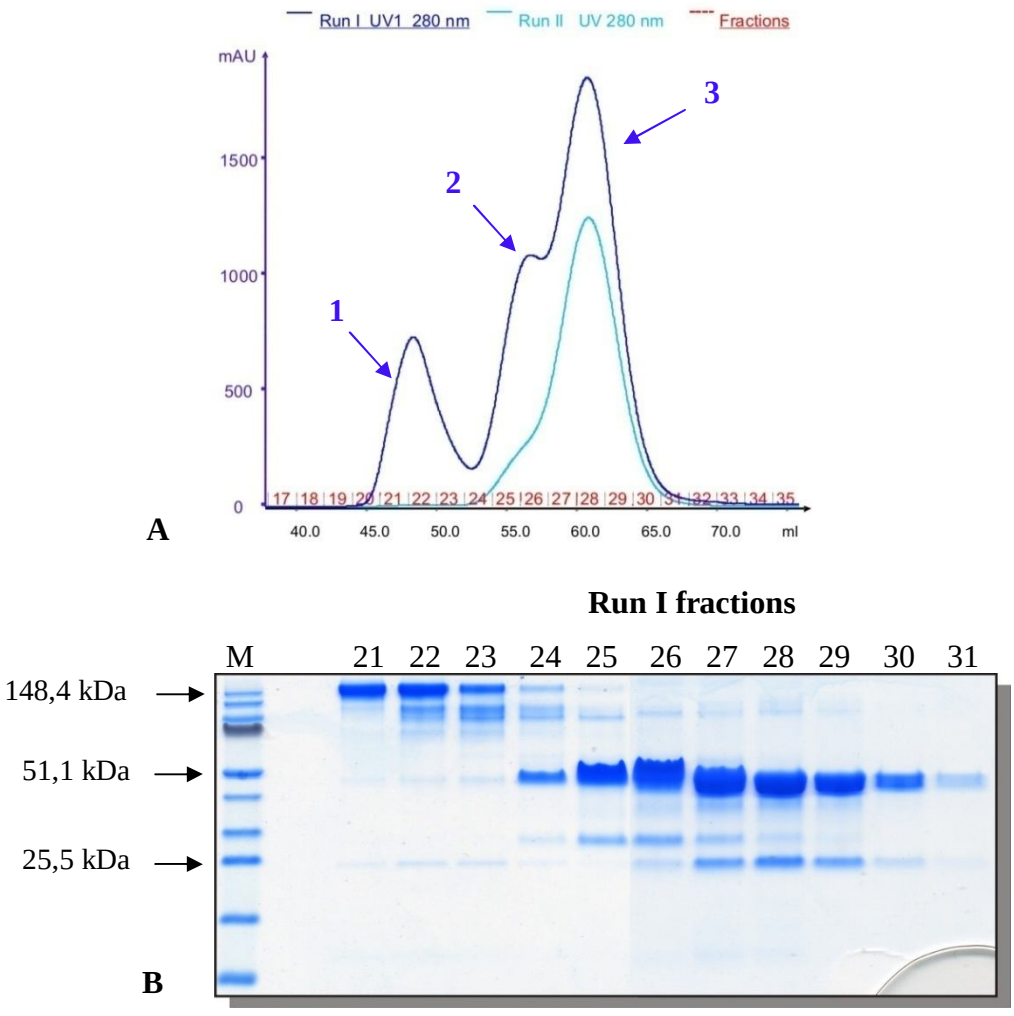


**Figure 3.15: Purification of proteolytic antibody fragments via double size exclusion chromatography.**

A: Gel filtration elution profile, comparison of run I (dark blue trace) and run II (turquoise trace), described in the text. B: 10% SDS-PAGE. M: molecular mass standard (PageRuler™ Prestained Protein Ladder, Fermentas). Run I fractions correspond to fractions eluted in the first run (see A, blue trace).

In the first gel filtration experiment (run I, Figure 3.15 A blue trace) the un- and partially digested IgGs (peak 1) were separated from lower molecular mass fragments (peaks 2 and 3). Antibody fragments of molecular mass of ~52 kDa contribute to peak number 2 (fractions 24-26, Figure 3.15 B) probably corresponding to Fab' or Fc fragments. The slightly smaller Fab Fragments were predominantly found in fractions 27-31 (peak 3) which were pooled, concentrated and reapplied to the column. In the second run (assigned as run II, Figure 3.15 A, turquoise trace) only a small portion of peak 2 was observed at the left shoulder of the main peak. Fractions 26-31 were combined and used for preparation of the CI/Fab co-complexes.

#### 3.3.4.2 Protein G spin columns followed by gel filtration

IgG as well as $(Fab)_2$ parts, both possessing antigen binding sites, were removed from the IPD mixture by including a gel filtration step in the purification procedure. The Fc fragments, having similar molecular mass as Fab fragments, could not be removed completely in this manner. To assure the highest purity of the proteolytic fragments used for crystallization trials, the Fc parts were separated from the Fab fragments by means of Protein G NAb™ Spin columns (Pierce). The antibody fragments were prepared using immobilized papain as described in 13.5.1.3 and affinity chromatography was performed according to 13.5.2.4. The fractions were analyzed in SDS-PAGE and on Western blot. The migration of the IgG 1F5 sample (lane A, Figure 3.16) was altered, probably due to reduction of the disulphide bonds. Most of the IPD mixture (lane D) was detected as ~25 kDa band. This might have been due to disintegration of the antibodies during prolonged storage in the presence of cysteine. The unbound fragments, the flow-through (ft) and wash fractions (w1-w3) contained the Fab fragments. The Fc fragments and whole IgGs were eluted from the column using low pH and were detected in a Western blot using anti-mouse alkaline phosphatase conjugate antibodies (Figure 3.16, e1-e3, right panel). Summarizing, apart from removal of the Fc parts, the protein G chromatography eliminates other Fc-containing molecules, such as the un-digested IgGs. The flow-through as well as all three wash fractions were pooled and applied to the gel filtration column for a final purification step. The peak fractions, (26-30, Figure 3.17) were pooled, concentrated and analyzed by SDS-PAGE and Western blotting (Figure 3.16, lane F). It is remarkable, that all antibody species were recognized by anti-mouse alkaline phosphatase conjugate antibodies. When anti-mouse alkaline phosphatase conjugate antibodies supposed to be specific for Fab fragments were used, the result was identical (data not shown), indicating low specificity of the immunoglobulins used for analysis of antibody fragmentation.

The Fab fragments prepared using the procedure described in this section were used in the co-crystallization trials.

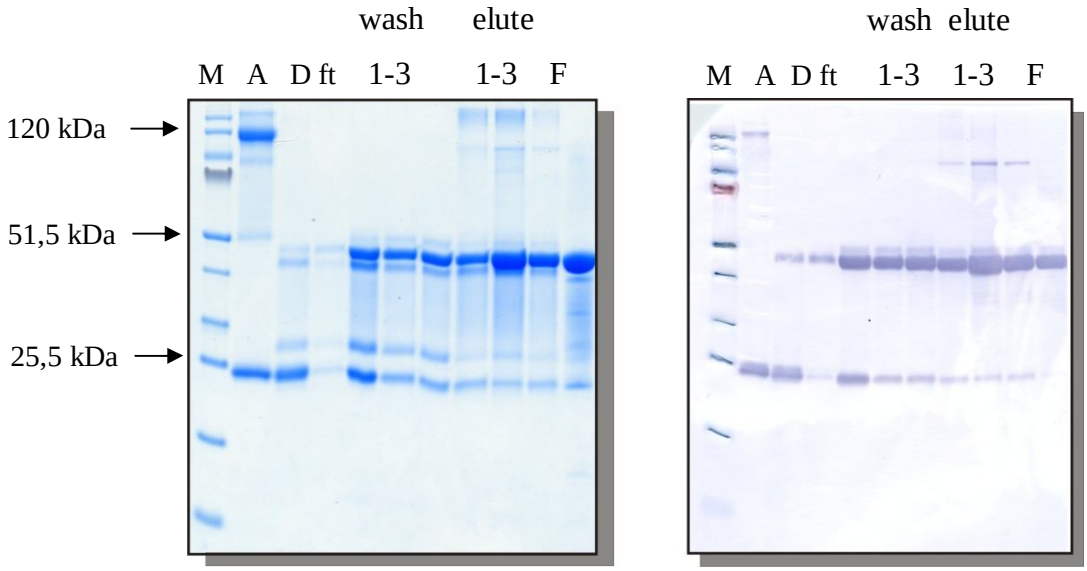


**Figure 3.16: Purification of the 1F5 IPD mixture over protein G NAb™ Spin Columns.**

Left: 10% SDS-PAGE, non-reducing conditions. Right: developed Western membrane. M: molecular mass standard (PageRuler™ Prestained Protein Ladder, Fermentas), A: mAb 1F5; D: 1F5 IPD mixture; ft: flow-through sample; wash 1-3: wash fractions; elute 1-3: eluted fractions; F: Fab 1F5.

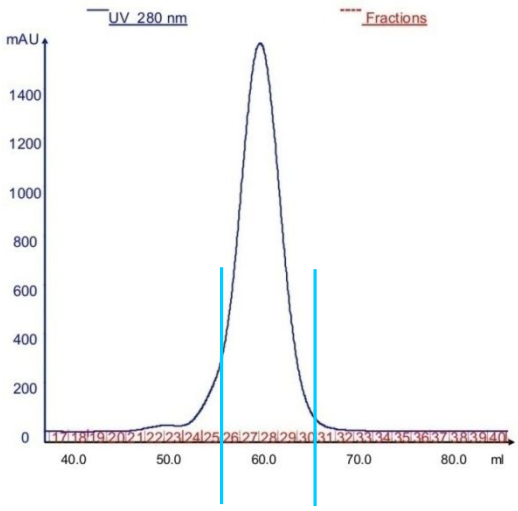


**Figure 3.17: Final gel filtration step in the Fab preparation procedure.**

Elution profile (HiLoad Superdex 16/60 prepgrade 75, GE Healthcare**).** Turquoise lines indicate pooled fractions (26-30) and the sample is shown in Figure 3.16, lane F.

The 44G10 and 31A8 Fab fragments were prepared according to the same procedure as described for antibody 1F5. A comparative elution profile is shown in Figure 3.18 A. Different elution maxima indicated differences in the masses of the antibody fragments. The presence

of dissimilar papain digestion sites within the immunoglobulins under investigation is also seen in SDS-PAGE and Western blot (Figure 3.18 B). The proteolytic fragments originating from the clones 31A8 and 44G10 eluted from the gel filtration column at the same volume, whereas 1F5 Fab seemed to be of a lower molecular mass. It is also remarkable, that the ~25 kDa band is most prominent in case of the clone 31A8, whereas negligible for 1F5. It may be speculated, that the 31A8 fragment was in some way disrupted during the papain digestion, resulting in higher sensitivity of the Fab towards SDS (Fab fragments separate more easily into the light and heavy chain under non-reducing conditions in the presence of SDS). The proteolytic fragment of the antibody 44G10, eluted from the gel filtration column as a uniform peak. The same sample, when analyzed in SDS-PAGE displayed presence of a double band in the ~ 50 kDa region.

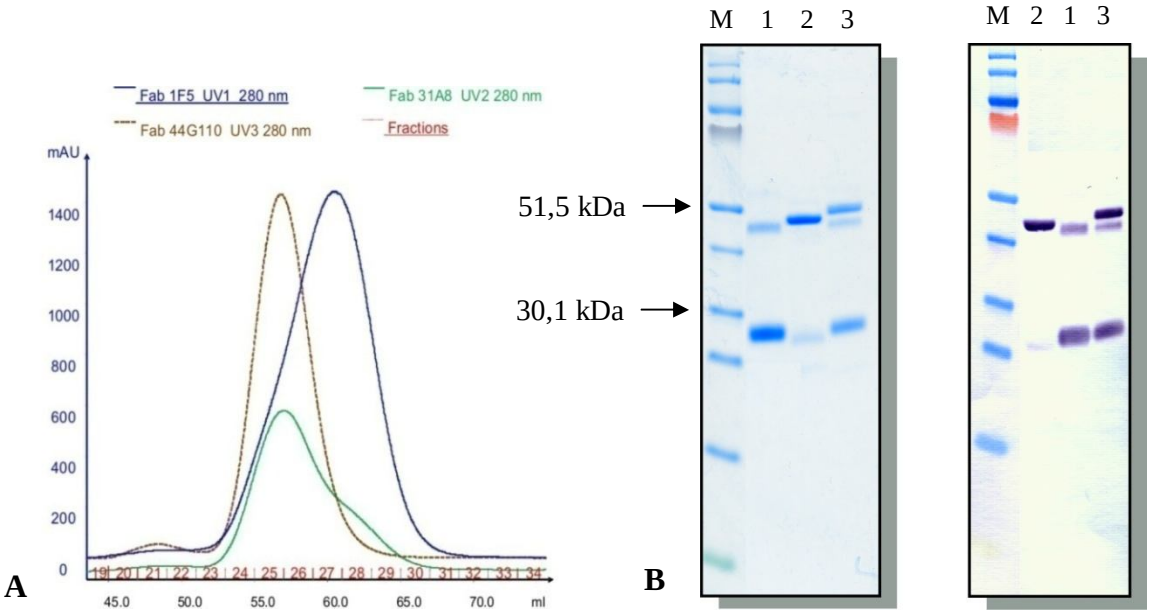


**Figure 3.18: Purified Fab fragments used in co-crystallization trials: 31A8, 1F5 and 44G10.**

A: Comparative gel elution profile for all three Fab fragments used for crystallization trials in this work. B: Left: 10% SDS-PAGE under non-reducing conditions. Right: developed Western blot membrane. M-molecular mass standard (PageRuler™ Prestained Protein Ladder, Fermentas); 1: Fab 31A8; 2: Fab 1F5; Fab 44G10.

# 4 SURFACE PLASMON RESONANCE MEASUREMENTS

## *4.1 AFFINITIES OF THE MONOCLONAL ANTIBODIES AND THE Fab FRAGMENTS TO COMPLEX I*

The affinities of the monoclonal antibodies towards complex I were assessed by surface plasmon resonance using two different protocols. In the first approach, the antibody was used as the ligand and complex I as the analyte. The immunoglobulins were indirectly immobilized on the CM5 sensor chip via an anti-mouse capture antibody, which in turn was covalently bound to the carboxymethylated dextran surface by amine coupling. Since the monoclonal antibody was immobilized on the surface, thereby avoiding avidity effects, the responses could be described by a simple 1:1 interaction model. The experiments were performed as described in 13.4. The affinity data obtained using this approach, were verified by a different technique. In the second protocol, complex I, used as the ligand, was attached to the NTA sensor chips via a His-tag, whereas the antibodies were used as analytes. The measurements were done according to the protocol described in 13.4. The affinity of the Fab fragments towards complex I was measured using only the second immobilization system. The results obtained by the two approaches were very similar and reproducible. The highest affinity, in the picomolar range, was measured for the monoclonal antibody 1F5. Its corresponding Fab fragment, bound to the antigen with only slightly lower affinity, but still with the same order of magnitude. The antibody 44G10 and its Fab fragment displayed nanomolar affinity towards complex I. The lowest response was measured in the case of the antibody 31A8, which was reflected by the highest $K_d$ value. It was not possible to measure the affinity of Fab 31A8 to complex I, due to a very weak binding signal. This result was in agreement with the data obtained for gel filtration chromatography of the CI/Fab co-complexes, where it was not possible to detect significant binding of the Fab 31A8 to complex I (see Figure 5.3 and Figure 5.4)

## *4.2 INFLUENCE OF CONFORMATION ON THE BINDING OF THE MONOCLONAL ANTIBODIES TO COMPLEX I*

The antibody 44G10 is Western blot negative, which indicates its conformational specificity. The same seems to be the case for the 31A8 antibody. In contrast, antibody 1F5 recognizes only a linear epitope and is Western blot positive. In order to address the binding of the antibodies to complex I displaying different conformations, NADPH that had shown to change the pattern fragments of peptides obtained by limited proteolysis of complex I [96;97] was

included in the experiments. To this end, antibodies were immobilized on the sensor chip via a capture antibody and complex I was used as the analyte. The substrate was pre-incubated with complex I, at final concentrations of 0.1, 1, 5, and 10 µM for at least 30 minutes on ice, as described in 13.4. In the first cycle complex I without bound NADPH was used as a control. The relative plasmon resonance response at the end of each injection was plotted against the NADPH concentration for all immunoglobulins. For both conformation specific antibodies 44G10 and 31A8 no effect on the binding to the enzyme was observed upon incubation with NADPH (Figure 4.1). In contrast, a significant drop in the binding signal of the 1F5 was observed for NADPH concentrations above 1 µM.

An interesting observation was recorded for the binding experiments, where an 'aged' complex I sample was used. The complex I dilutions were kept at 4°C for several days. The data collected during subsequent days indicated that the affinity of 31A8 and 44G10 antibodies to the enzyme decreased constantly with time, until it reached a constant level of approximately 70 % of the initial readings. In the case of the immunoglobulin 1F5 no correlation between age of the antigen sample and affinity towards it, was observed.

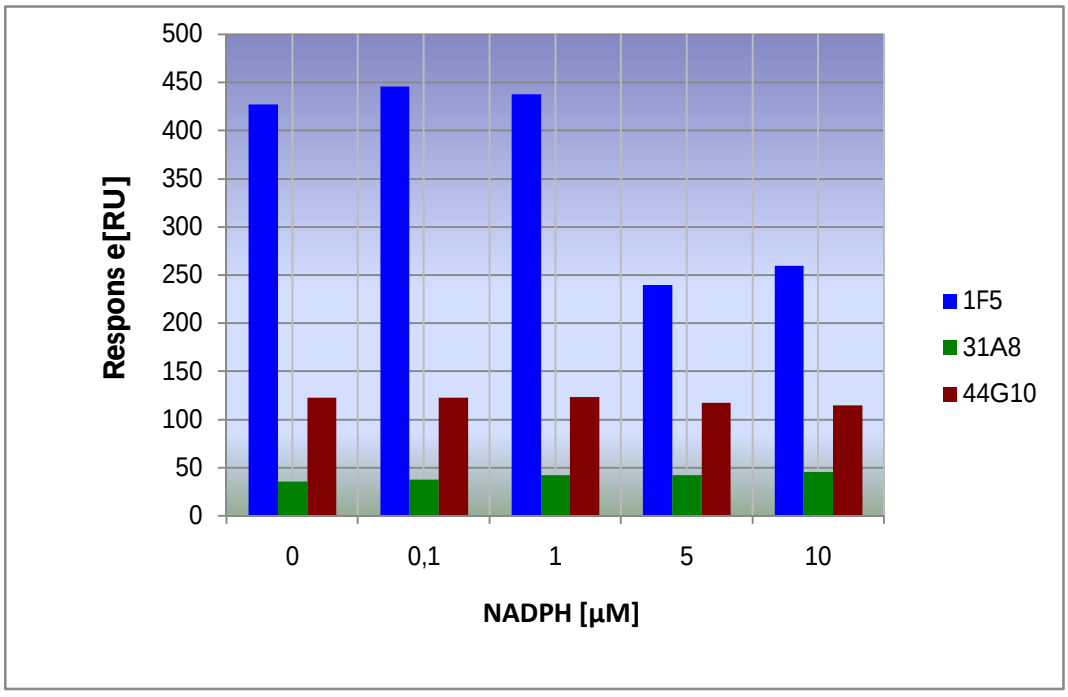


**Figure 4.1: Effect of NADPH on binding of the monoclonal antibodies to complex I.**

No effect of NADPH on binding to complex I was observed for the monoclonal antibodies 31A8 and 44G10. In contrast, the response upon binding of antibody 1F5 to complex I was decreased by approximately 40 % when NADPH was present at concentrations above 1µM.

# 5 PREPARATION OF THE CI/Fab CO-COMPLEXES

The functionality and stability of the prepared Fab fragments was verified in a standard binding experiment (13.7).

## *5.1 CI/1F5 Fab CO-COMPLEXES*

The Fab fragments of antibody 1F5 were prepared using immobilized papain. The digestion mixture was purified by protein G chromatography (protein G NAb™ Spin Columns, Pierce), followed by gel filtration (HiLoad Superdex 16/60 prepgrade 75, GE Healthcare). The pure Fab was added to complex I in a 1.3:1 molar ratio. The stability of the co-complex was analyzed using size exclusion chromatography and Western blotting. The gel filtration profile of the CI/Fab 1F5 co-complex exhibited a shift towards the higher molecular weight region as compared to the native complex I (Figure 5.1 A). As the mass attached to CI was 20 times smaller than the enzyme, the shift was relatively small. The Fabs 1F5 were shown to bind tightly to CI, as proven by Coomassie stained SDS PAGE and Western blotting (Figure 5.1 B).

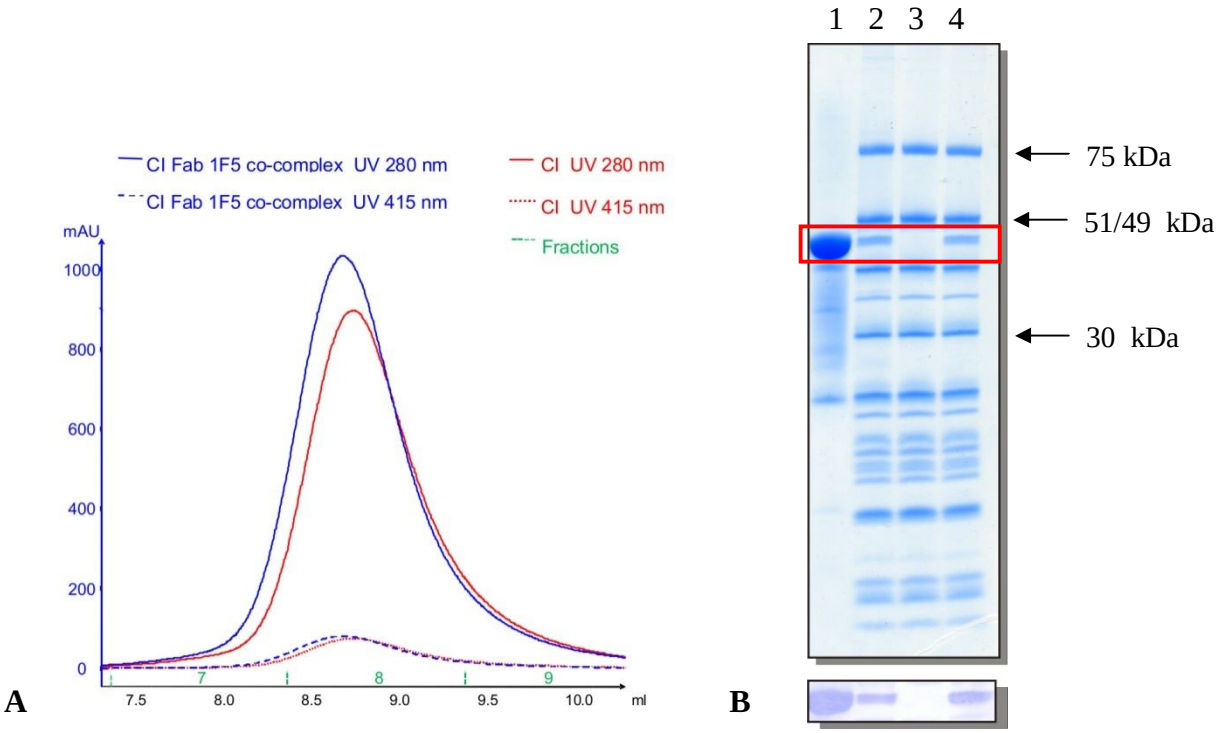


**Figure 5.1: Preparation of a CI/Fab 1F5 co-complex.**

A: Gel filtration profile; CI (red) vs. CI/Fab (blue). B: 10% SDS PAGE and developed Western membrane inset. 1: pure Fab 1F5; 2: mixture of Fab and CI in 1.3:1 molar ratio; 3: complex I; 4: CI/Fab 1F5 co-complex after gel filtration.

## *5.2 CI/Fab 44G10 CO-COMPLEXES*

The immobilized papain digest of antibody 44G10 was purified by gel filtration, without subsequent Protein G affinity chromatography. The Fab fragments were mixed with complex I at a 2:1 molar ratio. The amount of the Fab fragments needed for the two fold molar excess of the fragments over complex one was calculated taking into account the presence of the Fc parts. The stability of the resultant mixture was analyzed by size exclusion chromatography. The peak fractions were shown to represent co-complex fractions and the 44G10 Fab fragments were detected by Western blot using anti-mouse alkaline phosphatase conjugate antibodies. The unbound antibody fragments eluted as a minor peak and were also detected by Western blot (data not shown). CI/Fab 44G10 co-complex was also prepared with Fab fragments generated following to an improved procedure. This method included a Protein G affinity purification step following the papain digestion to remove the Fc parts. These Fab 44G10 proteolytic fragments were incubated with complex I, in 3 fold molar excess, to assure saturation of the enzyme with the fragments. The CI/Fab 44G10 co-complex was stable and the Fab fragment could be detected under non-reducing conditions in Western blot using anti-mouse alkaline phosphatase conjugate antibodies after gel filtration chromatography (Figure 5.2 A, B).

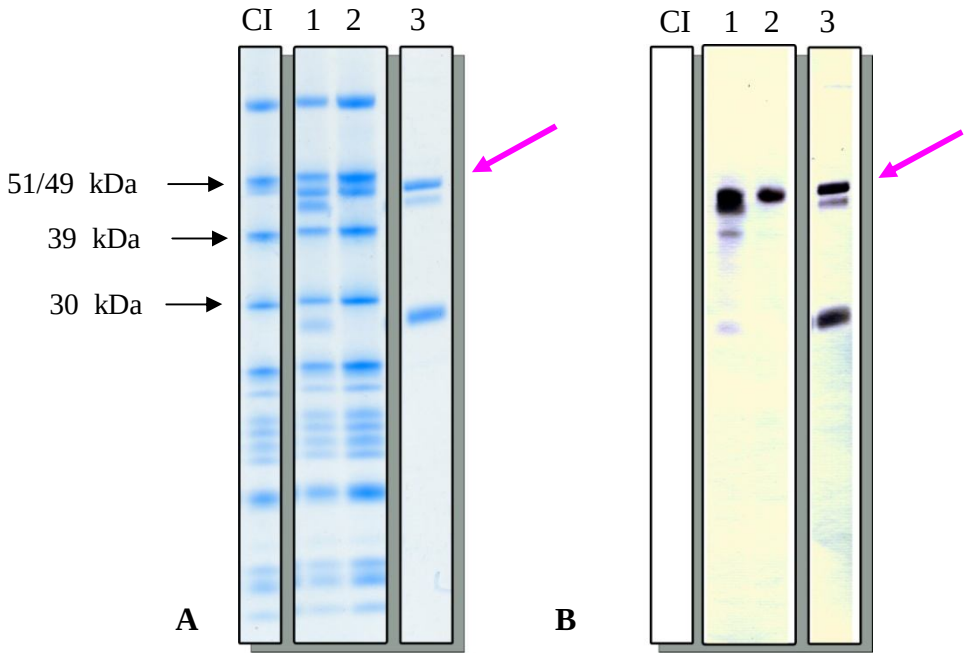


**Figure 5.2: Preparation of s CI/Fab 44G10 co-complex.**

A: 10% SDS PAGE under non-reducing conditions. CI: complex I; 1: mixture of Fab and CI in 3:1 molar ratio; 2: CI/Fab 44G10 co-complex after gel filtration; 3: Fab 44G10 used for the preparation of the co-complex. B: Western blot.

Both, Coomassie stain and Western blot indicated the presence of two bands in the region of ~50 kDa (Figure 5.2 A/B, lane 3). The double band was present in the mixture of complex I and the antibody fragment (Figure 5.2 A, B, lane 1), but absent in the sample after gel filtration chromatography (Figure 5.2 A, B, lane 2), where only the upper band (marked with pink arrow) was detected. This may indicate presence of two isoforms in the Fab 44G10 preparation with only one isoform binding to complex I.

## *5.3 CI/Fab 31A8 CO-COMPLEXES*

The antibody 31A8 was fragmented using immobilized papain. The digestion mixture was purified using Protein G magnetic beads according to the manufacturer's procedure. The unbound sample containing Fab fragments (without further purification) was mixed with pure complex I in a ratio corresponding to 2.5 molar excess of the Fab fragments. The co-complex eluted from a gel filtration column as a homogenous peak (Figure 5.3 A) and the preparation was analyzed on an SDS gel and by Western blotting. The Fab bands of the peak fractions (Figure 5.3 B, lanes 7-8) were much less prominent than the complex I subunits, what indicated a sub-stochiometric binding of the Fab fragments to complex I. Additionally, there was a double band observed in the region of 50 kDa for the Fab sample (Figure 5.3 B, lane F) as well as for all the peak fractions.

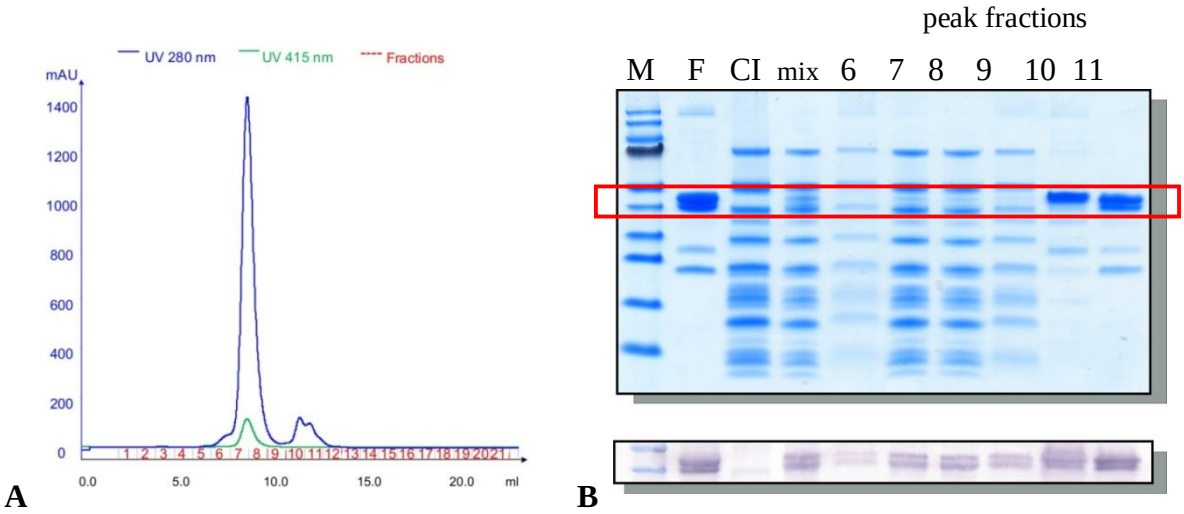


**Figure 5.3: Sub-stochiometric binding of the Fab 31A8 fragments to complex I.**

A: gel filtration elution profile. B: upper panel: 10% SDS-PAGE; lower panel: developed Western blot membrane. M: molecular mass standard (PageRuler™ Prestained Protein Ladder, Fermentas); F: protein G magnetic beads unbound fraction. CI: complex I; mix: mixture of fraction F and complex I in a 2,5 molar excess of Fab; 6-11: peak fractions.

The antibody fragment excess eluted behind the main peak as a double peak. The main components of fractions 10 and 11 were shown to have a different molecular mass (Figure 5.3 B, lanes 10 and 11) possibly cooresponding to Fab' and Fab fragments. Ideally, the Fc parts would have been removed in the magnetic beads protein G chromatography. The effect of the sub-stochiometric binding of Fab to complex I on co-complex crystallization will be discussed in the last chapter.

In an optimized procedure the Fab fragments were prepared by immobilized papain digestion of IgG 31A8, followed by protein G affinity chromatography and subsequent gel filtration. The Fab 31A8 was used in a 3 fold molar excess to form the co-complex. The CI/Fab mixture was applied to a gel filtration column in order to examine the stability of the co-complex and remove the unbound sample. The elution maximum of the resultant peak corresponded to the retention time of the native enzyme (Figure 5.4 A). Western blot analysis of the co-complex after size exclusion chromatography showed no signal in the range of the Fab fragment (Figure 5.4 B, lane CI/Fab). Lack of binding of the Fab 31A8 to complex I most probably resulted from damage of the antigen binding region, caused by papain digestion. Under native conditions, the non-complexed Fab (Figure 5.4B, lane 4) disassembles into light and heavy chain more easily than the Fab bound to complex I (Figure 5.4, lane 2).

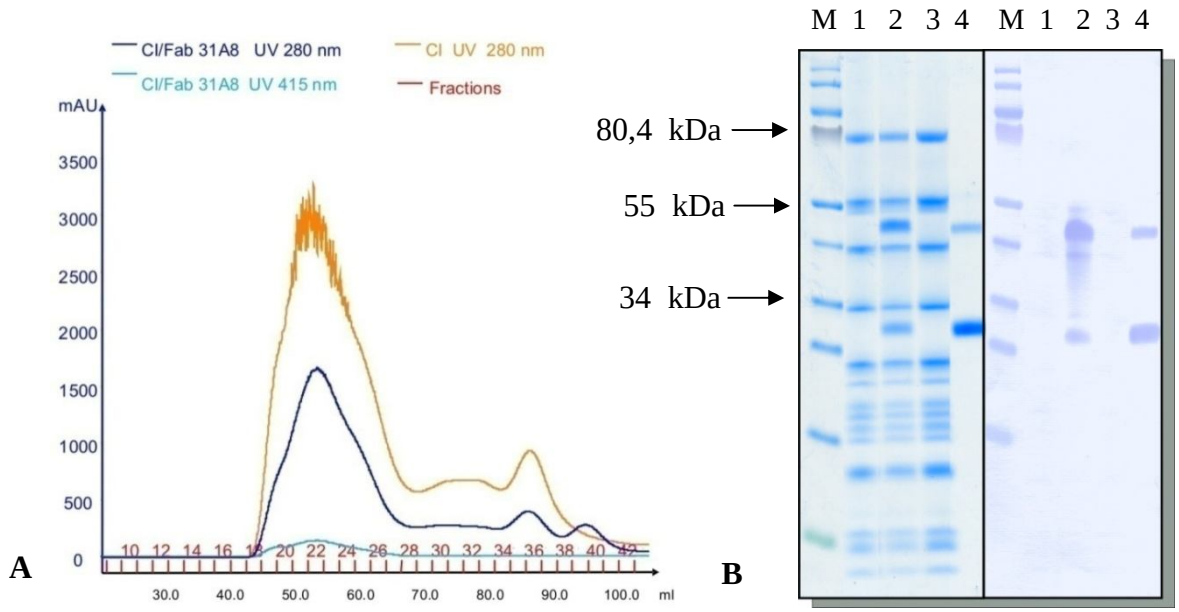


**Figure 5.4: Preparation of a CI/Fab 31A8 co-complex.**

A: Comparison of the gel filtration profiles for the co-complex (blue) and the native complex (orange). B: 10% SDS PAGE (left panel) and a developed Western membrane (right panel). M: molecular mass standard (PageRuler™ Prestained Protein Ladder, Fermentas); 1: complex I; 2: CI/Fab co-complex with 3 fold molar Fab excess; 3: the CI/Fab 31A8 mixture after gel filtration; 4: Fab 31A8 used for the co-complex preparation.

## *5.4 ACTIVITY ASSAYS AND PHOSPHATE DETERMINATION OF CI/Fab CO-COMPLEXES*

To test whether binding of the Fab fragment affected catalytic activity, pooled complex I fractions eluted from the $Ni^{2+}$ NTA column ($Ni^{2+}$ NTA pool) were divided into two equal parts. The first half was subjected directly to further purification steps (gel filtration and concentration). To the second part 1F5 Fab fragments were added in a molar excess of 2:1. This co-complex was purified in parallel to the native enzyme. Activity assays were performed as described in 13.6.6. The presence of the Fab complexes did not significantly affect the measured specific NADH:HAR oxidoreductase activity at any stage of the preparation (Table 5.1). Table 5.2 shows that also the specific dNADH:DBQ oxidoreductase activity was not affected by the presence of the Fab fragment.

| **Purification stage** | **Protein** | | **dNADH:HAR activity** | | **Yield** |
|---|---|---|---|---|---|
| | **mg** | **%** | **[µmol $min^{-1}$]** | **[µmol $min^{-1}$ $mg^{-1}$]** | **%** |
| **Membranes** | 4576 | 100 | 5678 | 1,2 | 100 |
| **Lauryl maltoside extract** | 2252 | 50 | 6280 | 2,8 | 110 |
| **$Ni^{2+}$ NTA Pool** | 69 | 1,5 | 1969 | 29 | 35 |
| **TSKgel G4000sw pool** | 12/**9,5** | 0,5/**0,4** | 689/**623** | 57/**66** | 24/**22** |
| **Complex I** | 10/**9** | 0,45/**0,4** | 610/**588** | 60/**64** | 21/**20** |

Table 5.1: Purification table of complex I vs. complex I/Fab 1F5 co-complex (red).

| | **NADH:HAR** [µmol $min^{-1}$ $mg^{-1}$] | **dNADH:DBQ** [µmol $min^{-1}$ $mg^{-1}$] |
|---|---|---|
| **Complex I** | 56 | 6,1 |
| **Co-complex** | 60 | 6,4 |

Table 5.2: NADH:HAR and dNADH:DBQ activities of the 1F5 co-complex and the native enzyme.

The results obtained for the co-complexes of Fab 31A8 and 44G10 were similar to those recorded for Fab 1F5 complex (not shown). Determination of organic phosphor taken as a measure for the phospholipid content of preparations of complex I and the co-complexes was performed as described in 13.6.9. Typical values obtained for the co-complex preparation were between 100-180 nmol phosphor/mg enzyme and were similar to the values obtained for the complex I in the absence of antibody fragments (data not shown).

# 6 CRYSTALLIZATION OF CI/Fab CO-COMPLEXES

## *6.1 CI/Fab 31A8 CO-COMPLEX CRYSTALLIZATION*

Preparation of the CI/Fab 31A8 co-complexes was difficult due to impeded binding of the Fabs to CI (see previous chapter). It was concluded, that the antigen binding region of the 31A8 antibody fragments became distorted during the proteolytic digestion procedure. Depending on the batch and/or technique used for the Fab preparation, either weak or no binding to pure complex I was observed for the 31A8 antibody fragments. Figure 6.1 represents initial crystallization conditions for the co-complex for which a weak binding of the Fab fragments was observed. The conditions were selected after screening with the PEG/Ion™ crystallization screen (Hampton Research). The quality of the crystals was not satisfying. Twinning, crystal shower and other undesirable features resulted most probably from non-homogeneous mixture of CI particles with and without Fab fragments. Crystals from the experiments presented in Figure 6.1, A were cryoprotected by soaking in cryosolution (11% PEG 3350, 100 mM sodium formate, 30% glycerol, pH 6.0) and shock frozen in liquid nitrogen.

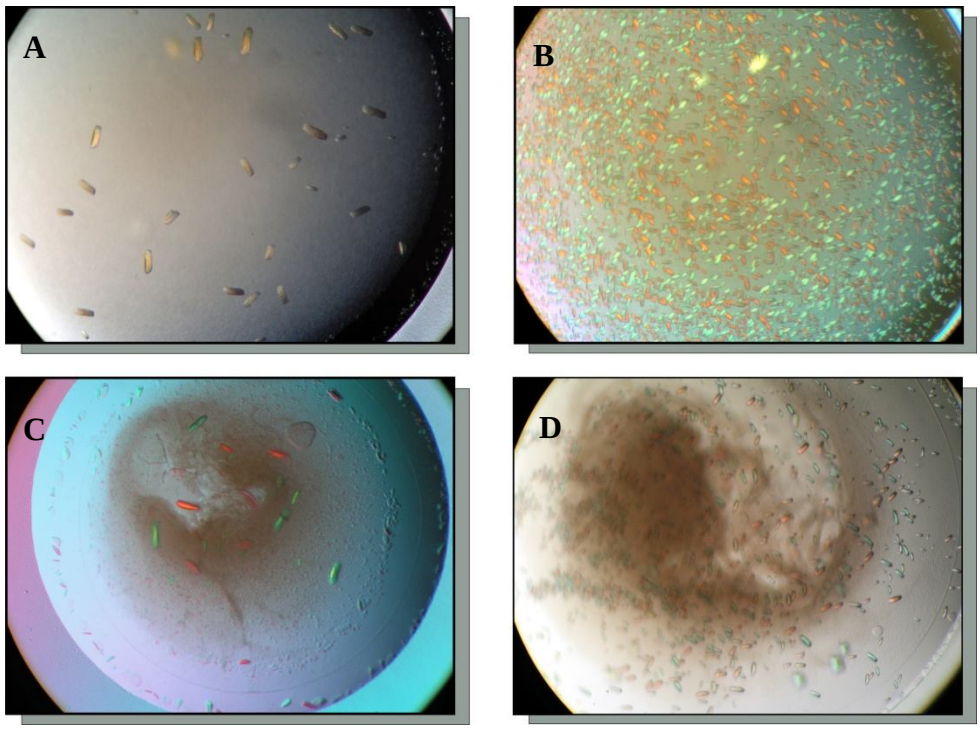


**Figure 6.1: Initial conditions for CI/Fab 31A8 co-complex crystallization.**

PEG/Ion crystallization screen (Hampton Research) was used for screening for suitable conditions. A: 9% PEG 3350, 100 mM sodium formate, 10% glycerol, pH 6.0; B: 8% PEG 3350, 100 mM ammonium acetate, 10% glycerol, pH 7.1; C: 9% PEG 3350, 100 mM sodium formate, 10% glycerol, pH 6.4; D: 9% PEG 3350, 100 mM sodium potassium phosphate, 10% glycerol, pH 5.2.

The frozen crystals did not diffract X-rays when measured in cryo-conditions at the ID14 beamline at the European Synchrotron Radiation Facility (ESRF) in Grenoble, France. Next, the conditions identified in the initial crystallization screen were optimized by varying precipitant concentration and pH values in different directions. It was possible to control the nucleation process by manipulating the pH value of the crystallization solution. As an example, crystallization conditions for 0.1 M sodium potassium phosphate, 8% PEG 3350, 10% glycerol are depicted in Figure 6.2. At pH 5.0-5.2 the sample crystallized as crystal shower (Figure 6.2, A), whereas only minimal increments of pH resulted in growth of only several crystals (Figure 6.2 B and C). Nevertheless, the quality of the crystals was not improved.

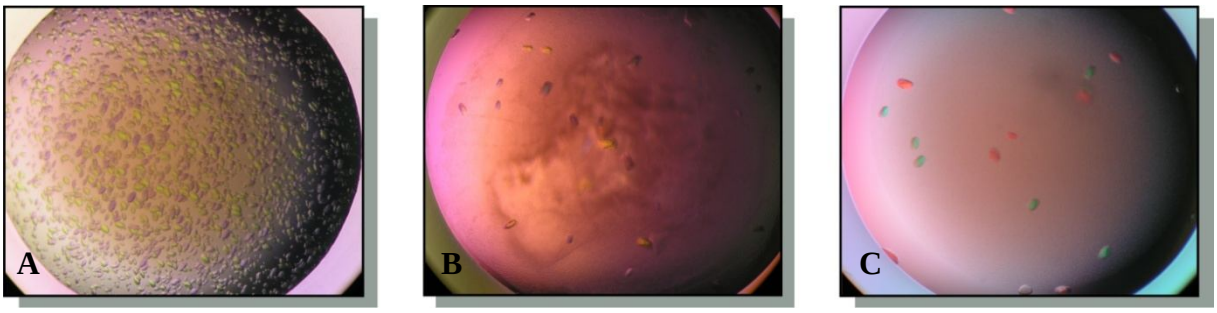


**Figure 6.2: Controlled nucleation of crystallization of CI/Fab 31A8 co-complex.**

0.1 M sodium potassium phosphate, 8% PEG 3350, 10% glycerol pH 5.0-5.6. Minimal changes in the pH of the crystallization buffer significantly influence on the nucleation process. A: pH 5.0-5.2; B: pH 5.4; C: pH 5.6.

The CI/Fab 31A8 sample described in 5.3 was crystallized, although no binding of the proteolytic fragments was detected. Screening for appropriate conditions was carried out using the Mosquito crystallization robot and commercial, as well as self designed crystallization screens. Additionally, an additive screen (Hampton Research) was performed for crystallization conditions working with the native protein. The conditions for which crystals were observed in the nano scale were transferred to the 24-well scale. The crystals, regardless whether grown as sitting or hanging drops, were similar in form to those observed for the same conditions for the un-complexed CI. In order to verify their composition, the crystals (Figure 6.3A) were dissolved and analyzed in SDS-PAGE and Western blot (Figure 6.4). The signal obtained for the CI/Fab 31A8 crystallization sample (Figure 6.4, lane 2) shows the presence of minor amounts of the Fab 31A8 fragments in the complex I sample.

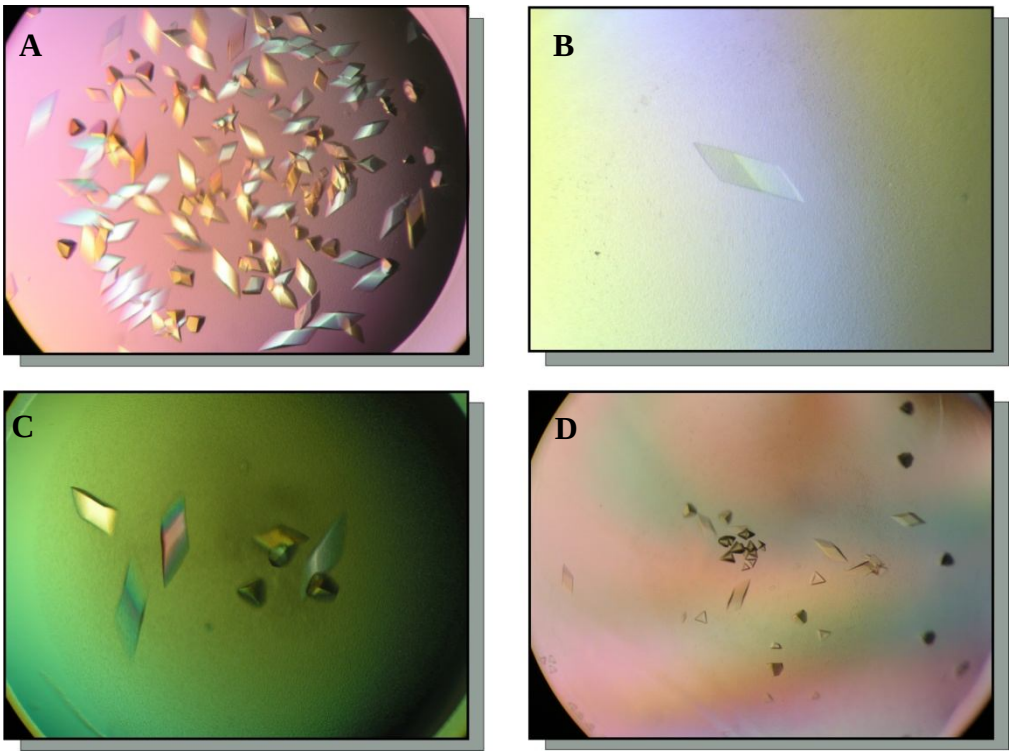


**Figure 6.3: Crystallization of CI with Fab 31A8.**

The CI/Fab 31A8 co-complex was crystallized under standard conditions for the crystallization of the native complex. A: hanging drop, 24-well plate scale - 7% PEG 3350, 40 mM calcium acetate, 12% glycerol, pH 7.3; B: sitting drop, nanoliter scale - 7% PEG 3350, 40 mM calcium acetate, 12% glycerol, pH 7.3 + 10 mM urea; C: hanging drop, 24-well plate scale - 8% 3350, 40 mM calcium acetate, 12% glycerol, pH 7.3; D: sitting drop, 24-well plate scale - 8% 3350, 40 mM calcium acetate, 12% glycerol, pH 7.3.

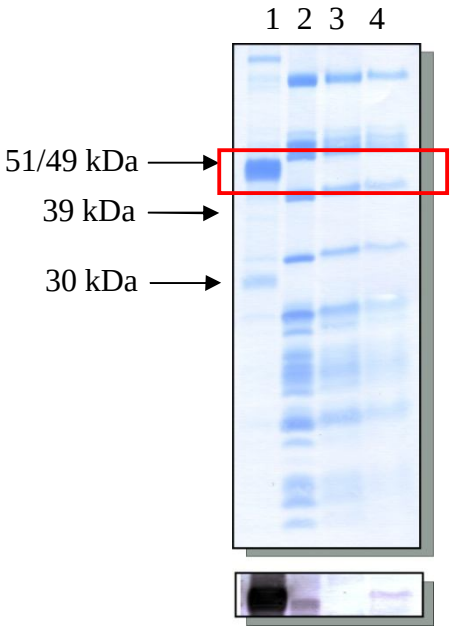


**Figure 6.4: Verification of the CI/Fab 31A8 co-complex crystals.**

Upper panel: 10% SDS-PAGE; lower panel: developed Western membrane; non-reducing conditions. 1: Fab 31A8, 2: CI/Fab 31A8 co-complex sample after gel filtration; 3: dissolved CI crystals (Fig 6.3A); 4: CI/Fab 31A8 sample dissolved crystals.

The signal for the Fab fragments in the dissolved crystals was even less pronounced (Figure 6.4, lane 4). This indicated that the binding of the antibody fragment to the antigen was negligible and most probably the Fab did not participated in the crystal contacts formation. The detected antibody domains could be present in the aqueous regions within crystal lattice. As speculated earlier in this work, the antigen binding region was most likely disrupted during the proteolytic digestion procedure using the immobilized papain. Furthermore, the crystals presented in the Figure 6.3 were analyzed by means of x-ray crystallography at the ESRF in Grenoble, beam line ID14. The crystallographic characteristic of the crystals were identical to those obtained for complex I without bound antibody fragments (data not shown).

## *6.2 CI/Fab 44G10 CO-COMPLEXES CRYSTALLIZATION*

The Fab fragment of the antibody 44G10, as well as its co-complex with complex I was prepared according to the procedure described in 5.2. The Fab fragment 44G10 was shown to bind tightly to the purified complex I. The crystallization sample was prepared in a dilution buffer containing 0.015% $C_{12}E_9$ and 0.4% Cymal4 ™/phosphocholine or 0.4% Cymal4™/DQA. An extensive screening for suitable crystallization conditions was performed for the prepared sample. The crystallization robots Mosquito™ (TPP Labtech) and Cartesian MicroSys™ (Genomic Solutions) were employed for high throughput screening of ~1200 commercially available crystallization solutions (listed in Materials and Methods section). Crystallization was performed at 18 °C and 4 °C for the sample at a concentration of 35 mg/ml.
In the 4 °C setups amorphous precipitate was much more abundant in comparison to the crystallization plates that were prepared and incubated in 18 °C.

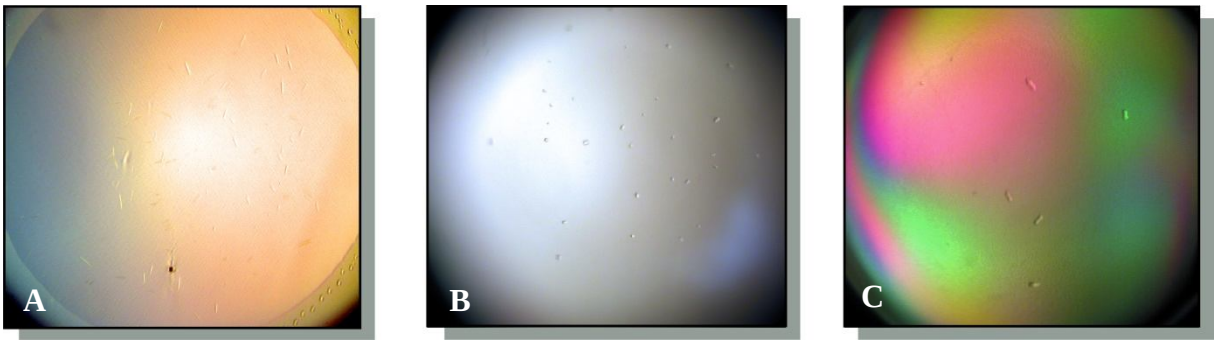


**Figure 6.5: Initial crystallization results for CI/Fab 44G10 co-complex.**

A: 18% PEG 400, 0.1 M MES pH 6.5, 0.1 M $MgCl_2$; B: 2 M $MgCl_2$, 0.1 M Bicine pH 9.0; C: 30% [w/v] PEG 4000.

For three out of more than thousand tested crystallization solutions small crystals could be observed after 24 hours from setting the drops (Figure 6.5). Self-designed crystallization buffers, based on the initial screening procedure, were prepared for optimization and scale-up of the results. Only in case of the solution 18% PEG 400, 0.1 M MES pH 6.5, 0.1M $MgCl_2$ it was possible to grow crystals at the 24-well scale. Nonetheless, the crystals shown in Figure 6.5 A were proven to be Ugp1p crystals (see 10, page 80). It is likely, that the crystals presented in Figure 6.5 C were PEG crystals. Reproducible crystals of CI/Fab 44G10 co-complex at the 24-well plate scale were observed for the standard conditions used for crystallization of the un-complexed enzyme (8% PEG 3350, 40 mM calcium acetate, 12% glycerol, pH 7.3). In comparison to complex I crystals, the co-complex crystals were much smaller and not well defined (Figure 6.6 A). In order to improve crystal quality, phosphocholine (PC) was directly added to the crystallization samples. Upon addition of ~10-20 molecules of PC per complex I particle, no difference was observed between the co-complex crystals and those of complex I alone. When ~ 30 molecules of PC/CI were added, the resultant crystals were smaller and irregular (Figure 6.6). Further addition of lipids abolished crystallization and only heavy precipitate was observed in the setups regardless of the pH used. Subtle changes of the PEG concentration in the crystallization sample and/or bottom solution were used in the following screening procedure. To influence the nucleation process, the co-complex crystallization sample was mixed with the precipitant solutions (7-8% PEG 3350, 40 mM calcium acetate, 12% glycerol, pH 7.3) and placed over wells containing buffers with increasing concentration of PEG (7-10%).

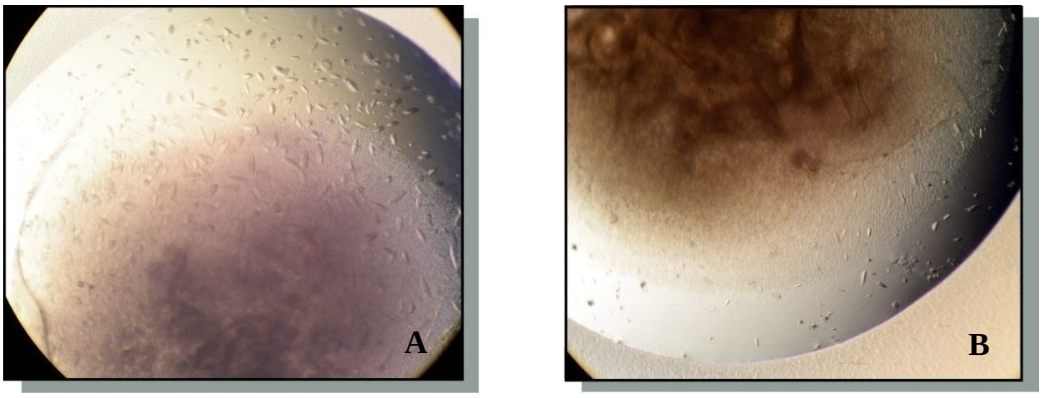


**Figure 6.6: Influence of lipids on the crystallization of a CI/Fab 44G10 sample.**

A: CI/Fab 44G10 co-complex crystals grown from 8% PEG 3350, 40 mM calcium acetate, 12% glycerol, pH 7.3; B: CI/Fab 44G10 co-complex crystals grown from 8% PEG 3350, 40 mM calcium acetate, 12% glycerol, pH 7.3, where ~ 30 PC molecules/CI were added to the crystallization sample.

Although an extensive screening procedure was applied in search for suitable crystallization conditions for the Fab 44G10 co-complex of complex I, it was not possible to grow crystals of satisfying quality. It is likely that the Fab fragment 44G10 has a detrimental influence on the crystallization of complex I. Even if the antibody fragment represents only a twentieth of the complex I mass, it may greatly influence the formation of crystal contacts. In the case of the CI/Fab 44G10 co-complex, it seems that the Fab fragments introduced significant disorder into the system and as a result impeded the crystallization process.

## *6.3 CI/Fab 1F5 CO-COMPLEXES CRYSTALLIZATION*

### *6.3.1 Initial crystallization conditions*

CI/Fab 1F5 co-complex was prepared and purified according to the technique described in 5.1. Using SDS-PAGE and Western blotting it was shown that the 1F5 antibody fragment formed a stable co-complex with complex I. The CI/Fab co-complex crystallization sample was prepared in a buffer containing 0.015% $C_{12}E_9$ in addition to 0.2% Cymal 4™/0.072% PC or 0.12% Cymal 5™/0.072% PC. The initial crystallization conditions were based on the standard complex I crystallization buffers and the experiments were carried out at 18 $^{o}$C. The characteristics of the crystallization sample and the growth conditions are summarized in Table 6.1. The sample remained soluble at 10 mg/ml for all tested buffers. At a concentration of 20 mg/ml small crystals grew in the wells where the PEG 3350 concentration was more than 10%. The largest crystals grew at a sample concentration of 35 mg/ml during the third day after setting the drops and achieved their maximal size by the sixth day. It seemed, that the equilibration took place very fast resulting in large crystals (up to 1 mm) of miscellaneous forms independent of the system used (hanging/sitting drop) (Figure 6.7). Use of Cymal 5 instead of Cymal 4 resulted in crystals of similar appearance. Western blot analysis proved the presence of Fab fragments in re-dissolved crystals. The crystals were cryoprotected by sequential transfer into growth buffers with increasing concentrations of glycerol (20%, 25%, 30% glycerol) and were finally shock frozen in liquid nitrogen or liquid propane. Data collected at the ID14 beamline at the ESRF in Grenoble, France, did not reveal any significant difference between the data qualities of the crystals frozen using either method. At low temperatures the crystals diffracted X-rays up to a resolution of 15 Å. When removed from the cryo-stream, the crystals annealed rapidly and no diffraction pattern could be observed. The following crystallization buffers were preselected for further screening procedure:

* 9% PEG 3350, 10% glycerol, 100 mM sodium potassium phosphate, pH 5.2

* 8% PEG 3350, 12% glycerol, 40 mM calcium acetate, pH 7.3

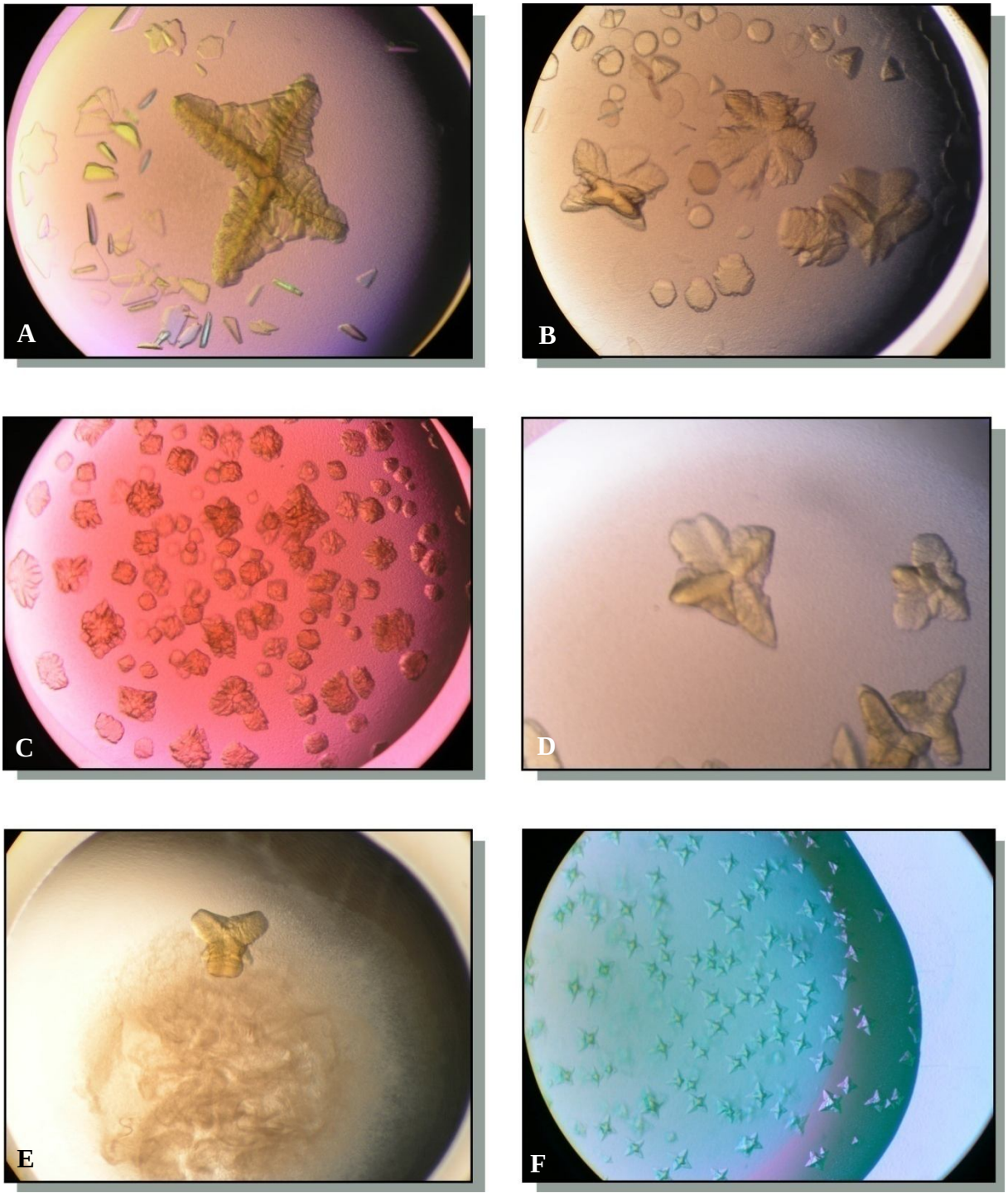


**Figure 6.7: Initial crystals of CI/Fab 1F5 co-complex.**

**A**: 10% PEG 3350, 10% glycerol, 100 mM sodium potassium phosphate, pH 5.2, drop 2µl (1+1); **B**: 11% PEG 3350, 10% glycerol, 100 mM sodium potassium phosphate, pH 5,2; **C**: 10% PEG 3350, 10% glycerol, 100 mM sodium potassium phosphate, pH 5.2, drop 2+1; **D**: 10% PEG 3350, 12% glycerol, 100 mM lithium acetate, pH 7.8; **E**: 8% PEG 3350, 12% glycerol, 40 mM calcium acetate, pH 7.3; **F**: 9% PEG 3350, 12% glycerol, 100 mM magnesium formate, pH 5.9.

| **Sample characteristic** | |
|---|---|
| Protein concentration | 10, 20 and 35 mg/ml |
| Phospholipid content | nmol /mg co-complex |
| Native lipids | 162 |
| Added lipids | 55 |
| Total | 217 |
| Specific activity | µmol $min^{-1}$ $mg^{-1}$ |
| NADH:HAR oxidoreductase | 61 |
| dNADH:DBQ oxidoreductase | 3.5 |
| **Crystal growth conditions** | |
| Temperature | 18 $^{o}$C |
| System | Vapor diffusion, hanging and sitting drop |
| Drop volume | 1-3 µl |
| Reservoir volume | 1 ml |
| Detergent | 0.015% $C_{12}E_9$ |
| Additive | 0.2% Cymal 4/0.072% PC<br>0.12% Cymal 5/0.072% PC |

Table 6.1: Characteristics of CI/Fab 1F5 crystallization samples after initial screening.

### *6.3.2 Optimization of crystallization conditions*

#### 6.3.2.1 Additive screen

As the obtained crystals appeared in irregular shapes, the optimization procedure was aimed at growing crystals in regular forms. The crystallization conditions selected from the initial experiments were employed for an additive screen (Hampton Research). The sample characteristics were similar to those presented in Table 6.1. Use of sitting and hanging drop systems had little or no effect on the crystallization results. Upon addition of salts (10 mM), only amorphous precipitate was observed in all wells. 10 mM phenol promoted growth of rock-like crystals, in contrast to a different dissociating agent, dimethyl sulfoxide (3%) which resulted in precipitation of the protein. Linkers generally abolished formation of crystals. Addition of 10 mM urea amounted in growth of large irregular crystals.

For the oxidized, but not for the reduced form of L-glutathione crystals of flower- and rock-like shapes could be observed. Non detergent sulfobetaines (NDSB) caused protein precipita-

tion. Heavy precipitate was observed in wells where detergents like LDAO or n-octyl-β-D-glucoside were used as an additive. When non-volatile organic compounds were included in the crystallization buffer, this led to sample precipitation. In contrast, addition of volatile organic compounds such as acetone (4%) or 1,4-dioxane (3%) promoted formation of single, large crystals. The experiments were easily reproducible, but the presence of the additives in the crystallization buffers did not influence the form of the crystals, which were similar to those obtained without additives (Figure 6.8).


**Figure 6.8: Crystallization of CI/Fab 1F5 co-complex in presence of additives.**

The crystals grew in hanging drops at 18 °C from 8% PEG 3350, 10% glycerol, 100 mM sodium potassium phosphate, pH 5.2, supplemented with additives: A: 3% 1,4-dioxane; B: 4% acetone; C: 0.12% Cymal 5.

#### 6.3.2.2 Oils in crystallization of CI/Fab co-complexes

Judging from the irregular forms and size, the CI/Fab 1F5 crystals grew too fast. Oils were employed during crystallization of the co-complexes to reduce the growth rate and to control the nucleation process. In the microbatch experiments using the 72 well Terasaki plates (Hampton Research) heavy whitish precipitate was observed in all wells. The experiments were performed at 18 °C. Presence of oils in the setups abolished crystallization, regardless of the oil type and volume. The results were similar when crystallization was carried out in 96 Well IMP@CT™ plates (Greiner Bio-One), with controlled-evaporation-rims, filled with crystallization buffer. Furthermore, introduction of an oil layer into standard vapor diffusion experiments, where the protein drop was not in contact with the oil, caused formation of a similar precipitate. Most likely the oils interfered with detergents present in the protein drop and/or glycerol present in the crystallization buffers. To sum up, addition of oils was not suitable for crystallization of CI/Fab co-complexes.

### 6.3.2.3 Seeding

In order to obtain CI/Fab 1F5 crystals of a better quality seeding experiments were performed in three variants described in 13.9.6. Both, sitting and hanging drop systems were tested. In the seeding experiments, self-nucleated crystals appeared already after several hours independent of the seed stock dilution used. The quality of the crystals was similar to those observed under standard conditions.

### 6.3.2.4 Lipids and the crystals quality

A strict relationship between the crystals' quality and the amount of the native lipids[1] was observed for the CI/Fab 1F5 co-complex. It was possible to grow crystals from 8% PEG 3350, 10% glycerol, 100 mM sodium potassium phosphate, pH 5.2 in a reproducible manner at 18 $^{o}$C. However, the best quality crystals originated from preparations, where the amount of lipids[1] was around 150 nmol lipids/mg co-complex (Figure 6.9).

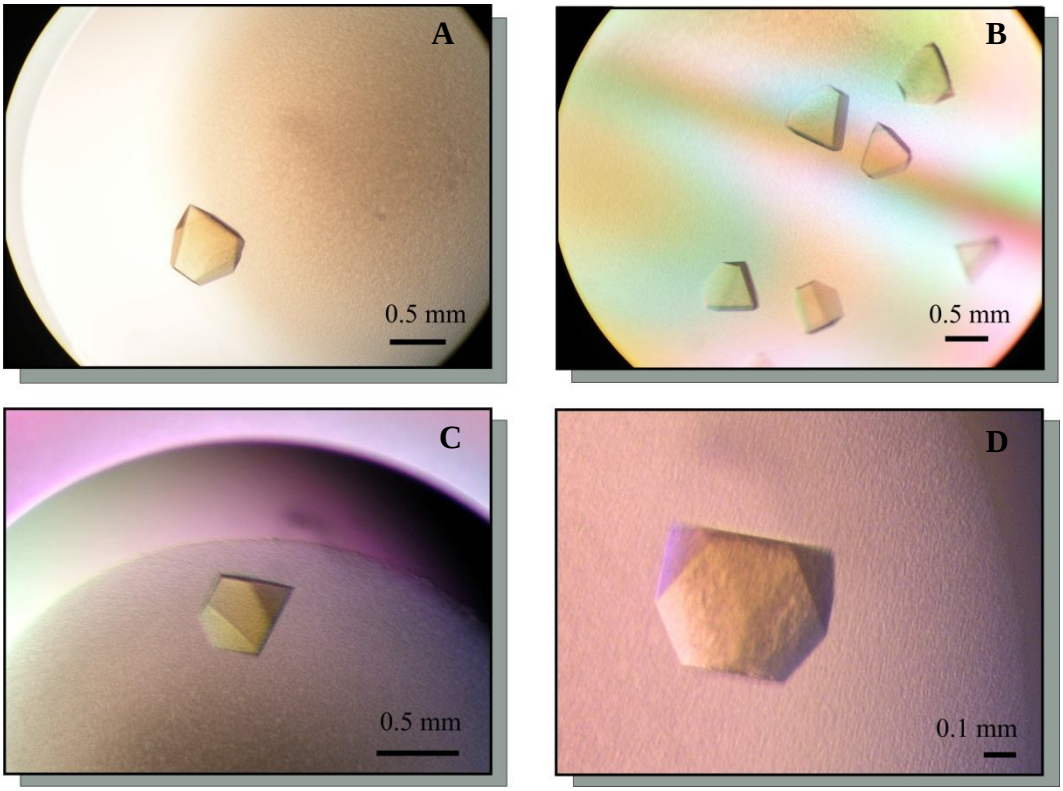


**Figure 6.9: High quality crystals of the CI/Fab co-complex.**

The crystals grew from 8% PEG 3350, 10% glycerol 100 mM sodium potassium phosphate, pH 5.2, in hanging drops (A, C, D) and sitting drops (B). The crystallization sample contained ~ 150 nmol PC/mg co-complex what was a quality-determining factor.

[1] Determined by malachite green assay described in 13.6.9.

Single, large (~ 0.4 x 0.4 x 0.3 mm) and regular crystals appeared after 24 hours and achieved their maximum size by the fifth day after setting the drops. Generally, the crystals grew more eagerly in the sitting drop setups, although they were smaller and rarely only a single crystal was formed. The hanging drop setups, on the other hand, yielded large, single crystals. Preparations where the phospholipid content was below 110 nmol /mg co-complex did not crystallize. In case of the co-complex crystals from batches with more than 190 nmol phospholipids/mg co-complex grew as irregular forms of non-satisfying quality. The amount of the native lipids depended strongly on the purification procedure, and was not easily predictable or controllable. If a batch of complex I had a low lipid-content, external PC was added to balance the difference. The degree of delipidation correlated with the amount of detergent molecules per complex I during the $Ni^{2+}$-NTA affinity as well as size exclusion chromatography. The differences in the sample characteristics are obvious from comparing Table 6.1 and Table 6.2. First of all, the amount of total lipids was significantly higher for the initial conditions. Secondly, although the amounts of native lipids were the same, the specific dNADH:DBQ oxidoreductase activity was almost two times higher for the sample giving rise to high quality crystals, when comparing to the initial crystals.

#### 6.3.2.5 Temperature

Without doubt, the lipid content played a key role in the crystallization of the CI/Fab 1F5 co-complex. Temperature appeared to be second important factor. Interestingly at 18 $^{o}$C, CI/Fab 1F5 high quality crystals grew readily from 8% PEG 3350, 10% glycerol 100 mM sodium potassium phosphate, pH 5.2 but not 8% PEG 3350, 12% glycerol, 40 mM calcium acetate, pH 7.3. The situation was opposite at 10 $^{o}$C, where large, high quality crystals grew generally from the acetate buffer conditions.

#### 6.3.2.6 Crystal growth using pH gradient

It was possible to grow CI/Fab 1F5 crystals using pH gradient[2]. When the phosphate buffer was used (8% PEG 3350, 10% glycerol 100 mM sodium potassium phosphate, pH 4.5) the CI/Fab 1F5 crystals, although under heavy precipitate, were similar to these obtained, when grown in constant pH conditions (Figure 6.10 A). The same experiments conducted with calcium acetate buffer (6% PEG 3350, 12% glycerol, 40 mM calcium acetate, pH 6.0) resulted in growth of irregular crystals (Figure 6.10 B). No crystals were observed, when the protein was mixed with crystallization buffer containing PEG 3350 at concentration lower than 7%.

[2] Technique described in 13.9.2.5

| **Sample characteristic** | |
|---|---|
| Protein concentration | 35 mg/ml |
| Phospholipid content | nmol/mg co-complex |
| Native lipids | 148 |
| Added lipids | 0 |
| Total | 148 |
| Specific activity | µmol $min^{-1}$ $mg^{-1}$ |
| NADH:HAR oxidoreductase | 66 |
| dNADH:DBQ oxidoreductase | 6.8 |
| **Crystal growth conditions** | |
| Temperature | 18 °C |
| System | Vapor diffusion, hanging and sitting drop |
| Drop volume | 1-3 µl |
| Reservoir volume | 1 ml |
| Detergent | 0.015% $C_{12}E_9$ |
| Additive | 0.2% Cymal 4/0.072% PC |
| | 0.12% Cymal 5/0.072% PC |

Table 6.2: Characteristics of a CI/Fab 1F5 crystallization sample yielding high quality crystals.

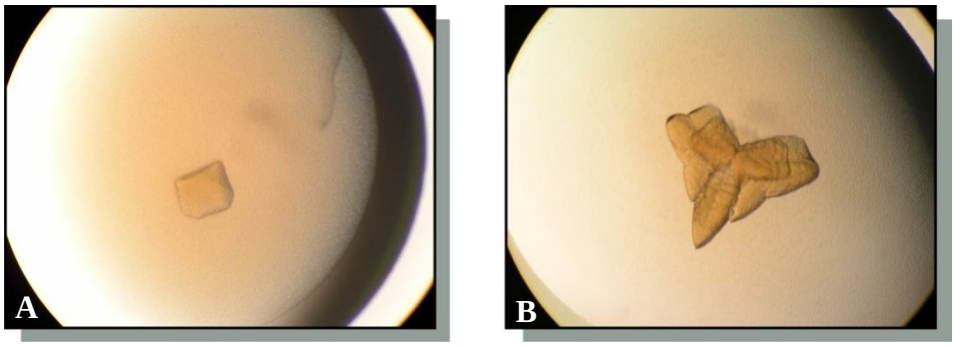


**Figure 6.10: Growth of CI/Fab 1F5 crystals under pH gradient conditions.**

A: Reservoir solution: phosphate buffer, pH 4.5, Drop solution: phosphate buffer, pH 5.2; B: Reservoir solution: acetate buffer, pH 6.0, Drop solution: acetate buffer, pH 7.0.

### 6.3.2.7 Dehydration of co-complex crystals

The aim of the dehydration experiments was to improve the diffraction properties of the co-complex crystals. Due to the fragility and temperature-sensitive nature of the co-complex crystals[3], the trials were performed at 10 $^{o}$C. As revealed by microscopic inspection, the crystals exposed to the dehydration solution for more than two hours suffered from dehydration damage. Crystals not displaying any signs of damage (dehydrated for 1,5 hours) were frozen in liquid nitrogen at 20 minutes intervals in the absence of additional cryoprotectant. When measured at the ESRF in Grenoble, France, the dehydrated crystals did not diffract x-rays. This was most likely due to excessive water removal and collapse of the crystals packing. An alternative to this experiment, would be controlled dehydration by means of a humidity chamber as the one described by Reiner Kiefersauer et al,. [98].

### 6.3.2.8 Soaking of the co-complex crystals in $Ta_6Br_{12}^{2+}$

The CI/Fab 1F5 crystals remained stable upon soaking in $Ta_6Br_{12}^{2+}$ solution. The compound was added to the drops containing crystals either as a solid (a couple of crumbs added directly to the drop) or as 10 mM solution in water. Microscopic inspection of the crystals did not reveal any cracks or damage after 24 hours incubation. An example crystal was measured at the ESRF in Grenoble, France. Unfortunately, no diffraction pattern was observed for this particular crystal. As the crystal was already over one month old, this might have been the reason for lack of diffraction. The experiments will be repeated with freshly grown crystals.

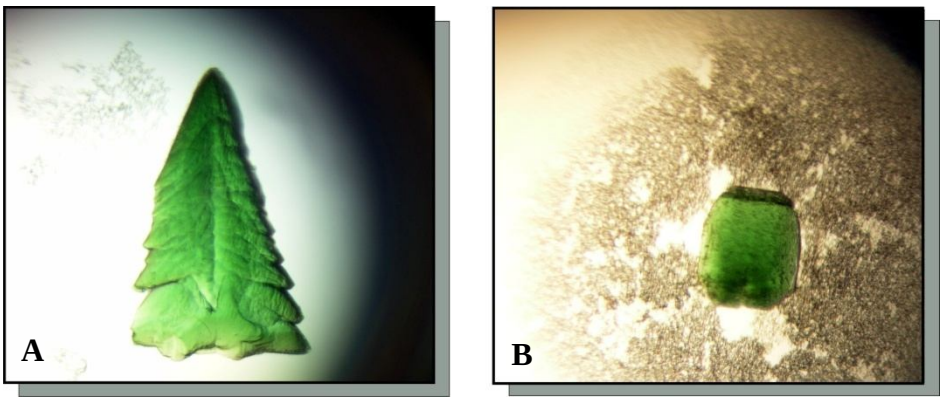


**Figure 6.11: CI/Fab 1F5 co-complex crystals after soaking in $Ta_6Br_{12}^{2+}$.**

A: Crystal grew from 11% PEG 3350, 12% glycerol, 40 mM calcium acetate, pH 7.3 with 0.12% Cymal 5 as additive. B: Crystal grew from 19% PEG 3350, 12% glycerol, 40 mM calcium acetate, pH 7.3 with 0.12% Cymal 5. The crystals were soaked in 10 mM $Ta_6Br_{12}^{2+}$ for 24 hours at 10 $^{o}$C.

[3] The CI/Fab 1F5 crystals melted fast when exposed to air at room temperature.

### *6.3.3 Diffraction of CI/Fab 1F5 crystals*

The screening of the CI/Fab 1F5 co-complex crystals was performed at the ESRF beamline ID 14-2 in Grenoble, France, whereas the data sets were collected at the Swiss Light Source, beamline PXII in Switzerland. The best crystals diffracted X-rays to below a resolution of 7 Å. It was possible to collect a data set composed of 600 diffraction images from a single crystal without significant loss in data quality. An example diffraction image is depicted in Figure 6.12. Data collection parameters are summarized in the Table 6.3. The images were processed with the HKL suite package (Otwinowski, Minor). The preliminary results suggest that the crystal lattice is of the cubic type and display space group different from the one observed for native crystals.

| Data collection parameters | |
|---|---|
| Detector | MAR 225 mm CCD |
| Wavelength | 0.99187 Å |
| Detector to crystal distance | 700 mm |
| Oscillation range | 0.3˚ |
| Oscillation start | 0˚ |
| Beam centre | x 103 y 112.1 |

Table 6.3: Parameters of the data collection for a CI/Fab 1F5 crystal.

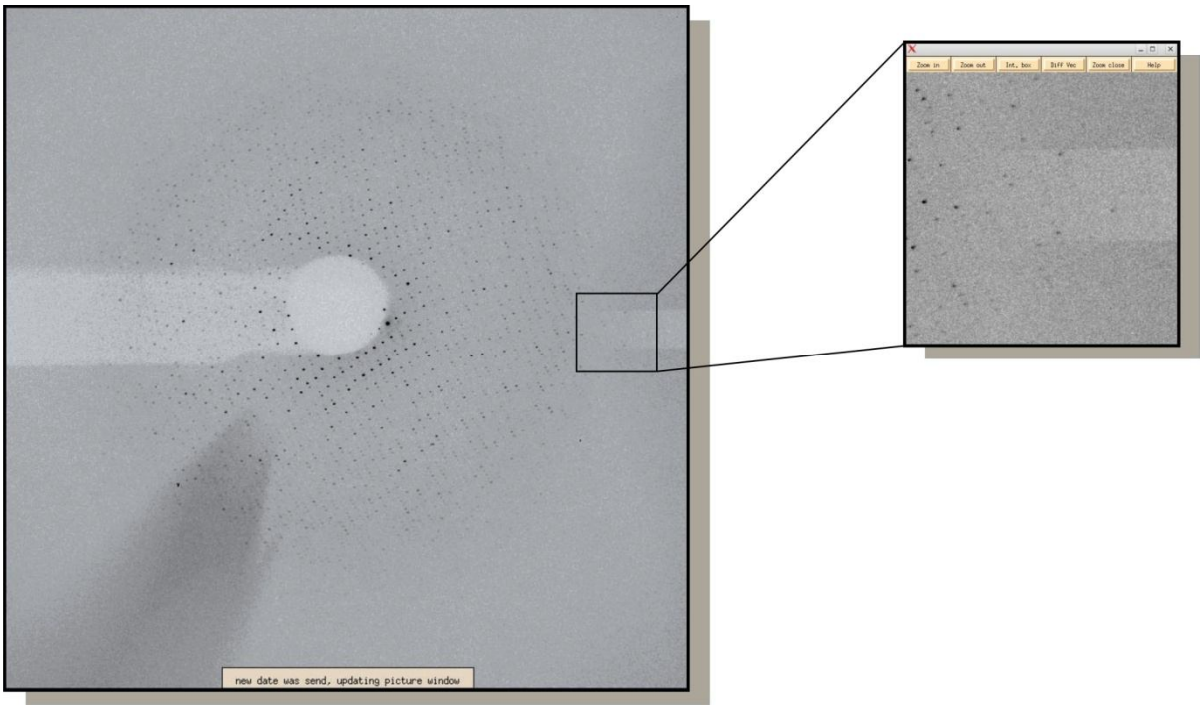


**Figure 6.12: Diffraction image of CI/Fab 1F5 co-complex crystal.**

The X-ray diffraction data were collected at the Swiss Light Source, beamline PX II. The crystal diffracted X-rays to a resolution of 7.2 Å. The shadow present on the image resulted from a detector defect, and at this stage was of a minor significance.

The unit cell dimensions calculated from indexing of the images with DENZO (HKL package) seem to be as follows: a = 471 Å, b = 471 Å, c = 472 Å, $\alpha = 90^{\circ}$, $\beta = 90^{\circ}$, $\gamma = 90^{\circ}$. Such an extremely large volume of the primitive cell is rarely seen for the protein crystal systems, but common for ribosomes [99]. Another interesting observation concerns the reflections, which lay in a close neighborhood to each other. This may be explained by the large unit cell dimensions. In order to address these questions, further processing of data and optimization of the crystal quality is required.

# Part I-Discussion

Structure of complex I

Generation of antibody Fab fragments

Purification of CI/Fab co-complexes

# 7 SOLVING THE X-RAY STRUCTURE OF MITOCHONDRIAL COMPLEX I

Until recently the structural information on complex I was derived mainly from electron microscopic studies [6;100-102]. Electron microscopic (EM) reconstruction of the *E. coli* complex I showed that the peripheral and the membrane arms are connected via a thin junction [3]. The peripheral arm of the bacterial enzyme was crystallized and a partial X-ray structure of the complex I from *Th. thermophilus* was solved [37]. Although the prokaryotic protein represents the minimal model of complex I, the peripheral arm structure from *Th. thermophilus* does not answer the key questions regarding the energy coupling. The available structural information on the membrane arm is very limited and the proton pumping mechanism has not been elucidated yet. The architecture of complex I has also been addressed using methods, such as studies of subcomplexes [25], site directed mutagenesis [103;104] and structure prediction. The tremendous structural and functional complexity of the enzyme is mirrored by extreme difficulties with its purification and crystallization. The L-shaped protein displays significant internal flexibility including bending motions of the peripheral and the membrane arm and other possible functional conformational changes [6]. This renders generation of high quality crystals diffracting to high resolution difficult, if not impossible. Nevertheless, a high resolution X-ray structure of the holoenzyme will be prerequisite for understanding the molecular machinery of the energy coupling by complex I. A well established purification protocol of *Y. lipolytica* complex I yields a highly pure and active enzyme in quantities suitable for crystallization attempts (protocol modified after [105]). In contrast to the bacterial enzyme, complex I from *Y. lipolytica* is very stable and crystallizes as a holocomplex. However, the quality of the native protein crystals is limited.

The role of antibody fragments as tools for structural studies has become increasingly important over recent years. Following the successful cases of the cytochrome *c* oxidase from *P. denitrificans* [61;68], cytochrome $bc_1$ complex from *Saccharomyces cerevisiae* [60], human β2 adrenergic G-protein coupled receptor [67] and KcsA $K^+$ ion channel from *Streptomyces lividans* [85], attempts were undertaken to apply the antibody fragment-mediated crystallization for complex I structural characterization.

## *7.1 PREPARATION OF HOMOGENOUS Fab FRAGMENTS*

Preparation of highly pure Fab fragments of IgG molecules suitable for crystallization trials was one of the important parts of this project. After a set of proteolytic enzymes and different fragmentation conditions were tested, an immobilized papain-based protocol was developed. Since the first reports in the late fifties [106] generation of antibody fragments by proteolytic digestion of γ immunoglobulins become a standard technique [107;108]. The mechanism of fragmentation by means of diverse proteolytic enzymes has been studied for antibodies from different species. Nevertheless, preparation of homogenous Fab fragments is not straightforward and has to be optimized separately for each antibody. Papain is a thiol protease with broad substrate specificity, which can give rise to undesired heterogeneous fragments. Variable digestion of the IgG molecule in the hinge region results in a mixture of Fab and Fab' fragments. The latter contains an additional small portion of the heavy chain constant domain. In some cases the impurity represented by this extra portion may disturb crystallization, while in other cases it may play an insignificant role. For example, the Fab fragment and the ten amino acids longer Fab' fragments from human myeloma IgG1 proteins were crystallized. Identical crystalline forms and diffraction patterns were observed, regardless of the size of the proteolytic fragment [109]. On the other hand, it can be anticipated, that the presence of oligosaccharides (derived from the Fc part heavy chain) in the Fab' fragment may introduce a significant inhomogeneity and abolish crystallization.

During the initial crystallization of the CI co-complexes, an un-purified papain digestion mixture was used as a source of Fab fragments. The resultant crystals were of low quality and difficult to reproduce. The most important step in the preparation of Fab fragments was separation of the un- and partially digested antibodies. Although whole antibody molecules were crystallized and their X-ray structures were solved [110-112], the flexibility in the hinge region is detrimental for crystallization. Furthermore, the bifunctionality of the un- and partially digested antibodies is undesired in crystallization experiments, since it introduces a pronounced inhomogeneity to the sample. With a size exclusion column having a separation range of 3-70 kDa it was not possible to resolve fragments with a mass difference smaller than 1 kDa. In order to separate proteolytic fragments with small mass differences, preparative isoelectric focusing (IEF) could be employed. Crystallization trials of the CI/Fab 1F5 co-complex included Fab fragments derived from a Protein G purified papain digest. The undigested and partially digested antibody fragments ($F(ab)_2$ or $F(ab')_2$) were separated from the mixture using gel filtration. A second round of size exclusion chromatography was employed

to achieve the highest possible purity of the sample. This procedure ensured production of homogenous Fab fragments as judged from size exclusion chromatography and SDS PAGE (Figure 3.18)

It has also been shown, that the mouse IgG subclasses display variable susceptibility to papain or pepsin [107;113;114]. The mouse IgG1 subclass exhibits the highest resistance to papain and the presence of 10 mM cysteine is necessary for Fab formation. Results of liquid chromatography-electrospray ionization mass spectrometry (LC/ESI-MS) of IgG1 papain digest indicated a two-step fragmentation mechanism [115]. During the first step IgG1 is cleaved to $F(ab')_2$ and Fc fragments. In the second stage, thiol reduction of the interchain disulphide bonds in the hinge region is crucial in the formation of the Fab fragments. The same study revealed that, the subclass IgG2a was easily cleaved to Fab and Fc fragments in the absence of cysteine.

The antibodies used in this project belonged to the subclass IgG1 (31A8 and 44G10), and to the subclass IgG2a (1F5). SDS-PAGE and gel filtration showed different papain–sensitive sites for all three monoclonal antibodies used. The largest Fab fragment (~50 kDa) resulted from fragmentation of the 44G10 antibody. Though the elution profile of Fab 44G10 was represented by a single, uniform peak, a double band in the region of 50 kDa was observed by SDS-PAGE (Figure 3.18). After incubation with complex I and subsequent size exclusion chromatography only the polypeptide corresponding to the upper band did bind to complex I and was detected in the co-complex, by Western blot (Figure 5.4). Most probably, proteolytic digestion produced two isoforms of Fab fragments, where only one (the upper one) possessed the ability to bind the antigen. The Fc fragment was removed from the sample during the Protein G affinity chromatography and could not account for the polypeptide represented by the lower band.

Antibody Fab 31A8 released the smallest Fab fragment (~ 46 kDa) compared to the 1F5 and 44G10. Interestingly, this fragment dissociated easily into light and heavy chain when incubated in SDS under non-reducing conditions. This indicated low stability, or even loss of native conformation which in turn may explain negligible binding to complex I. The affinity of 31A8 Fab fragments towards the antigen was almost undetectable in the SPR experiments confirming the binding data, where the Fab fragment could be separated from complex I on a gel filtration column. It was concluded, that the antigen binding site was most probably damaged during papain digestion.

Fragmentation of immunoglobulin 1F5 produced Fab fragments (~ 48 kDa), which appeared to be the most useful ones. Dissociation into light and heavy chain was minor (Figure 3.18)

and at the same time the affinity towards the antigen (measured using SPR) was the highest among analyzed Fab fragments. This fragment was successfully employed in co-crystallization trials with complex I.

## *7.2 Fab-MEDIATED CRYSTALLIZATION OF COMPLEX I*

The first co-crystallization experiments of complex I were carried out in the presence of Fv fragments. The recombinant Fv fragments of antibodies 31A8 were produced in the bacterial periplasm. Using Western blot it was shown that the Fv fragments formed a stable co-complex with complex I. Nevertheless, low yield of the bacterial expression was the limiting factor in the co-crystallization attempts [116]. Moreover under the tested conditions, no improvement in the crystal quality upon Fv binding was observed (Zickermann unpublished). Most probably the extra hydrophilic portion delivered by the Fv fragments was too small for formation of new crystal contacts. The Fv fragments represent the smallest portion of an immunoglobulin, which possess antigen binding ability, but the mass is roughly 30-40 times smaller than that of complex I.

The aim of this project was co-crystallization of complex I with proteolytic Fab fragments and structural characterization of the co-complexes. The monoclonal antibodies used for preparation of the fragments bind different epitopes within the complex I membrane arm at the intermembrane space site (Figure 7.1). The epitopes appear to be very attractive for the crystallization experiments, since they offer formation of possible crystal contacts involving the membrane part of the protein. The antibodies 44G10 and 31A8 are Western blot negative and were classified as conformation specific antibodies (Zickermann, unpublished). In contrast, the IgG 1F5 recognizes a linear epitope [17]. The immunoglobulins were digested using immobilized papain to gain Fab fragments, suitable for co-crystallization attempts.

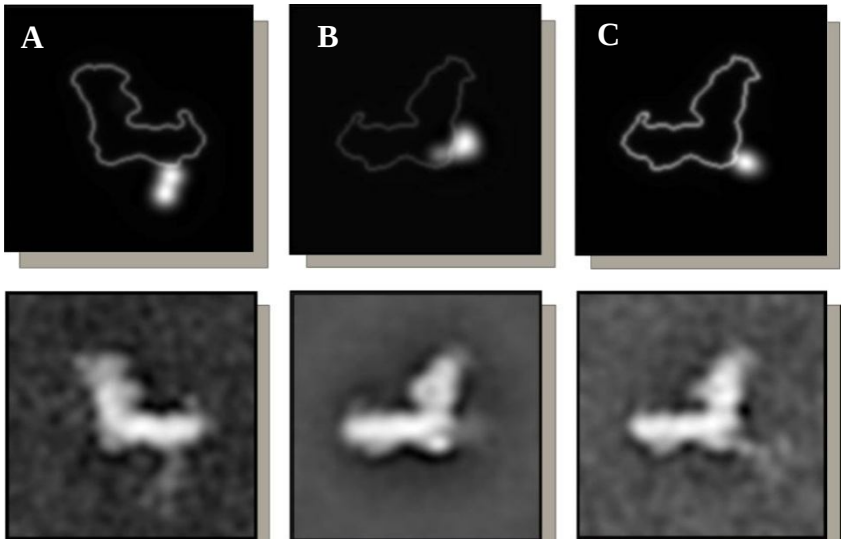


**Figure 7.1: Electron microscopy of complex I from *Y. lipolytica* decorated with monoclonal antibodies (Bostina et al. unpublished).**

The upper images represent average of the statistical analysis of the representations shown in the lower panel images. A: antibody 30C12 binding NESM subunit (analogously to antibody 1F5) [17]; B: conformation specific antibody 44G10. C: conformation specific antibody 31A8.

The major difference to the published co-complexes is the size ratio of the antibody fragment to the antigen. In case of the KcsA potassium channel, the Fab fragment comprises about 2.5 times the mass of the antigen, providing a hydrophilic domain reaching far beyond the detergent micelle and leading to formation of spacious crystal packing. The monomer of complex I from *Y. lipolytica* is roughly 20 times larger than the binding antibody fragment. Nonetheless, it was possible to grow crystals of Fab co-complexes of the NADH:ubiquinone oxidoreductase from *Y. lipolytica*, with X-ray diffraction properties indicating a different space group when compared to the native enzyme.

### *7.2.1 CI/Fab 1F5 crystals*

Data presented in this study suggest that the Fab 1F5 participates in crystal contact formation, since the co-complex crystallized in a space group different to the one observed for the native enzyme under the same conditions. The initial diffraction data suggested even crystal packing of a higher symmetry, when compared to the un-complexed protein. The Fab fragment binds to the NESM subunit in the distal part of the membrane arm. Significant improvement in diffraction quality of the CI/Fab 1F5 crystals was achieved. The initial crystals grown in conditions identical to the native protein diffracted X-rays to a resolution of 20 Å. Use of Fab fragments prepared according to the optimized protocol enhanced crystal quality. Further im-

provements involved optimization of the lipid content of the crystallization sample. Finally, the mentioned procedures together with growth under a pH gradient led to production of crystals diffracting X-rays to a resolution of 7 Å. Nevertheless, further enhancements of the crystal quality will be required in order to obtain structural information.

To this end, screening for better cryoprotection conditions will be employed in ongoing experiments. Preliminary optimization of the cryoconditions indicated that freezing in liquid propane is superior to freezing in liquid nitrogen. An improvement of diffraction limit from 16 Å to 12 Å resolution was observed. However, these results need to be verified, since it is well known that even crystals coming from the same drop may display very different diffraction quality.

For further expansion of the hydrophilic domain, a combinatorial crystallization technique could be considered [117;118]. Attachment of Fab binding domains such as protein L from *Peptostreptococcus magnus* (PpL), protein A from *Staphylococcus aureus* (SpA) and the streptococcal protein G (SpG), would provide an additional hydrophilic part, which in turn could greatly enhance crystallization. The disadvantage of this method could be internal flexibility resulting from the attachment of an extra polypeptide chain. This would be detrimental for crystallization trials.

Employment of a humidity chamber, which allows a controlled dehydration process, seems to be a promising technique for improvement of the diffraction quality of protein crystals [98]. In non-controlled dehydration experiments of CI/Fab 1F5 crystals using high concentrations of polyethylene glycol in the bottom solution a substantial amount of solvent was withdrawn from the crystals. As a result, the crystal lattice was most probably disrupted, since no diffraction pattern was observed when the crystals were measured at synchrotron radiation facility.

Once crystals of higher quality will be obtained, the structural characterization of the co-complexes is expected to be a valuable source of information on the structural architecture and function of eukaryotic complex I.

### *7.2.2 Crystallization with conformation specific antibody fragments*

If possible, co-crystallization with antibody fragments derived from conformation specific antibodies offers a unique approach of trapping a protein molecule in a particular conformational state. In the case of NhaA, a bacterial $Na^+/H^+$ antiporter, conformation specific antibodies were used for functional and structural studies [119]. The pH-mediated regulation of the activity was shown to be accompanied by a conformational change in the hydrophilic amino-terminus. Moreover, antibody 1F6 was shown to bind only to the alkaline state of NhaA

[120]. The crystals of the Fab co-complexes of the *E. coli* NhaA diffracted X-rays to a maximum resolution of 7.9 Å [Venturi, PhD thesis].

In another example HIV gp120 envelope glycoprotein was neutralized with antibodies recognizing the native protein [121]. The Fab fragments were used to identify two molecular surfaces with immunogenic potential, one competitive with the CD4 receptor and the other competitive with the chemokine receptors. A structure of the ternary complex of a partially deglycosylated HIV-gp120 core bound to a two-domain fragment of the CD4 cellular receptor and to Fab fragment against a CD4i (CD4-induced) epitope was solved at 2.5 Å resolution [122]. This work provided evidence for a conformational change upon CD4 binding, the nature of CD4-induced antibody epitope, and a specific mechanism of immune evasion.

Structural studies of the potassium channels using the Fab approach became almost a standard technique in the group of Roderick MacKinnon. In addition to expanding the hydrophilic domain, the antibody fragments were employed for determination of the phases to solve the structures. To address the function of the voltage-dependent KvAP potassium channel from *Aeropyrum pernix,* conformational Fab fragments were attached to the voltage sensor paddles to detect their motions. Combining results from the crystal structure, electrophysiological assays [123;124] and electron microscopic analysis [125] the authors proposed a new model of voltage-dependent gating, where the voltage-sensor paddles move across the membrane carrying the load of gating charges through the electric field [124].

Conformation specific antibodies used in this study (31A8 and 44G10) gave positive signals in the native ELISA test. It is however not known if these antibodies indeed stabilize a specific conformation of the native enzyme. Surface plasmon resonance (SPR) experiments (see 4) show, that presence of NADPH did not influence binding of the antibodies 31A8 and 44G10 to complex I. In contrast, the relative response of antibody 1F5 dropped significantly above NADPH concentrations of 1µM. This suggests that binding of antibody1F5 to the complex I conformation exerted by NADPH is limited. When an ‘aged’ sample of complex I was used in SPR measurements, the affinity of the antibodies 31A8 and 44G10 decreased with time, until it reached a constant value of approximately 70 % of the initial records. This was not the case for antibody 1F5, which affinity towards complex I did not change regardless to the age of the sample. This result correlates with the fact that 1F5, in contrast to the other two antibodies, recognizes a linear epitope within complex I.

Although, various fragmentation methods were employed, it was not possible to generate functional Fab fragments of the antibody 31A8. It was deduced, that the antigen binding site of the IgG 31A8 was distorted during the papain digestion step.

The Fab 44G10 was shown to bind tightly to complex I. Even though an extensive screening (over 2500 conditions at 4 $^{o}$C and 18 $^{o}$C) was carried out, no suitable crystallization conditions were found. The quality of the initial crystals obtained for CI/Fab 44G10 co-complex was not sufficient for crystallographic analysis. It was concluded that the Fab 44G10 fragments had a deleterious effect on the crystallization process. The IgG fragment, which binds possibly to the 39-kDa subunit (Zickermann, unpublished), must impose an unfavorable crystal packing, which abolishes crystallization.

# 8 PRÉCIS

Fab fragments suitable for co-crystallization with complex I were generated using an immobilized papain-based protocol. The binding of the antibody fragments to complex I was verified using Surface Plasmon Resonance and size exclusion chromatography. The binding constants of the antibodies and their respective Fab fragments were found to be in the nanomolar range.
This work presents the first report on successful crystallization of complex I (proton pumping NADH:ubiquinone oxidoreductase) from *Yarrowia lipolytica* with proteolytic Fab fragments. The quality of the crystals was significantly improved when compared to the initial experiments and the best crystals diffracted X-rays to a resolution of ~7 Å. The activity of complex I remained uninfluenced by antibody fragment binding. The initial diffraction data suggest that the complex I/Fab co-complex crystals represent a space group different to the one observed for the native protein. Ongoing experiments are aimed at further enhancements of the diffraction quality of the crystals.
Providing a different space group the CI/Fab co-complexes may become a very useful approach for structure determination of the enzyme. Moreover, the bound Fab offers an additional possibility to generate phase information. The antibody-mediated crystallization represents a valuable tool in structural characterization of the NADH:oxidoreductase subcomplexes or even single subunits.

# Part II-Theoretical introduction

UDP-glucose pyrophosphorylase

# 9 UGP1P –INTRODUCTION

## *9.1 UDP-GLUCOSE PYROPHOSPHORYLASE – THE REACTION MECHANISM*

UDP-glucose pyrophosphorylase (UGP1, Ugp1p, UTP:α-D-glucose-1-phosphate uridylyltransferase, UDPGP, EC 2.7.7.9) catalyzes the $Mg^{2+}$-dependent formation of UDP-glucose and pyrophosphate, from glucose-1-phosphate and UTP [126] (Figure 9.1). The $\Delta G^{\circ\prime}$ of the phosphoanhydride exchange between glucose-1-phosphate and UTP is close to zero. Thus the reaction is thermodynamically readily reversible.

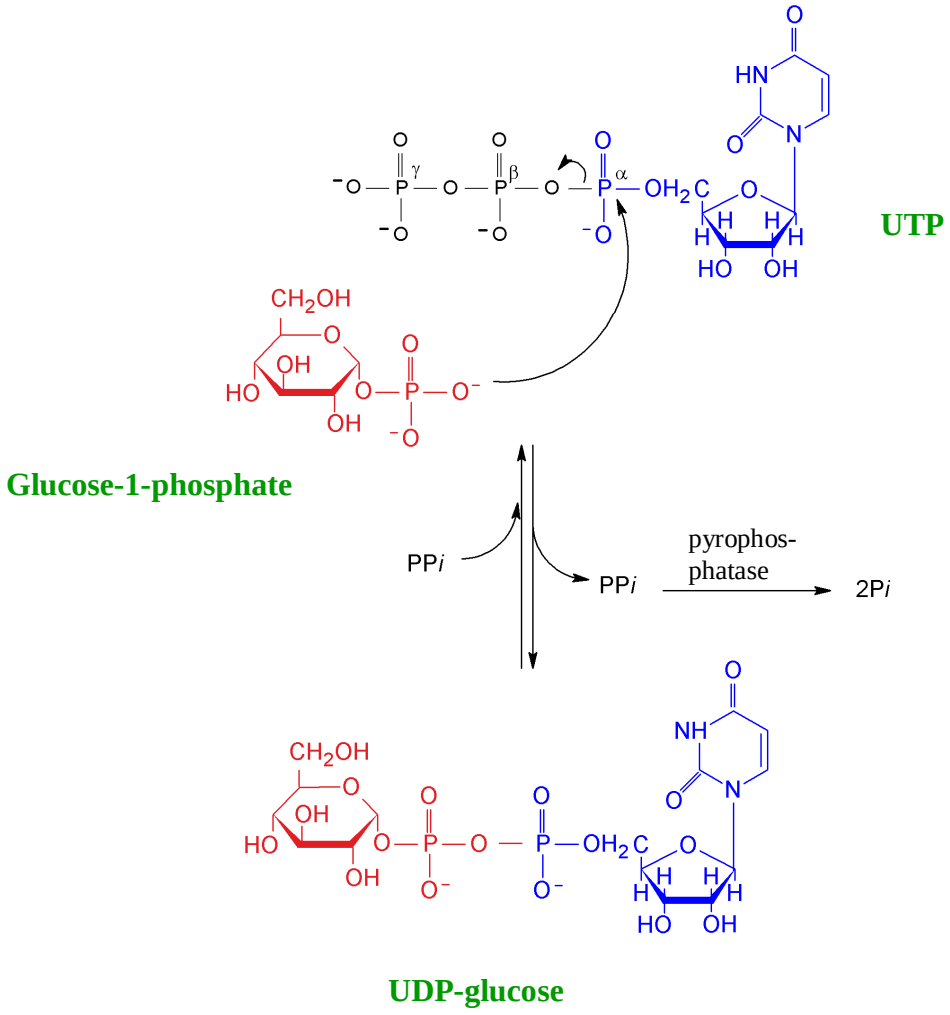


**Figure 9.1: The reaction catalyzed by UDP-glucose pyrophosphorylase.**

In the readily reversible reaction the phosphoryl-oxygen of glucose-1-phosphate attacks the α-phosphorus atom of UTP. As a result, UDP-glucose and pyrophosphate are formed. Pyrophosphatase hydrolyzes the inorganic pyrophosphate in a highly exergonic reaction, which renders the formation of UDP-glucose energetically favorable and physiologically irreversible.

Nevertheless, hydrolysis of the formed PP*i* (pyrophosphate) by the omnipresent inorganic pyrophosphatase is highly exergonic ($\Delta G^{\circ\prime} = -33.5$ kJ*mol$^{-1}$) and as a result the overall reaction of UDP-glucose formation is physiologically irreversible. The reaction kinetics follow an ordered bi-bi mechanism, which involves formation of a ternary enzyme/substrate complex, where the nucleoside phosphate binds prior to pyrophosphate or glucose-1-phosphate [127-129]. A similar uridylyl transfer reaction is catalyzed by galactose-1-phosphate-uridyl-transferase (see following chapter). In contrast to UDP-glucose pyrophosphorylase, the kinetics of this enzyme display double-displacement characteristics (ping-pong kinetics), with participation of a free uridyl enzyme intermediate [130-132]

## *9.2 UDP-GLUCOSE AT THE CROASSROADS OF SUGAR METABOLISM*

The universal distribution of UDP-glucose pyrophosphorylase in nature results from a global need for its major catalysis product UDP-glucose. UDP-glucose represents an activated form of glucose which due to the presence of the high energy bonds can transfer glucosyl units in numerous cellular reactions. In *S. cerevisiae,* UDP-glucose serves as a glucosyl donor for the synthesis of *β*-glucan (1,6-*β*-glucan and 1,3-*β*-glucan), which represents about 55% of the total cell-wall carbohydrates. This polymer is believed to be the key factor in determining the morphology and in maintaining the osmotic integrity of the yeast cells [133]. It was shown, that deletion of the UGP1 gene in *S. cerevisiae*, was lethal for the yeast cells [134]. Additionally, UDP-glucose is involved in trehalose synthesis in yeast. In animal cells UDP-glucose plays an important role in the synthesis of glycogen. Direct polymerization of glucose-1-phosphate units to glycogen under phosphate-release is thermodynamically impossible (positive $\Delta G^{\circ\prime}$). Since the discovery of Luis Leloir in 1957 it is known that glucose can be transferred onto the non-reducing end (atom C4) of the growing glycogen chain only in its activated form, as UDP-glucose. The transfer of glucosyl units of UDP-glucose to the glycogen chain results in formation of α(1→4) gylcosidic bonds and is catalyzed by glycogen synthase. Although the synthesis of glycogen is not exclusively dependent on the activity of UDP-glucose pyrophosphorylase, malfunction of the enzyme may affect polysaccharide levels [135]. In plants, UDP-glucose is an important precursor in the synthesis of sucrose [136] and direct or indirect precursor in the synthesis of cellulose, pectines and hemicellulose [137]. Moreover, in the reaction coupled to ADP-glucose pyrophosphorylase (AGPase) activity, UDP-glucose is directly converted to ADP-glucose, which participates in starch biosynthesis

[138]. The crystal structure of ADP-glucose pyrophosphorylase from potato tuber was solved by Jin *et al.* [139] without substrate and in co-complexes with ADP-glucose and ATP respectively (PDB 1YP2, 1YP3, 1YP4). Recently, a new structure from *Agrobacterium tumefaciens* was deposited in the PDB [140]. In all eukaryotes, UDP-glucose is involved in the synthesis of the carbohydrate moiety of glycolipids and glycoproteins as it participates in the formation of $Glc_3Man_9GlcNac_2$, which is necessary for N-glycosylation of proteins [141] [142]. According to some studies, UDP-glucose may participate in the synthesis of glucomannoproteins, which are present in the yeast cell wall [143]. The role of UDP-glucose in the synthesis of proteoglycans was described by [144]. It was also shown that UDP-glucose pyrophosphorylase is necessary for the production of the capsular polysaccharide, the virulence factor of *Streptococcus pneumonia* [145]. UDP-glucose pyrophosphorylase is also crucial for galactose metabolism. In order to utilize galactose in glycolysis, it has to be converted into glucose, or more precisely to glucose-6-phosphate. The two monosaccharides are epimers with different configuration only at the C4 atom, but the conversion of glucose to galactose is not a simple one step epimerization reaction. It requires the action of four enzymes: galactokinase, galactose-1-phosphate uridylyl transferase, UDP-galactose-4-epimerase and phosphoglucomutase. The so called Leloir pathway is represented schematically in Figure 9.2. In the first step of this pathway, galactose is ATP-phosphorylated at C1 by galactokinase. Next, galactose-1-phosphate uridylyl transferase transfers the uridylyl group of UGP-glucose to galactose-1-phosphate yielding glucose-1-phosphate and UDP-galactose. The latter, is epimerized to UDP-glucose by means of UDP-galactose-4-epimerase. This step is $NAD^+$ dependent indicating incolvement of a sequential redox mechanism at C4 atom of the monosaccharides. In the final reaction, glucose-1-phosphate is converted to glucose-6-phosphate, which can directly enter glycolysis. Malfunctioning of the enzymes of the Leloir pathway causes severe metabolic disorders, collectively referred to as galactosemia. The disease was first described by Goppert in 1917 [146]. Defects in the gene encoding galactose-1-phosphate uridylyl transferase (classic galactosemia) lead to poor growth in children, speech abnormality, mental retardation, cataract and liver damage (which may be lethal).

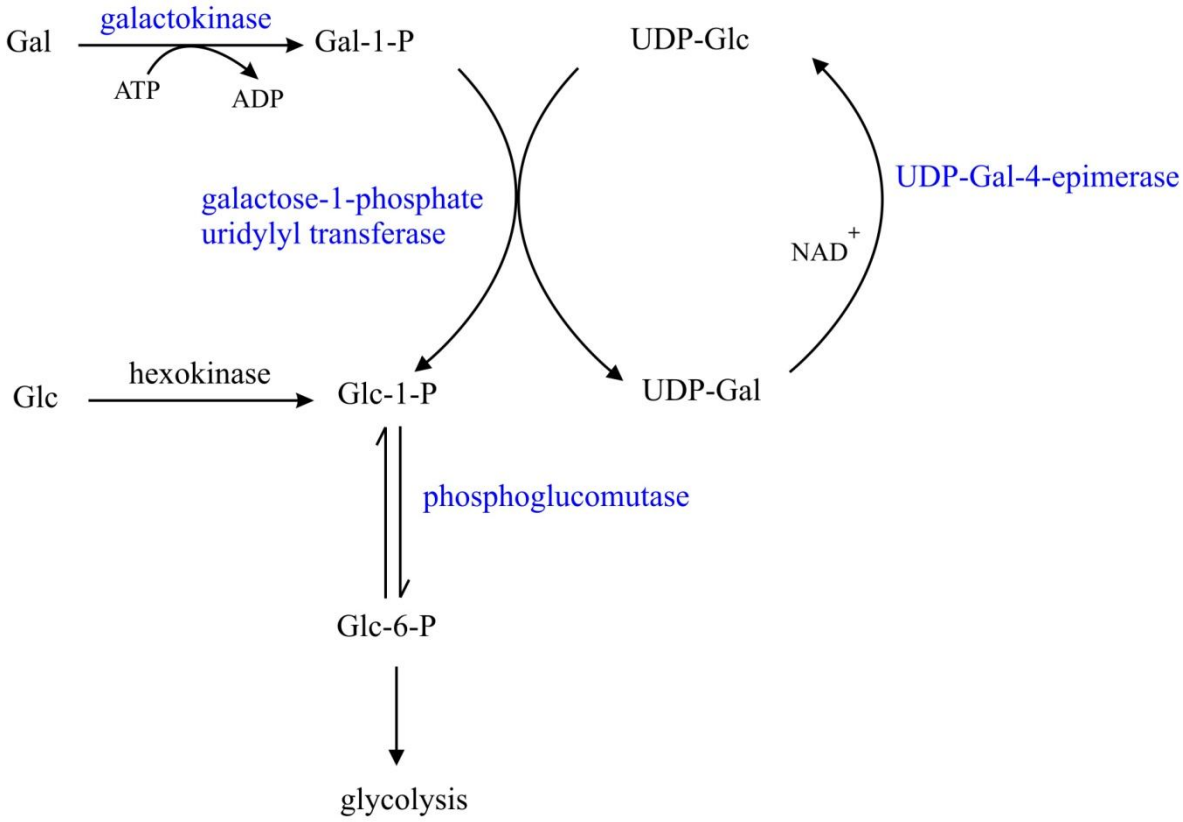


**Figure 9.2: Interconversion of galactose and glucose in the Leloir pathway.**

Galactose can enter glycolysis only after it is epimerized to glucose. This is achieved in the Leloir pathway, where galactokinase, galactose-1-phosphate uridylyl transferase, UDP-galactose-4-epimerase and phosphoglucomutase mediate the outlined reactions of galactose/glucose interconversion. Gal-galactose; Glc-glucose; P-phosphate; UDP-uridylyl diphosphate. The figure is based on Biochemistry, 2nd edition, Voet & Voet, p. 478, Figure 16-35.

Elimination of lactose and galactose from the diet can induce regression of the cataract (clouding of the eye lenses), but neurological complications are permanent. Overexpression of human UDP-glucose pyrophosphorylase (h*UGP2*) in *S. cerevisiae* was reported to rescue galactose-1-phosphate uridylyl transferase-deficient yeast [147]. Galactokinase deficiency (galactosemia type 2 or GALK deficiency), is characterized by an accumulation of galactose and galactitol as a consequence of disabled conversion of galactose to galactose-1-phosphate by galactokinase. Buildup of galactitol, a toxic sugar alcohol causes cataract [148;149]. Implementation of a galactose-free diet alleviate the symptoms of this genetic disorder. Galactosemia type 3 is very rare and results in clinical symptoms similar to classical galactosemia and also severe delays in both motor and cognitive skills [150].

## *9.3 UGPASES*

UGPases are ubiquitous cytosolic proteins which were purified from a variety of sources since their discovery [151]. The molecular mass of a monomer varies between 40 and 60 kDa depending on the species. The enzymes are most abundant in tissues displaying high polysaccharide synthesis activity. In the protein extractable from calf liver, the UGPases account for up to 0.2% [152], and they represent 1% of the total slime mold protein [153]. In tumor tissue, where the glycolytic activity is increased compared to normal cells, UGPase content is decreased by up to 50% [154]. In higher animals, the highest concentrations of UDP-glucose pyrophosphorylase are found in liver, while brain, spleen, lung and fat tissues contain rather low amounts of the enzyme [155]. In higher plants, UGPases activity levels are typically linked to the demand for starch and sucrose [126]. Chloroplasts and starch granules may also contain high concentrations of the enzyme.

Together with other glycosyltransferases, UGPases belong to the SGC superfamily (SpsA GnT I core domain), which was defined on the basis of structural similarity of *Bacillus subtilis* glycosyltransferase (SpsA) and *N*-acetylglucosaminyltransferase from rabbit (GnT I) [156]. The proteins, although possessing low sequence identity, are characterized by the presence of a signature called SGC fold [156;157] . An SGC fold is characterized by an eight-stranded β-sheet, flanked with α-helices (Figure 9.3). Furthermore, UGPases posses a characteristic motif in their active site (LxxGxGTxxxxxxPK) that is conserved throughout the superfamily.

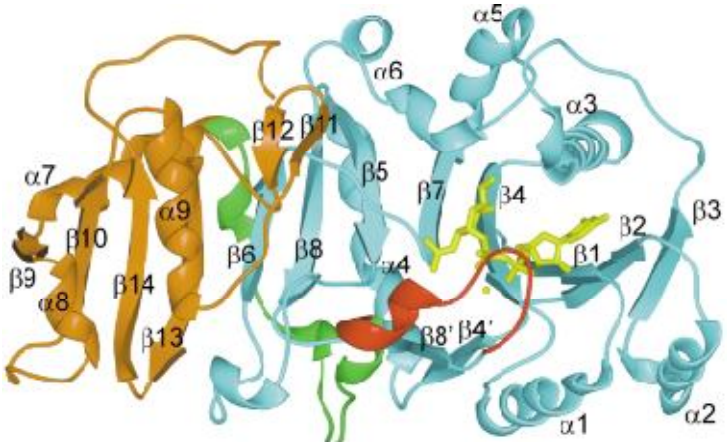


**Figure 9.3: Rabbit GnT I protein-the representative of SGC domain (SpsA GnT I core domain)**

GnT I ribbon diagram (Fig. 1. Unligil et al., 2000 [156]). The protein is composed of two domains: domain 1 (cyan) and domain 2 (orange). UDP-GlcNAc (UDP-N-acetylglucosamine) binding loop is shown in red, the linker connecting the domains in green. UDP-GlcNAc and $Mn^{2+}$ are depicted in yellow.

Although eukaryotic UGPases catalyze the same reaction as their bacterial counterparts, the proteins show no similarities in the amino acid sequences, nor in the three-dimensional structure [134;158]. The sequence similarity within eukaryotic enzymes lies between 42 to 95%. The UDP-glucose pyrophosphorylase from *Y. lipolytica* shows 70 % sequence identity to the protein from baker's yeast and 51% to the one from *A. thaliana* (Figure 9.4). A second isoform of UGPase, UGPA2, was found in the *S. cerevisiae* genome. The two isoforms display 41% sequence identity [159].

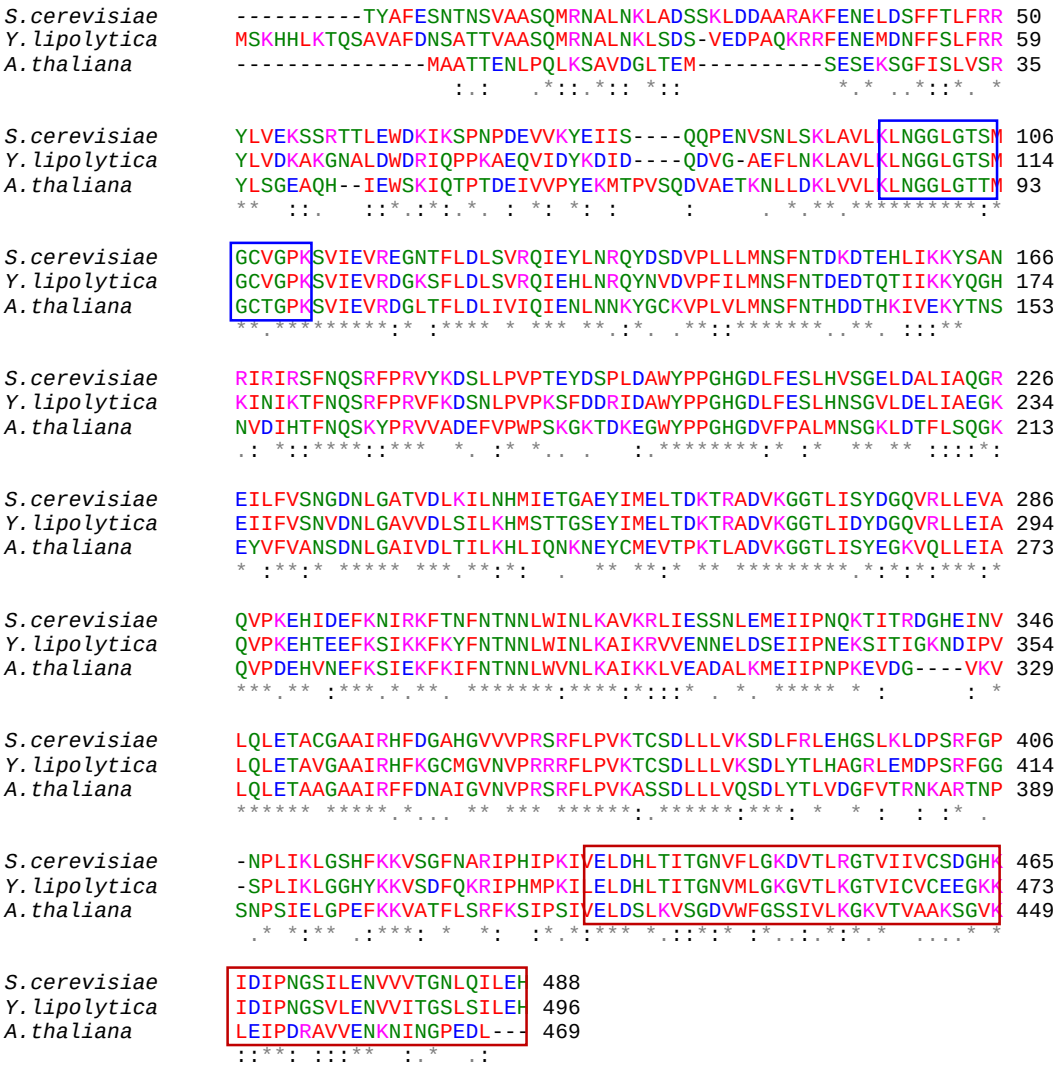


**Figure 9.4: UDP-glucose pyrophosphorylase sequence alignment; *S. cerevisiae, Y. lipolytica* and *A. thaliana.***

The sequence identity between the plant and yeast enzymes is 51% for *Y. lipolytica* and 52% for *S.cerevisiae,* whereas the sequence identity between the yeast proteins amounts to 70%. The nucleotide binding loop sequence is enclosed in the blue box, whereas the C-terminal region important for the oligomerisation-in red box. The sequence alignment was done using ClustalW2, EMBL-EBI tools.

The oligomerisation state of UDP-glucose pyrophosphorylases depends on the origin as well as environmental conditions. In *E. coli,* the UGPase that is a product of the *galU* gene was shown to be active in its tetrameric state [160]. The active Ugp1p from *S. cerevisiae* was purified as an octamer with a an apparent molecular mass of 448 kDa [161]. In case of the plant enzyme, the most active form was typically found as monomer. Dimers and higher order oligomers displayed very little or no catalytic activity. Therefore, it has been proposed that the oligomeric state of plant UGPases may regulate enzymatic activity [162].

## *9.4 REGULATION OF THE ENZYMATIC ACTIVITY OF UDP-GLUCOSE PYROPHOSPHORYLASE*

While yeast UDP-glucose pyrophosphorylase is subject to product inhibition, little is known on regulation of its metabolic activity. Glycogen synthesis is regulated at the level of glycogen synthase and glycogen phosphorylase and the regulation mechanism involves phosphorylation and allosteric interactions. In case of the mammalian enzyme, regulation of glycogen synthesis entails hormone-mediated substrate cycles and enzyme-catalyzed covalent modifications [163;163]. The activity of phosphoglucomutase determines the glucose-1-phosphate pool. In baker's yeast paralogous PAS kinases Psk1 and Psk2, additionally to glycogen synthase phosphorylate also Ugp1p [164]. Phosphorylation of a single residue Ser11 exerts a conformational change in Ugp1p, which is required for targeting the enzyme to the site of glucan synthesis in the cell periphery. Two forms of Ugp1p were isolated: isoform 1 (unphosphorylated) and isoform 2 (phosphorylated). Cells lacking the phospho-Ugp1p (either due to impairment of PAS kinase genes or mutation of the PAS kinase phosphorylation site) displayed a pronounced glycogen hyperaccumulation and a decrease in β-(1,6)-glucan, which is the major component of the cell wall. It was hypothesized, that isoform 1 is preferentially used for the glycogen synthesis, whereas the phospho-Ugp1p mediates synthesis of UDP-glucose for structural carbohydrates [165].

## *9.5 UGPASES – STRUCTURAL ANALYSIS*

UDP-glucose pyrophosphorylase was purified and successfully crystallized from a variety of organisms. Up to now there are five sources for which high resolution structures were deposited in the PDB. The structure of UDP-glucose pyrophosphorylase from *A. thaliana* was solved for the native enzyme (2q4j, 1z90), in complex with UTP (2icx) and UDP-glucose (2icy), which resulted in the highest resolution data set (1.64 Å) [166]. The structure of the

enzyme from the parasite *Leishmania major*, was solved to a resolution of 2.3 Å and there are two entries in the PDB: 2oef and 2oeg [167]. There are two structures available for the bacterial enzyme; from *E. coli* (2e3d) [168] and from *Corynebacterium glutamicum* (2pa4) [169]. The structure of Ugp1p from baker's yeast was solved by molecular replacement using the structure of the plant enzyme as a template [161]. As mentioned before, the amino acid sequence identity between the two proteins is 52%. A superposition of the monomers of the two structures (Figure 9.5) exhibits high structural similarity, especially in the SGC domain. The C-terminal region, which is important for oligomerisation, lacks the β18 sheet in case of the *A. thaliana* monomer, which is replaced by a short α-helix (blue trace, Figure 9.5). The C-terminus of yeast and metazoa is characterized by highly conserved hydrophobic residues, which are replaced by polar and charged amino acids in the plant enzyme sequences (Figure 9.4) [161;166]. The β18 sheet participates not only in the oligomerisation event, but also in the formation of a dimeric protomer. While UGPases from different species display high structural similarity in the active site region, the C-terminus shows pronounced differences.


**Figure 9.5: Superimposition of the X-ray monomer structures of UDP-glucose pyrophosphorylase from *A. thaliana* (blue) and *S. cerevisiae* (red).**

The high sequence identity correlates well with the structural similarity. The major difference is observed at the C-terminal (marked with an asterisk) of the monomer. In place of the β-sheet β18 in the yeast structure, a shorter $3_{10}$-helix is present in the plant enzyme. The figure was prepared using the CCP4 alignment tool (The CCP4 Suite: Programs for Protein Crystallography. Acta Cryst. D50, 760-763).

In the recently solved structure of Ugp1p from baker's yeast, C-terminal hydrophobic interactions of the monomers mediate the formation of a dimeric protomer per unit cell (Figure 9.6 A) as well as the association of the protomers into an octameric assembly (Figure 9.6 B). The native crystals diffracted X-rays to a resolution of 3.1 Å and were classified to belong to the *I*222 space group [161].

Ugp1p from *Y. lipolytica* has not been characterized so far. The protein displays 70% and 52% sequence identity to the one from *S. cerevisiae* and the plant enzyme respectively. It is likely that the domain architecture is similar to the one observed for other SGC domain proteins. Since the sequence of the active site of the yeast enzyme is conserved, one may assume that the secondary structures of this region should be very similar. It will be interesting to see, if and how the protein forms oligomers and what will be the mechanism of regulation of the enzymatic activity. In order to address at least some of these questions a structural characterization of the enzyme will be required.

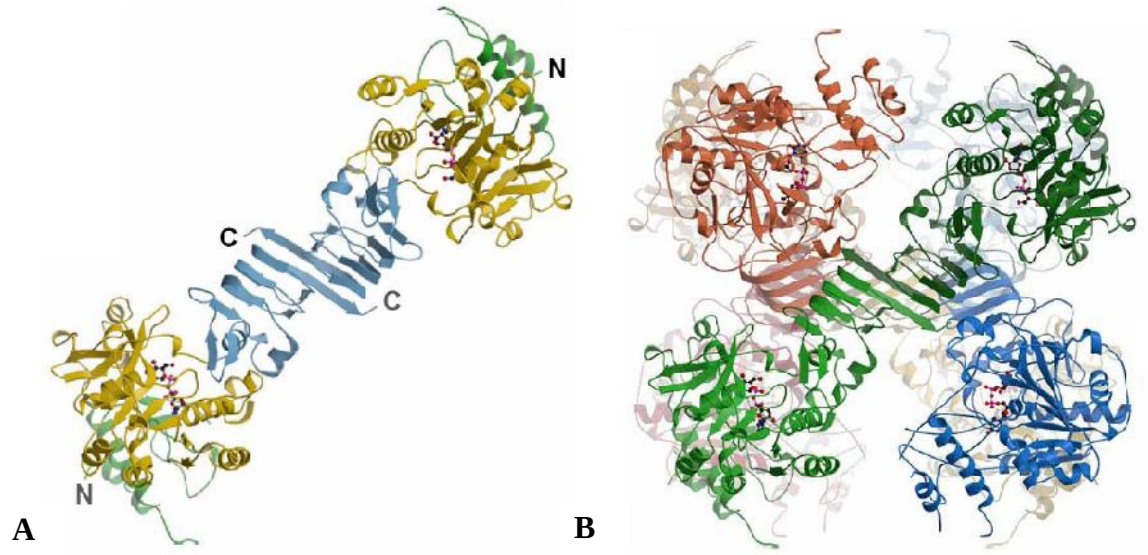


**Figure 9.6: Crystal structure of UDP-glucose pyrophosphorylase from *S. cerevisiae*.**

A: An asymmetric unit contains a dimeric protomer formed by hydrophobic interaction of the C-terminal β sheets. B: Side view of octameric Ugp1p. The N-terminal domain is shown in green, the central (SGC) domain in yellow, the C-terminal domain in blue. UDP-glucose in ball-and-stick representation was modeled into the presumed active site. Figure reprinted from Roeben et al., 2006 [161].

# Part II-Results

UDP-glucose pyrophosphorylase

# 10 UGP1P - RESULTS

UDP-glucose pyrophosphorylase from *S. cerevisia*e displays affinity towards $Ni^{2+}$-NTA (prof. Andreas Bracher, personal communication). The same was observed for Ugp1p from *Y. lipolytica* and the enzyme was co-purified during affinity chromatography of His-tagged complex I. Ugp1p was detected in the CI/Fab 44G10 co-complex preparation, after it crystallized in a crystal form different from those observed for the co-complexes before. MALDI mass spectrometry (MS/MS) in collaboration with Benjamin Rietschel (AG Karas, Goethe University Frankfurt) was employed to characterize the dissolved crystals. 20 small crystals were collected for SDS-PAGE composition analysis. To remove precipitate the crystals were washed thoroughly in a stabilizing buffer, which was the growth solution supplemented with 10% glycerol. No crystal damage was observed upon crystal soaking in the stabilizing solution.

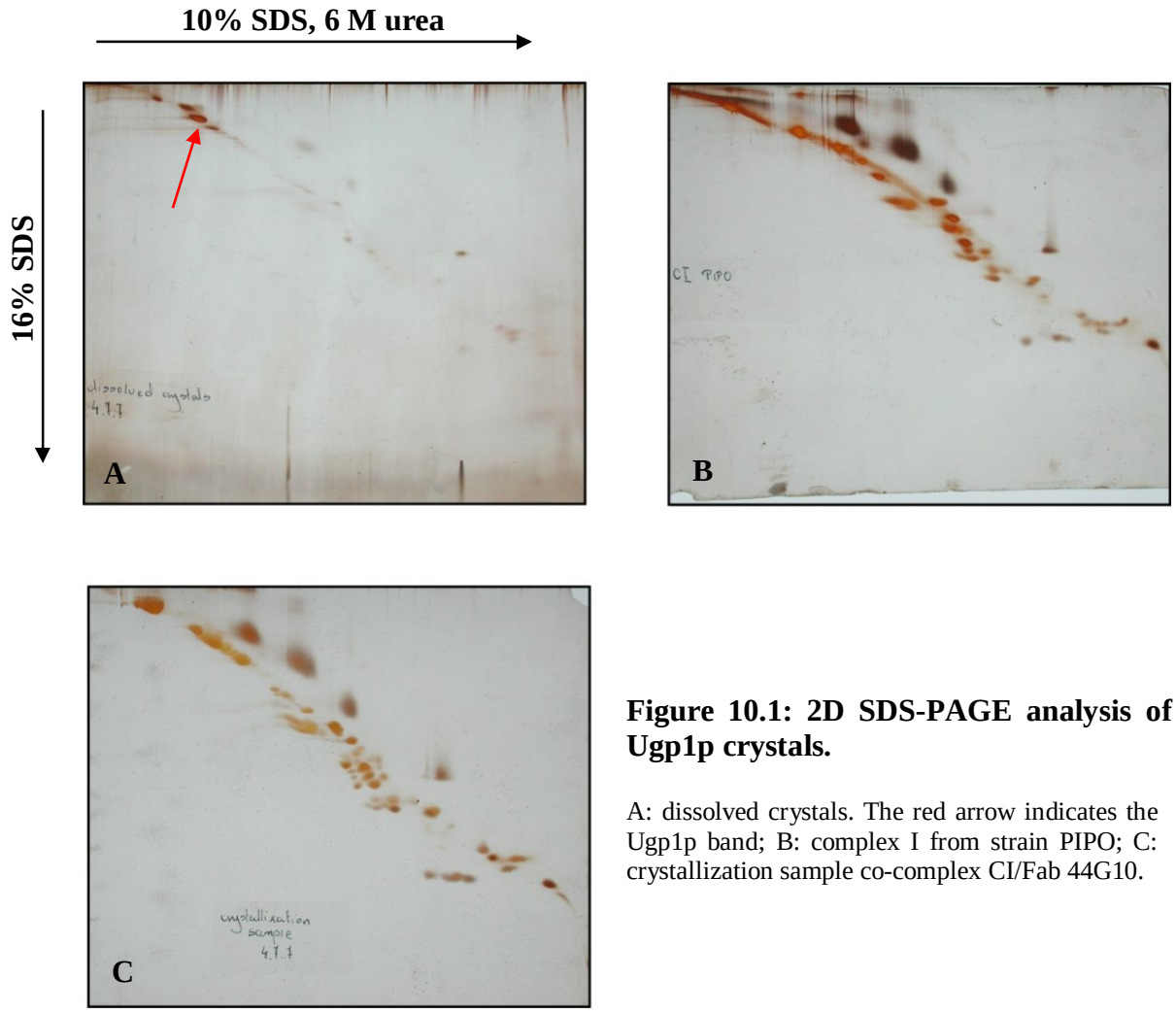


**Figure 10.1: 2D SDS-PAGE analysis of Ugp1p crystals.**

A: dissolved crystals. The red arrow indicates the Ugp1p band; B: complex I from strain PIPO; C: crystallization sample co-complex CI/Fab 44G10.

The washed crystals were dissolved in water and the same amount of SDS-PAGE loading buffer was added. The dissolved crystals were analyzed by 2D SDS-PAGE as described in 13.6.5. In the first dimension the bands were separated by SDS-PAGE (10% acrylamide, 6M urea) and a 16% SDS gel was used to resolve the protein bands in the second dimension [170] (Figure 10.1).Residual amounts of protein precipitate produced a slight background of complex I subunits (Figure 10.1). The band marked with a red arrow was cut out and analyzed by mass spectrometry. The band was unambiguously identified as UDP-glucose pyrophosphorylase with sequence coverage of 72%. The monomer mass calculated on the basis of the MS polypeptide was 55614 Da. In the 2D SDS-PAGE (Figure 10.1 A) Ugp1p migrates slightly above the 49/51-kDa subunits of complex I. The band was absent in the complex I control sample (Figure 10.1 B).

## *10.1 PURIFICATION OF UGP1P*

Ugp1p co-purified with complex I during the $Ni^{2+}$ NTA affinity chromatography step. The protein eluted from the size exclusion column following complex I. The elution volume corresponded to a mass of roughly 450 kDa, which would indicate an octameric state of the enzyme (Figure 10.2 A). The fractions were analyzed by 10% Laemmli gel and pooled accordingly (Figure 10.2 B).

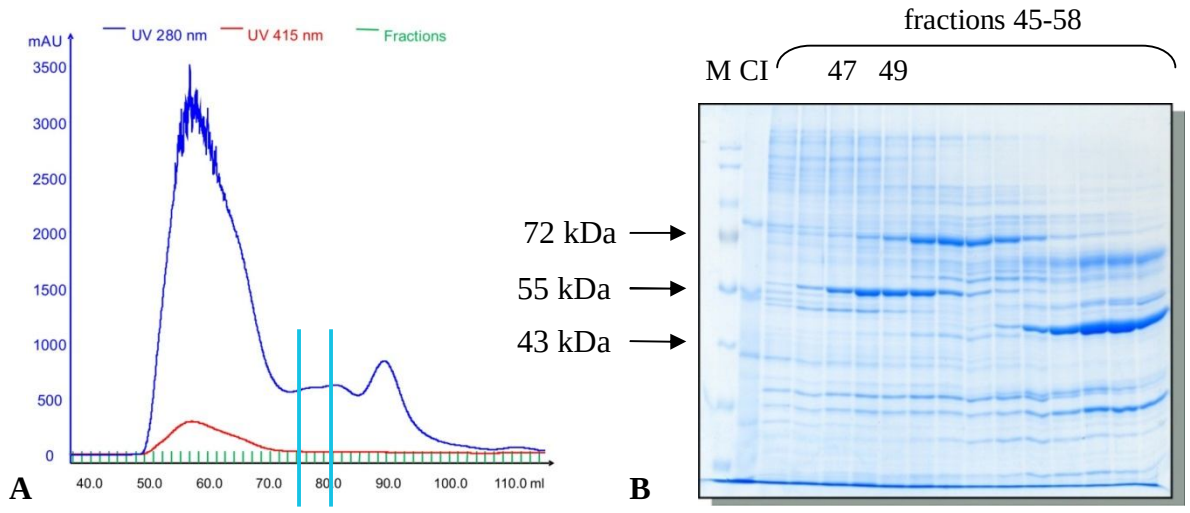


**Figure 10.2: Co-purification of Ugp1p with complex I.**

A: gel filtration elution profile. Fractions 47-49 (marked by turquoise bars) were pooled for ion exchange purification. B: 10% Laemmli gel [171]. M: molecular mass standard (PageRuler™ Prestained Protein Ladder, Fermentas); CI: complex I; fractions 45-58: fractions eluted from a gel filtration column (see A).

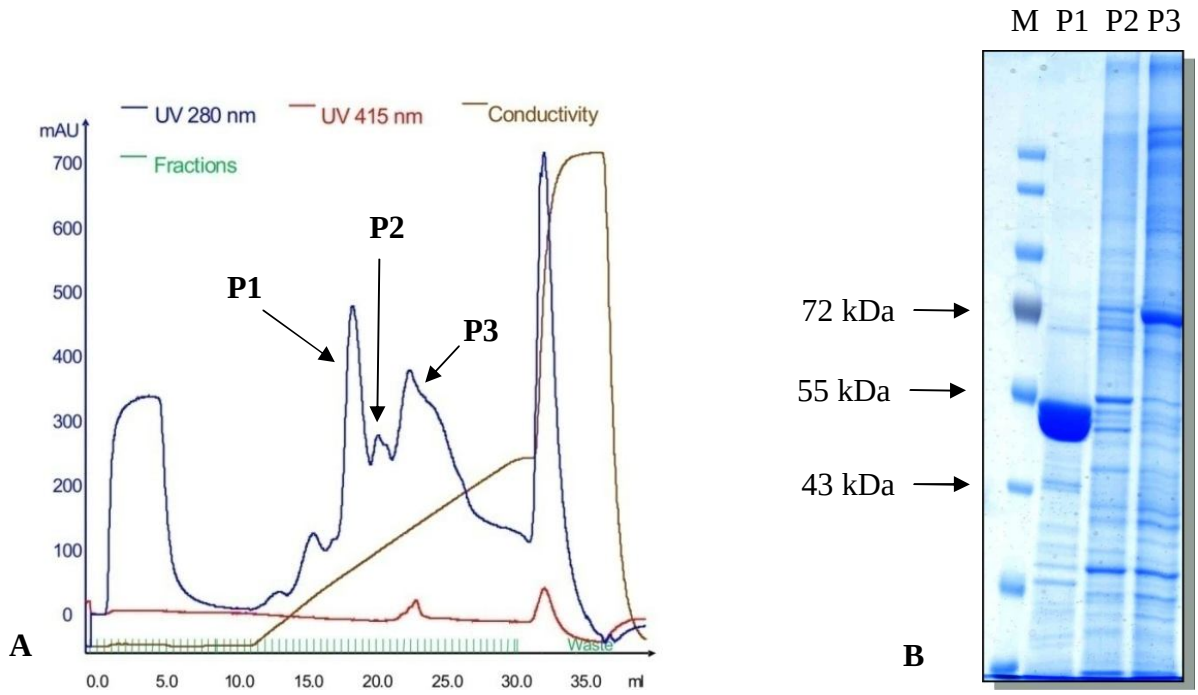


**Figure 10.3: Purification of Ugp1p using ion exchange chromatography.**

A: Mono Q elution profile. B: 10% Laemmli gel [171]. M: molecular mass standard (PageRuler™ Prestained Protein Ladder, Fermentas); P1: peak 1; P2: peak 2; P3: peak 3.

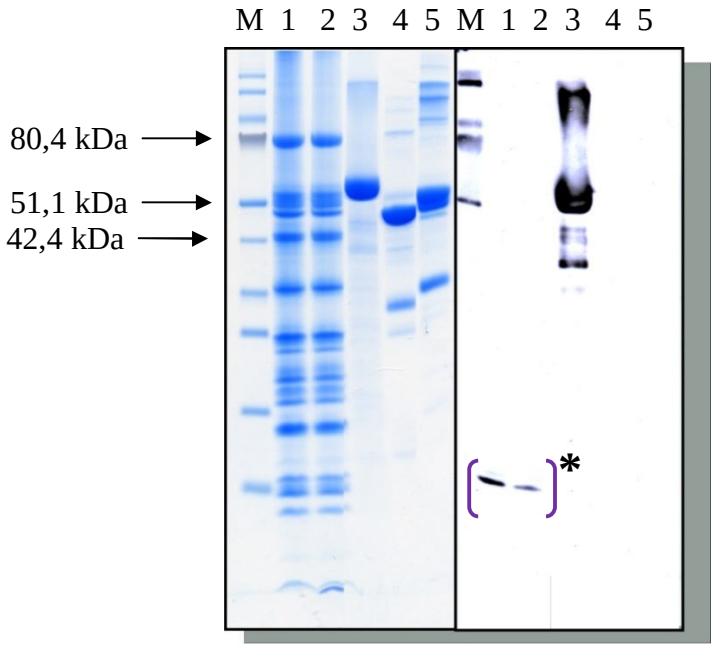


**Figure 10.4: Western blot detection of purified Ugp1p.**

Left: 10% SDS-PAGE. M: molecular mass standard (PageRuler™ Prestained Protein Ladder, Fermentas); 1: CI/Fab 1F5 co-complex; 2: CI/Fab 1F5 crystallization sample; 3: purified Ugp1p; 4: Fab 1F5; 5: Fab 44G10.

The pooled fractions were purified using anion exchange chromatography as described in 13.8. The resultant peaks were analyzed on a 10% Laemmli gel (Figure 10.3 A, B). Peak 1 represented a highly pure Ugp1p fraction. The Ugp1p band migrated in the Laemmli gel with an apparent molecular mass below the 55 kDa marker band (Figure 10.3 B, lane P1). The purified Ugp1p was detected in a Western blot using anti-Ugp1p antibodies directed against the baker's yeast enzyme (courtesy of dr. Jared Rutter, University of Utah, USA; Figure 10.4). The low molecular weight Western blot signals observed for lanes 1 and 2 in the Figure 10.4 and marked with brackets (*) represented an unspecific cross-reaction.

## *10.2 OLIGOMERS OF UGP1P FROM Y. LIPOLYTICA*

A purified sample of Ugp1p was analyzed using laser-based mass spectrometry method LILBID (laser-induced liquid bead ion desorption) in collaboration with Lucie Sokolova (AG Brutschy, Goethe-University, Frankfurt).

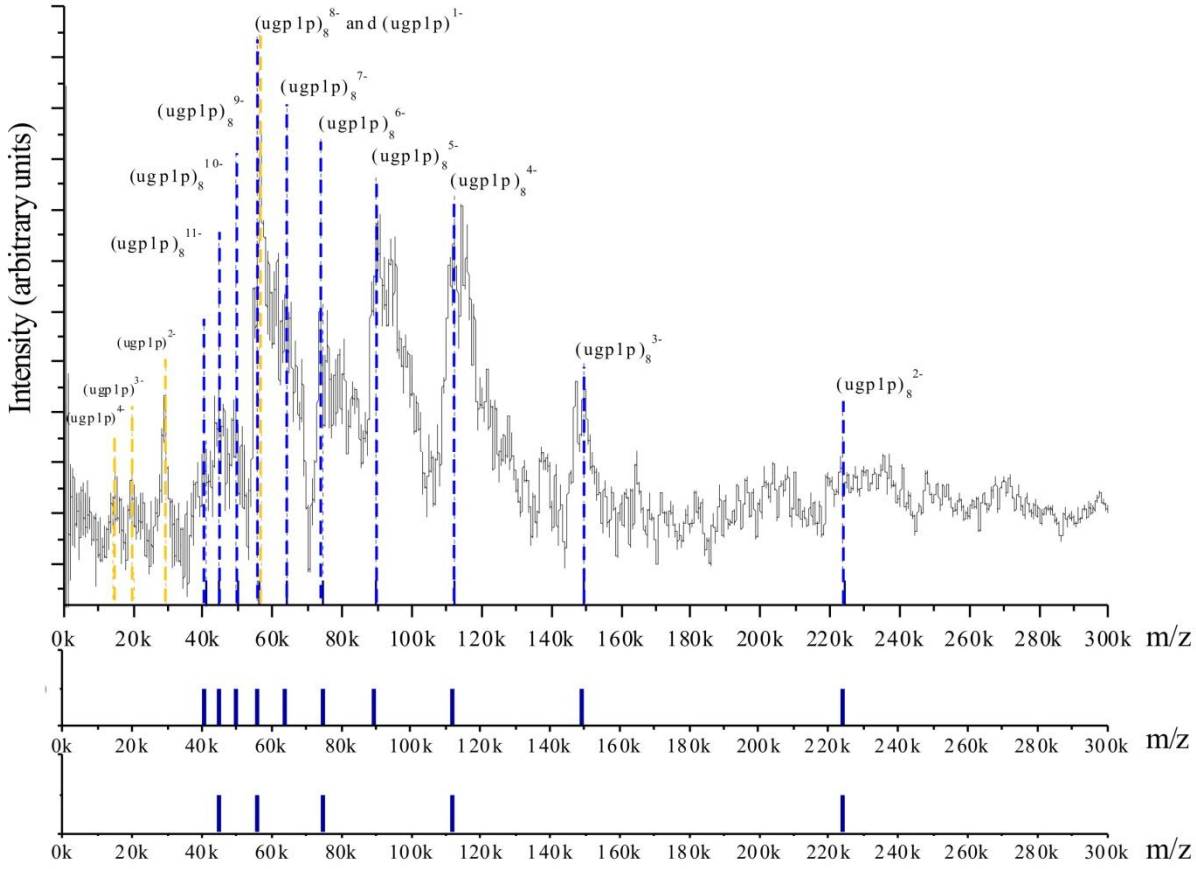


**Figure 10.5: Ugp1 from *Y. lipolytica* forms octamers as indicated by MS LILBID.**

A: (MS) LILBID spectrum of Ugp1p. The blue bars represent a charge distribution of an octamer of Ugp1p. The yellow ones represent a charge distribution of a monomer. Theoretical charge distributions for the Ugp1p, calculated in B for an octamer and C for a tetramer.

The sample in 30 mM ammonium acetate buffer of pH 7 was measured at ultrasoft conditions. The peaks in the spectrum corresponded to a charge distribution of a molecule of a mass about 450 kDa, which implies that Ugp1p is an octamer of a total mass 448 kDa (Figure 10.5).

## *10.3 CRYSTALLIZATION OF UGP1P*

### *10.3.1 Initial crystallization conditions*

The initial crystals of the purified Ugp1p grew in 300 nL hanging drops in vapor diffusion experiments carried out using Mosquito crystallization robot (TTP Labtech, UK). The crystals grew as thin needles (Figure 10.6 A). The mother liquor was composed of 18% PEG 400, 0.1 M MES, pH 6.5, 0.1 M $MgCl_2$. In order to facilitate crystal handling and analysis the crystallization conditions were scaled up to 4 µl drops set up in 24 well plates. In the larger scale crystals appeared more eagerly in the sitting drop setups, as thicker better defined needles, not longer than 100 µm (Figure 10.6 B).

Further screening for suitable crystallization conditions was conducted using the Mosquito crystallization robot and commercial crystallization screens: Crystal Screen and Crystal Screen 2 (Hampton Research). Out of 96 conditions, three resulted in good quality crystals.

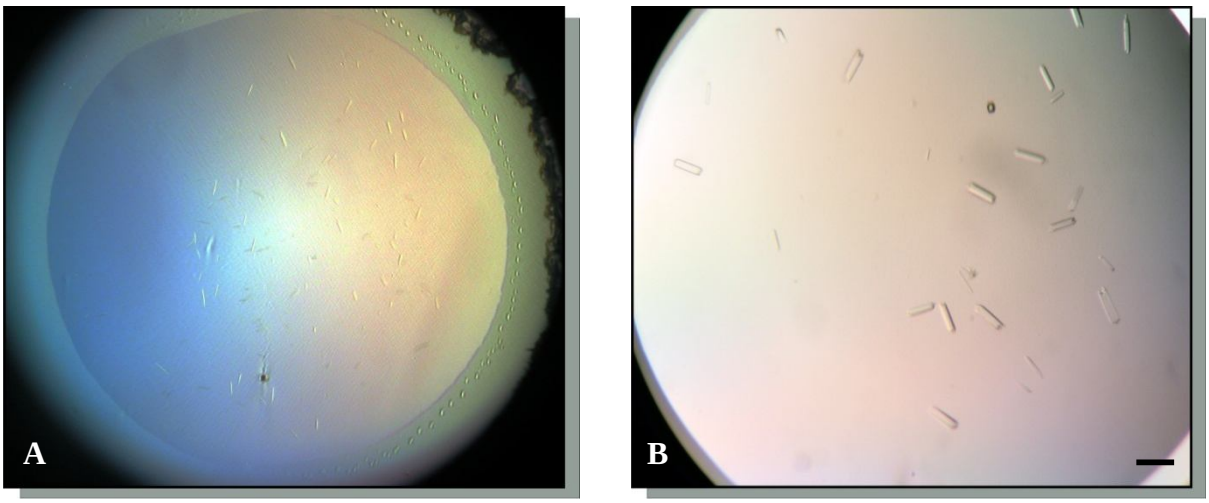


**Figure 10.6: Initial crystals of Ugp1p from *Y. lipolytica*.**

The crystals grew from 18% PEG 400, 0.1 M MES, pH 6.5, 0.1 M $MgCl_2$. A: Crystals which appeared in 300 nL hanging drops setups, prepared using Mosquito crystallization robot (TPP Labtech). B: The initial conditions were scaled up to standard conditions (24 well plates, 4 µl drops). The crystals grew in sitting drop setups up to 100 µm (black bar).

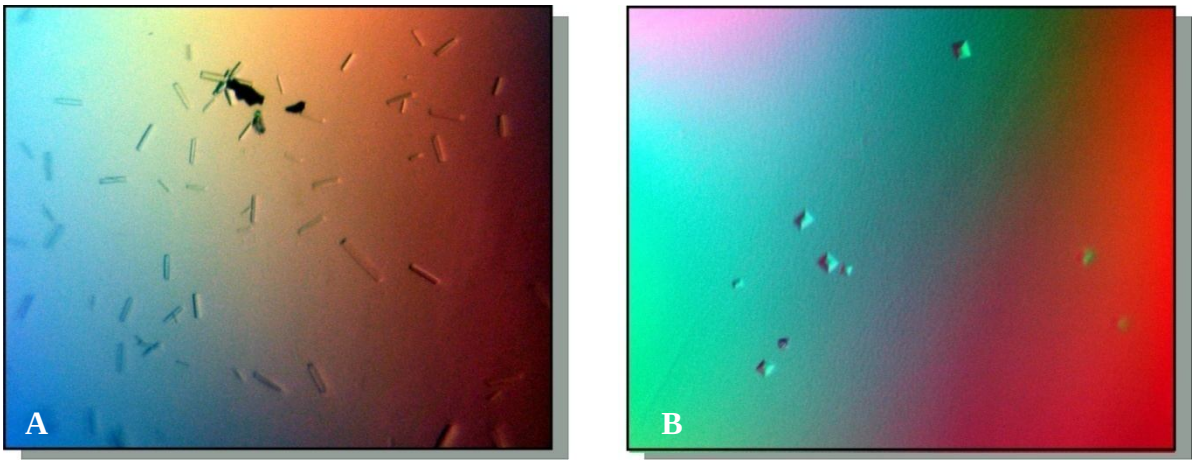


**Figure 10.7: Crystals obtained using Mosquito crystallization robot and commercial screens.**

A: 0.2 M calcium chloride , 0.1 M HEPES sodium, pH 7.5, 28% PEG 400 (Crystal Screen solution 14); B: 0.5 M ammonium sulfate, 0.1 M sodium citrate tribasic pH 5.6, 1 M lithium sulfate (Crystal Screen 2 solution 15).

Figure 10.7 represents crystals grown in 300 nL sitting drops. It was not possible to reproduce the crystals in the 24 well plate scale. The results obtained in the third condition (20% PEG MME 550, 0.1 M NaCl, 0.1M BICINE, pH 9.0) selected from the screening procedure could be easily reproduced at larger scale. The initial crystals appeared in a sitting drop system (Figure 10.8 A). In the upscaled conditions, larger crystals were observed in the hanging drops in comparison to sitting ones (Figure 10.8 B, C). The crystals appeared to be very fragile and became easily damaged during fishing with a nylon loop.

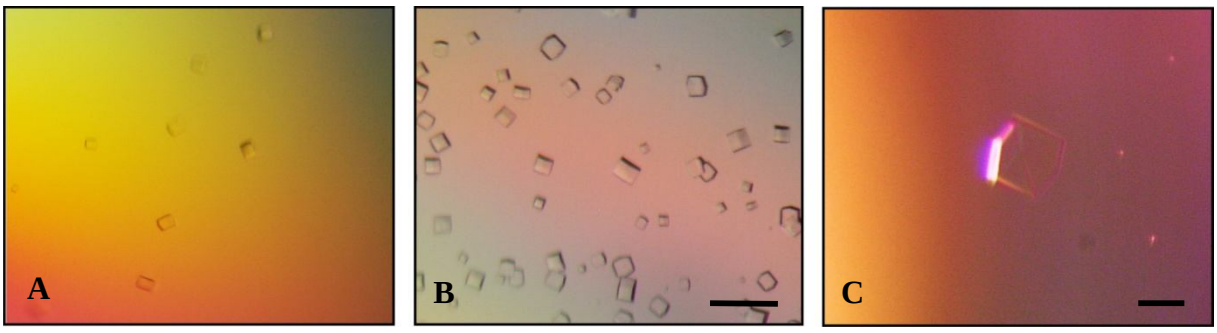


**Figure 10.8: Ugp1p crystals grown from 20% PEG MME 550, 0.1 M NaCl, 0.1 M BICINE, pH 9.0.**

A: Initial crystals obtained using Mosquito crystallization robot-sitting drop; B: crystals grown in 24 well plate in sitting drop; C: crystal grown in 24 well plate in hanging drop. Black bar indicates approximately 100 µm.

### *10.3.2 Optimization of the crystallization conditions*

It was possible to control the nucleation process by manipulating the pH of the mother liquor together with precipitant concentration. The basic condition used in this experiment was 18% PEG 400, 0.1 M MES, pH 6.5, 0.1 M $MgCl_2$. The nucleation process was slower when the PEG (precipitate) concentration increase was accompanied by higher pH values of the crystallization buffer. At 14% PEG 400 the optimum for crystallization was found for 0.1 M MOPS pH 7.0 (Figure 10.9 A). There were fewer crystals present in the drop. At the same time, the crystals were longer and thicker in comparison to the ones observed for pH 6.5. For PEG concentrations of 16 and 18% the pH optimum was shifted towards 7.0 (0.1 M MOPS)/7.5 (0.1 M HEPES) (Figure 10.9 B and C). The largest crystals grew at pH 7.5, whereas a crystal shower was recorded for pH 6.5. No crystals were observed for solutions containing PEG at pH 8.0 and above.

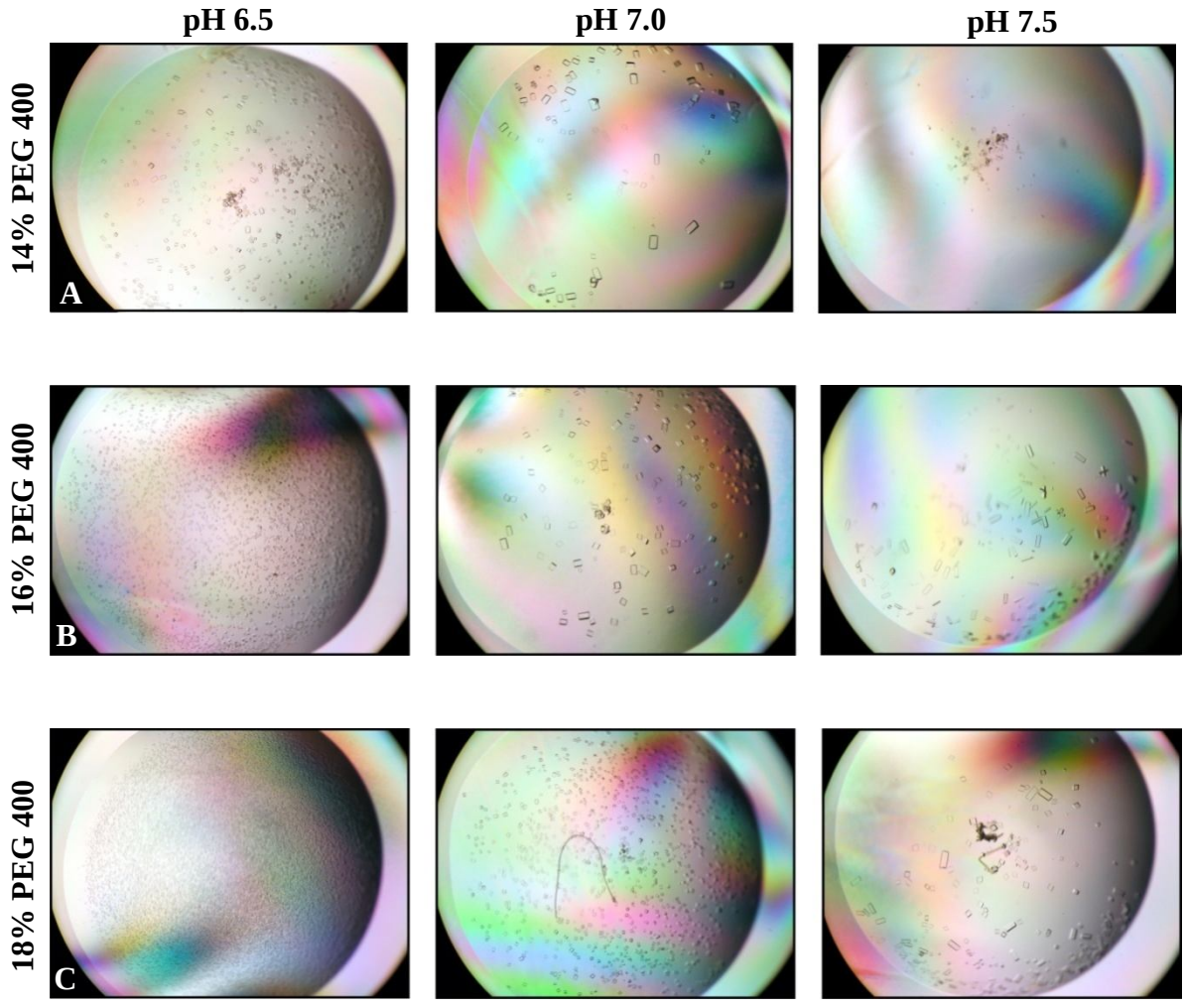


**Figure 10.9: Controlled nucleation process of Ugp1p crystals. PEG/pH dependence.**

### *10.3.3 Ugp1p crystallization under oil*

Microbatch experiments were carried out as described in 13.9.5, page 117. In these experiments the crystallization drop is sealed with an oil layer consisting of Al's oil or mixtures of silicon and paraffin used at different ratios. In addition to Al's oil, a 65% paraffin: 35 % silicon mixture was selected for further experiments. The screening for suitable conditions was performed around the standard precipitant solution (14-18% PEG 400, pH 6.5-7.5, 0.1 M $MgCl_2$). The equilibration of the supersaturation state was significantly slowed down by the oil barrier, resulting in larger size of the Ugp1p crystals. Regardless of the oil or oil mixture used, the best results were observed for 12% PEG and pH 7.0 (0.1 M MOPS). The largest crystals (up to 200 µm) grew under a layer of paraffin/silicon mixture (65%/35%).

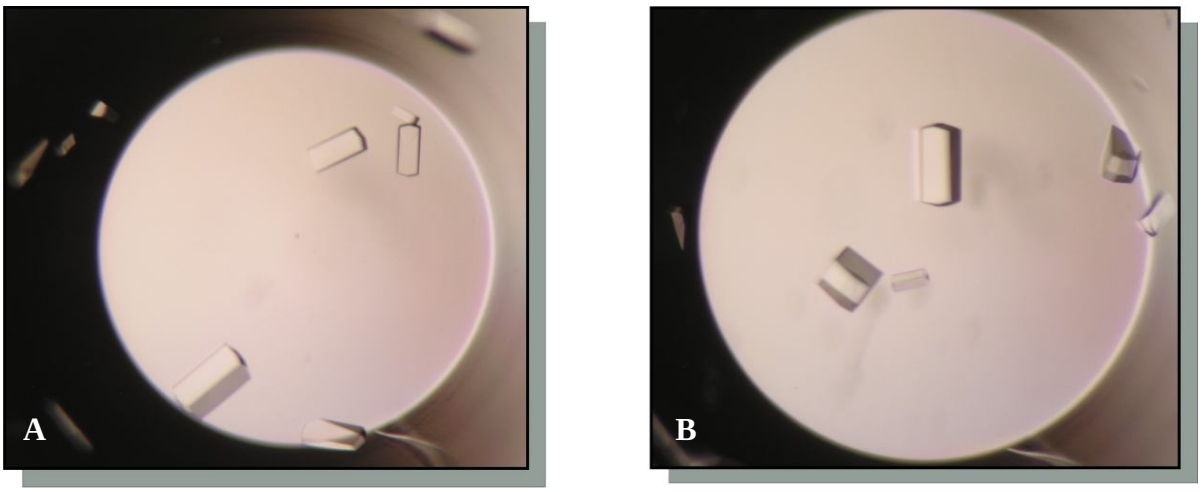


**Figure 10.10: Ugp1p crystals grown using microbatch technique.**

A: Crystals grown under Al's oil; B: crystals grown under a mixture 65% paraffin : 35% silicon. The crystals grew up to 200 µm.

Introduction of an oil barrier into vapor diffusion experiment (13.9.2.6, page 116) significantly improved the crystal size. A 500 µl film of an equal mixture of paraffin and silicon was placed on the top of 1 ml crystallization solution in a 24 well plate sitting drop experiment. The equilibration process was slower and the crystals grew longer and thicker in comparison to wells without the oil layer (Figure 10.11 A, B).

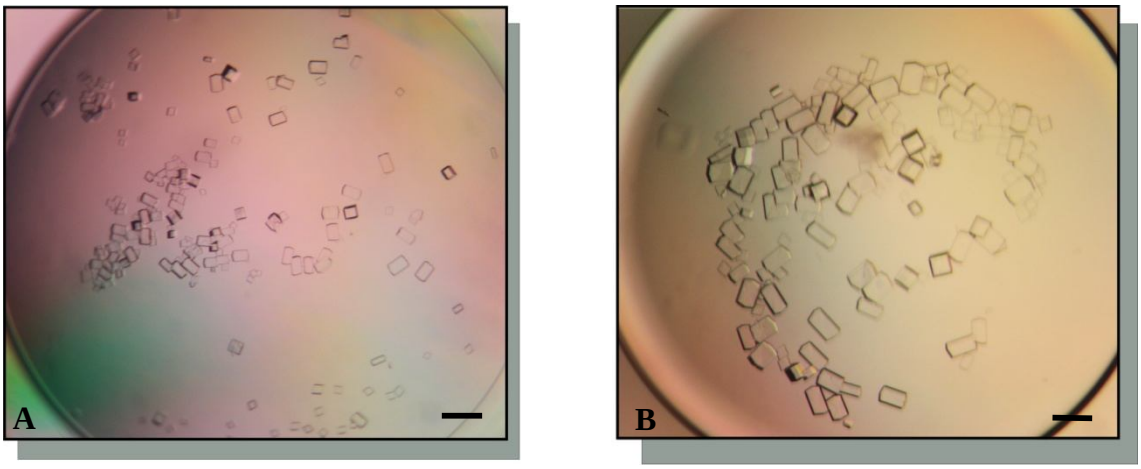


**Figure 10.11: Ugp1p crystals grown in vapor diffusion sitting drop experiments with an oil barrier.**

Well conditions: 14% PEG 400, 0.1 M MOPS, pH 7.0, 0.1 M $MgCl_2$. A: Crystals, which grew without an oil barrier. B: 500 µl Al's oil layer was placed over the well solution White bar represents ~ 100 µm.

## *10.4 DIFFRACTION OF UGP1P CRYSTALS*

The Ugp1p crystals were frozen and stored in liquid nitrogen. Use of 22 % PEG 400 in growth solution was a good cryoprotection agent. The diffraction data were collected on beamlines ESRF, ID 14, France and SLS, PX II, Switzerland. The crystals displayed high stability and the quality of the diffraction images remained unchanged after prolonged exposition to X-ray radiation. The best crystals diffracted X-rays to a resolution of 3.2 Å. The calculated space group was *I*4 and the unit cell dimensions as follows: a = 295 Å, b = 295 Å, c = 110 Å, α = 90˚, β = 90˚, γ = 90˚.

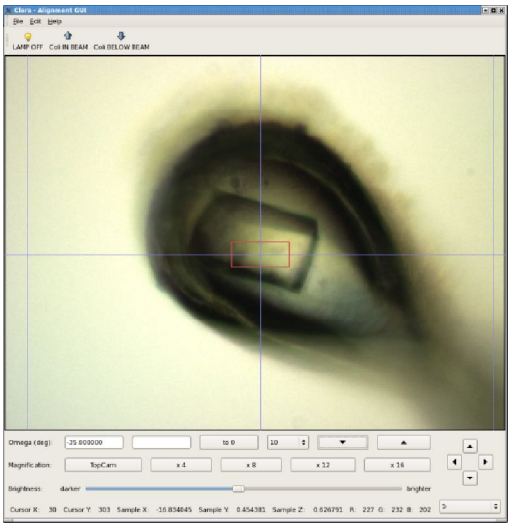

**Figure 10.12: Ugp1p crystal used for the X-ray data collection.**

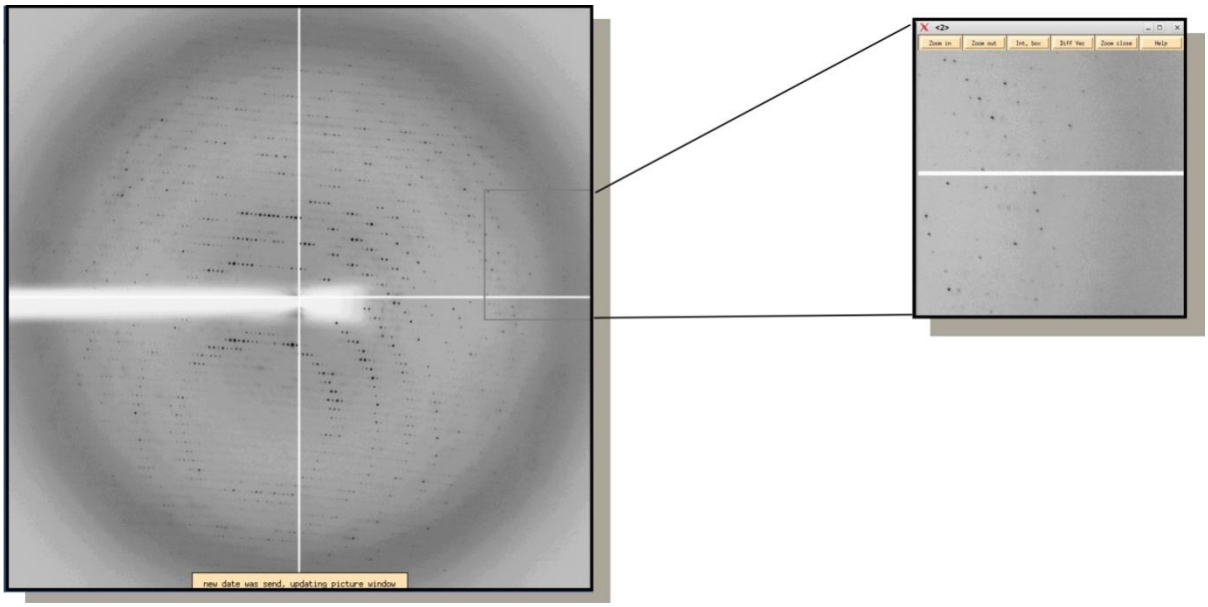


**Figure 10.13: Diffraction image of Ugp1p crystal.**

The data were collected at beamline ID14, ESRF, France. Data collection parameters: distance 300 mm, exposition time: 5 sec, oscilation range 0.4˚, wavelength 0.933 Å.

# Part II-Discussion

UDP-glucose pyrophosphorylase

# 11 DISCUSSION

## *11.1 CO-PURIFICATION OF UGP1P*

Due to some affinity towards $Ni^{2+}$-NTA Ugp1p was co-purified with complex I during the affinity purification step. In the following gel filtration experiment, the proteins were separated from each other and Ugp1p could be purified according to the procedure described in Materials and Methods. This phenomenon was also observed for UDP-glucose pyrophosphorylase from *S. cerevisiae* (Prof. Andreas Bracher, personal communication). The reason for nickel binding is unclear. Analysis of the surface residues of the structural model did not reveal any obvious histidine motifs that could be responsible for metal binding.

## *11.2 DOMAIN ARCHITECTURE OF UGP1P FROM Y. LIPOLYTICA*

UDP-glucose pyrophosphorylase form *Y. lipolytica* displays a high sequence similarity to other known UGPases. It contains a signature motif $LX_2GXGTX_6PK$, which is typically found in the active site of the SGC-domain proteins (Figure 11.2) [156;172-175]. The closest homologues with known structures are the enzyme from *S. cerevisiae* with 70 % sequence identity, followed by UDPGP from *Arabidopsis thaliana* with 52 % sequence identity. Based on the amino acid similarity, a structural model was built using the structure of the baker's yeast protein with the QuickPhyre server [176] and CCP4 Molecular Graphics [177] (Figure 11.1: Model of Ugp1p from *Y. lipolytica*.). It was possible to superpose the predicted structure of Ugp1p from *Y. lipolytica* with the solved structure of UDPGP from *A. thaliana* (PDB code 1z90) with a root mean square deviation (r.m.s.d) of only 1.22 Å over 437 $C^{\alpha}$ atoms. The model shows α/β architecture characteristic for pyrophosphorylases and consists of three domains: the amino-terminal domain, the SGC domain (central domain) and carboxy-terminal domain. The domains are arranged in a linear manner, where the N- and C-terminal domains are on opposite sides of the protein and do not contact each other (Figure 11.1). The N-terminal domain is the smallest one and is formed by two long α-helices and a β-hairpin structure. The central domain shows characteristics of the SGC domain family and is built of eight-stranded β-sheets, which are flanked by six α-helices [156]. In addition, a β-hairpin structure formed by a small two-stranded antiparallel β-sheets is observed in the core domain of the eukaryotic enzymes.

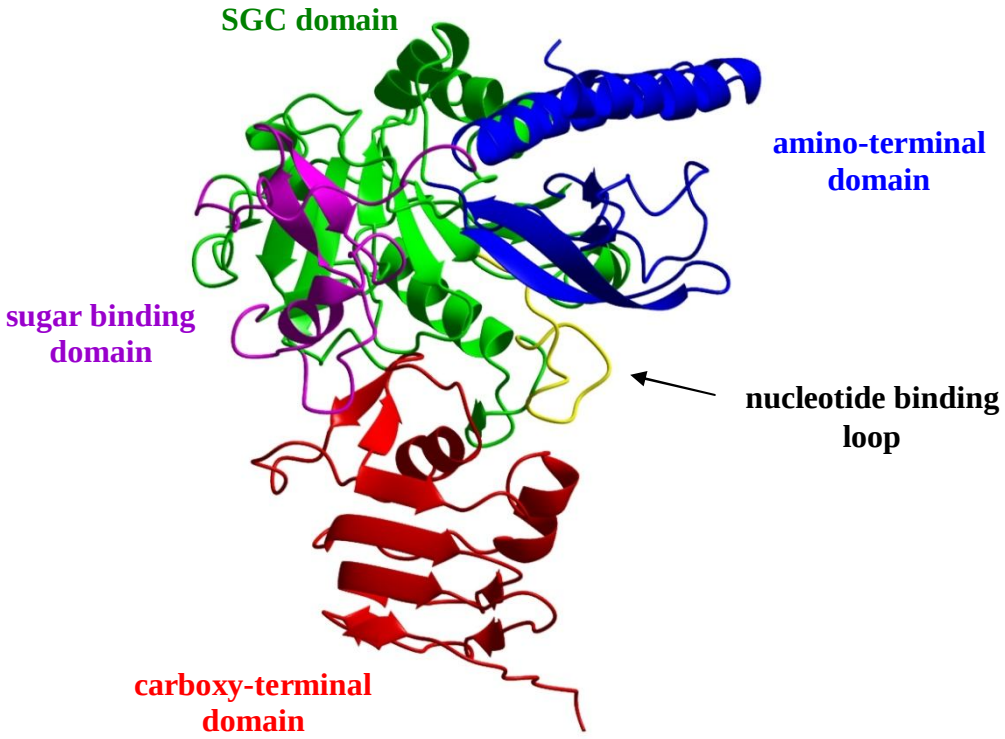


**Figure 11.1: Model of Ugp1p from *Y. lipolytica*.**

Ugp1p from *Y. lipolytica* displays a domain architecture characteristic for UGPases, with core domain typical for the SGC family proteins. The active site is located at the interface of the depicted domains. The model was based on the known structure of baker's yeast enzyme (PDB code 2i5k). The sequence similarity of the two proteins equals 70 %. The modeling was performed using QuickPhyre [176] and CCP4 Molecular graphics [177].

The sugar-binding domain[4] (Thr 268 - Ile 282) is conserved between baker's yeast and *Y. lipolytica*, and highly similar to the protein from *A. thaliana*. It is composed of α-helices and a four-stranded, antiparallel β-sheet. The interface of the four domains builds the active site of the enzyme which will be discussed in detail in the following paragraphs. The SGC domain signature motif harbors the nucleotide binding loop (Leu 105 – Lys 119) which is conserved throughout in eukaryotes (Figure 11.2). This loop is involved in conformational rearrangements upon substrate binding. The carboxy-terminal domain is characterized by the presence of a left-handed β-helix structure. This is formed by parallel β-strands, which clasp around a triangular core of hydrophobic side-chains. The β-helix arrangement is interrupted by an α-helix and a loop insertion in case of both yeast proteins and the *A. thaliana* enzyme. The terminal β-strand β18, which seem to be important for oligomerisation, is absent in the plant

[4] Regarded as a part of the central domain in the case of *S. cerevisiae* [161] and a separate domain in the case of the *A. thaliana* enzyme [166].

structure. This is in agreement with the fact that the active plant proteins were found exclusively as monomers.

| | | |
|---|---|---|
| *Yarrowia lipolytica* | LKLNGGLGTSMGCVGPKSV | 121 |
| *Saccharomyces cerevisiae* | LKLNGGLGTSMGCVGPKSV | 113 |
| *Schizosaccharomyces pombe* | LKLNGGLGTTMGCVGPKSI | 130 |
| *Hordeum vulgare* (barley) | LKLNGGLGTTMGCTGPKSV | 104 |
| *Solanum tuberosum* (potato) | LKLNGGLGTTMGCTGPKSV | 107 |
| *Arabidopsis thaliana* | LKLNGGLGTTMGCTGPKSV | 101 |
| *Homo sapiens* | VKLNGGLGTSMGCKGPKSL | 128 |
| *Bos taurus* (bovine) | VKLNGGLGTSMGCKGPKSL | 128 |
| *Danio rerio* (zebrafish) | VKLNGGLGTSMGCKGPKSL | 143 |

**Figure 11.2: Sequence alignment of the signature motif typical for SGC-domain proteins.**

The signature motif $LX_2GXGTX_6PK$ resides the nucleotide binding loop (Leu 105 – Lys 119) of the UDP-glucose pyrophosphorylases. Residues important for substrate or metal binding are conserved (red) in the active centre of the SGC-family proteins. Sequence alignment was performed using ClustalW2, EMBL-EBI tools.

## *11.3 ARCHITECTURE OF THE ACTIVE SITE OF UGP1P*

The model of Ugp1p from *Y. lipolytica* was constructed on the basis of the sequence similarity to the baker's yeast protein (PBD 2i5k), of which structure had been solved by molecular replacement using the known structure of UDPGP from *Arabidopsis thaliana*. The following chapter will refer to the original plant structure which was solved as the native enzyme (PDB code 1z90), with bound UDP-glucose (PDB code 2icy) and with bound UTP (PDB code 2icx). Since the residues involved in substrate binding are conserved between Ugp1p and UDPGP and the secondary structure displays high similarity, it seems very likely that the architecture of the active sites is conserved. The residues are numbered according to the *A. thaliana* structure of the chain A and the numbering of the predicted model of *Y. lipolytica* enzyme is included in brackets.

### *11.3.1 Active site with bound UDP-glucose*

The interior of the substrate binding pocket is laid-out with positively charged amino acids (Figure 11.3 A). The amino-terminal residues involved in UDP-glucose binding include Gln 162 (182) and Gly 191 (211) coordinating the uridyl group and His 192 (212) coordinating the β-phosphate. The central-domain residues binding UDP-glucose are Asn 220 (240) and Asn 293 (313) coordinating the glucosyl unit, Gly 87 (107) coordinating the uridyl group, Leu 85 (105) coordinating the ribose group, and Lys 99 (119) coordinating the α-phosphate. The three residues Gly 87 (107), Leu 85 (105) and Lys 99 (119) are found on the nucleotide binding loop. Sugar binding domain residues involved in UDP-glucose binding, are Gly 258 (278)

and Glu 271 (291) coordinating the glucose portion and Lys 256 (276) coordinating the β-phosphate. The only C-terminal residue in contact with UDP-glucose is Lys 360 (382) coordinating the α-phosphate.

### *11.3.2 Active site with bound UTP*

Coordination of the uridine portion in the UTP complex is similar to the one observed for UDP-glucose complex. The sugar binding loop displays a conformation which is analogous to the one seen in the native structure. Temperature factors of this area recorded for chains A and B are higher when compared to neighboring residues indicating enhanced structural flexibility of the loop, when UTP is present [166]. Coordination of the α-phosphate is mediated by Lys 360 (382) and Lys 99 (119) similar to the situation for UDP-glucose, whereas the β-phosphate is no longer coordinated by His 192 (212).

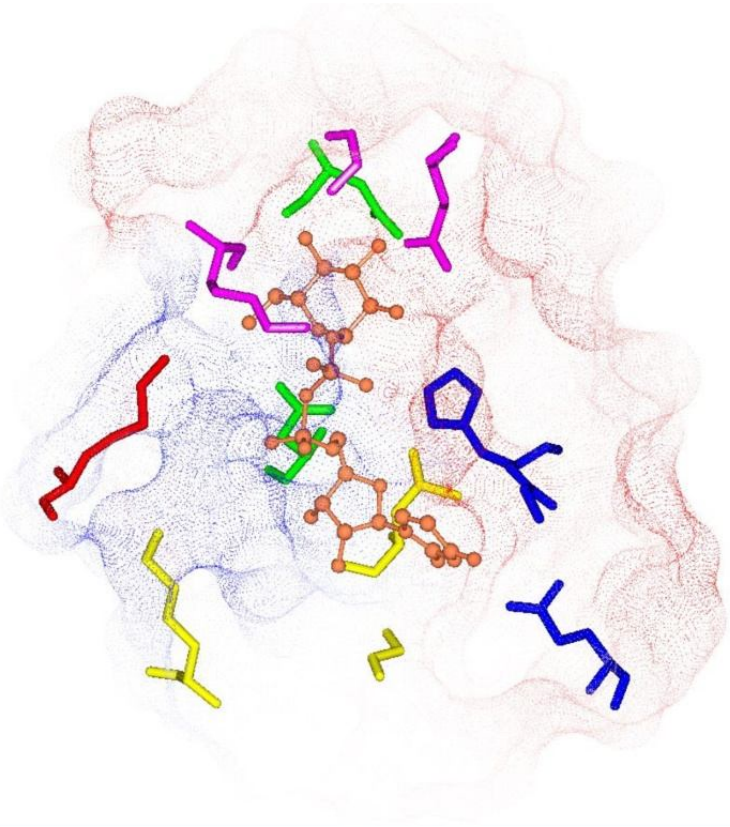

**Fig 11.3 A**

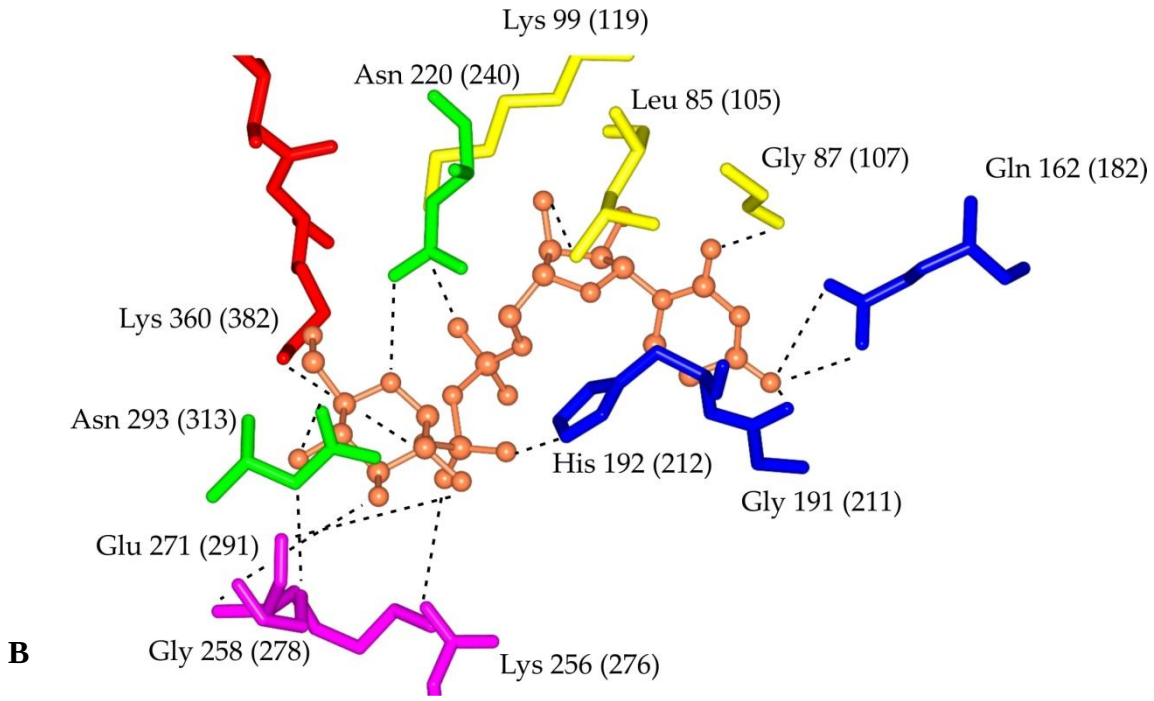


**Figure 11.3: Architecture of the active site of UDP-glucose pyrophosphorylase from *A. thaliana* with bound UDP-glucose.**

A: electrostatic representation of the substrate binding pocket; B: the active site close-up; Numbering corresponding to *Y. lipolytica* model is included in brackets. The amino terminal amino acids are depicted in blue, SGC domain amino acids-green, nucleotide-binding loop-yellow, sugar-binding domain-magenta, carboxy-terminal domain-red. UDP-glucose is shown in coral. The images were prepared using CCP4 Molecular Graphics.

## *11.4 CONFORMATIONAL CHANGES UPON SUBSTRATE BINDING*

UDP-glucose pyrophosphorylase from *A. thaliana* undergoes a conformational change upon substrate binding [166]. The functional equivalent from *Y. lipolytica* displays high sequence and structure similarity and is likely to show the same conformational modifications exerted by binding of the substrates. As the reaction catalyzed by UDPGP follows an ordered bi-bi mechanism, the nucleoside phosphate or UDP-glucose bind prior to glucose-1-phosphate or pyrophosphate. This mechanism is mirrored by a conformational change, where the nucleotide binding loop (Gly 87 - Lys 99, *A. thaliana* numeration) moves towards the nucleotide component of the substrate when UDP-glucose or UTP are present. This involves displacement of the β-helix structure in the direction of the substrate. In the native structure the nucleotide binding loop is relaxed and placed away from the nucleotide binding site (Figure 11.4). The second structural alteration is observed for the sugar binding loop (Thr 248 - Ile 261, *A. thaliana* numeration), which is in a closed conformation only in the presence of UDP-glucose. The *Y. lipolytica* Ugp1p model built on the basis of known *S. cerevisiae* structure

(2i5k) is in agreement with the native conformation (data not shown). Crystallization of the protein in the presence of the substrates is planned for Ugp1p.

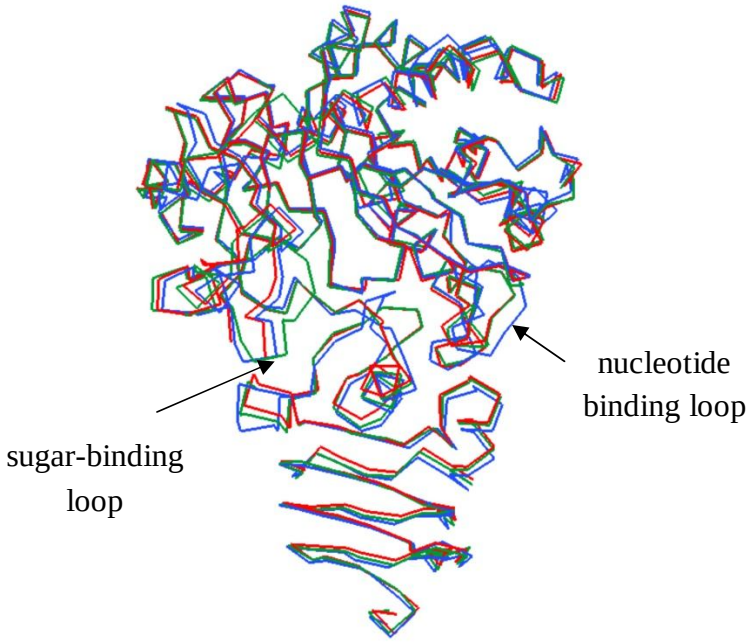


**Figure 11.4: Conformational changes of the UDPGP from *A. thaliana* upon substrate binding.**

Superposition of native (1z90, blue), UDP-glucose complex (2icy, green) and UTP complex (2icx, red) structures. The most evident conformational changes concern the nucleotide binding loop and the sugar binding loop. The image was prepared using PyMol, DeLano Scientific LLC.

## *11.5 OLIGOMERISATION OF UGP1P FROM Y. LIPOLYTICA*

Plant UDP-glucose pyrophosphorylases were found to be active exclusively as monomers [178], whereas the active mammalian counterparts displayed different oligomerisation states. Ugp1p from *S. cerevisiae* was shown to be active only as an octamer [161]. Comparison of the carboxy-terminal regions of UGPase representatives from yeast, plant and protozoa revealed the presence of highly conserved hydrophobic residues. Ugp1p from baker's yeast was crystallized as a dimeric protomer. Analysis of the oligomerisation interface disclosed a set of hydrophobic residues His 448, Thr 450, Ile 469, Val 470, Val 489 and Thr 491 (*S. cerevisiae* numbering). In the plant sequences, the residues are exchanged for polar and charged amino acids such as Ser 434, Lys 450, Thr 468, Asp 489, Asn 491, P 493 and Glu 494, which prevent formation of oligomers. Additionally, the C-terminal β18 strand, which was identified as being important for protomer formation, is replaced by a short α-helix in the plant structures. A characteristic C-terminal sequence Leu-Glu-His, with His 499 at the end is conserved throughout yeast and metazoa, but not in plants. The β18 strand as well as the hydrophobic

residues identified at the oligomerisation interface are conserved in Ugp1p from *Y. lipolytica*. Gel filtration experiments and initial LILBID data indicated that Ugp1p forms octamers.

# 12 PRÉCIS

UDP-glucose pyrophosphorylase from *Yarrowia lipolytica* displays affinity towards $Ni^{2+}$ NTA and was first detected in a contaminated sample of complex I. Following, separation from complex I, Ugp1p was purified using anion exchange chromatography. Sequence similarity studies revealed high identity to other known pyrophosphorylases. As indicated by laser-based mass spectrometry method (LILBID) Ugp1p from *Y. lipolytica* builds octamers similarly to the enzyme from *Saccharomyces cerevisiae.* The initial crystals grew as thin needles favorably in sitting drop setups. The size of the crystals was increased by employment of a micro batch technique. The improved crystals diffracted X-rays to a resolution of 3.2 Å at the synchrotron beamline. Structural characterization is under way using a molecular replacement approach based on the published structure of baker's yeast UGPase.

# Materials and Methods

For Part I and II

# 13 MATERIALS AND METHODS

## *13.1 MATERIALS*

### *13.1.1 Cell culture materials*

PANSERIN 401, serum free allround medium (Pan Biotech, P04-710401)

Hybridoma express medium, animal derived component free (PAA, U15-001)

Hybridoma cloning factor, growth adjunct (PAA, S05-015)

Hybridoma enhancing factor (Sigma-Aldrich, H2900)

L-Glutamine 200mM (Sigma-Aldrich, G7513)

Fetal bovine serum (Sigma-Aldrich, F2442)

Interleukin-6 (Sigma-Aldrich, I9646)

Water, cell culture grade (Sigma-Aldrich, W3500)

D-(+)-Glucose monohydrate (Fluka, 49159)

Dimethyl sulfoxide (Sigma, D2650)

Trypan blue 0.5% (Biochrom AG, L 6323)

MycoAlert, mycoplasma detection assay (Cambrex, LT07-118)

ELISA reagents (NaCl, $Na_2CO_3$, TrisCl, BSA, $MgCl_2$, Tween 20)

N-Dodecyl-β-maltoside (Glycon, D97002C)

Diethanolamine (Sigma-Aldrich, D8885)

Alkaline phosphate yellow liquid substrate for ELISA-pNPP (Sigma-Aldrich, P 7998)

Anti-mouse IgG (whole molecule) alkaline phosphatase conjugate (Sigma-Aldrich, A5153)

Anti-mouse IgG (Fab specific) alkaline phosphatase conjugate (Sigma-Aldrich, A2179)

Protein G Sepharose™ 4 Fast Flow (GE Healthcare, 17-0618-01)

Ni-NTA HisSorb Strips™ (Qiagen, 35023)

### *13.1.2 Proteolytic Fab production*

Immobilized ficin (Pierce, 44881)

Crystalline papain (Roche Diagnostics, 10108014001)

L-Cysteine HCl (Sigma, C7477)

N-Ethylmaleimide (Pierce, 23030)

Immobilized papain (Pierce, 20341)

Mono Q HR 5/5 (GE Health Care, 1ml, 17-0546-01)

S Hyper D (Bio Sepra, 142310)

Dynabeads® Protein G (Dynal Biotech, 100.03)

NAb™ Protein G Spin Columns (Pierce, 89957)

HiLoad 16/60 Superdex 75 prep grade (GE Health Care, 17-1068-01)

### *13.1.3 Protein chemistry*

Bacto™ Peptone (BD, 211820)

Bacto™ Yeast Extract (BD, 212720)

Agar (BD, 212304)

HAR (hexa-ammine-ruthenium III-chloride) (Sigma, 262005)

dNADH (Sigma, N8129)

DBQ (Alexis, 270-293-M010)

NADPH (Sigma, N7505)

Dodecyl-nonaethylene-glycol-ether – $C_{12}E_9$ (Sigma, P9641)

Viva Spin concentrators 30, 000 MWCO (Sartorius, VS0424)

Viva Spin concentrators 100, 000 MWCO (Sartorius, VS0444)

Centriprep YM-50 concentrators 50,000 MWCO (Millipore, 4310)

Chelating Sepharose™ Fast Flow (GE Health Care, 17-0575-01)

Gel filtration column TSK G4000sw, 21,5 mm x 30 cm (TOSOH Bioscience, 06729)

PVDF membrane (Millipore, IPVH07850)

Serva Blue G (Serva, 35050)

p-Coumaric acid (Sigma, C9008)

Luminol sodium salt (Sigma, A4685)

SigmaFast™BCIP®/NBT tablets (Sigma, B5655)

Anti-mouse IgG (Fab specific) alkaline phosphatase conjugate (Sigma, A2179)

Anti-mouse IgG alkaline phosphatase conjugate (Sigma, A5153)

Ani-rabbit IgG peroxidase conjugate (Sigma, A0545)

Anti-mouse IgG peroxidase conjugate (Sigma, 2554)

SeeBlue® Plus2 Pre-Stained Standard, molecular mass standard (Invitrogen, LC5925)

PageRuler™ Prestained Protein Ladder, molecular mass standard (Fermentas, SM 0671)

### *13.1.4 Surface plasmon resonance*

Sensor chip CM5 (BR-1000-14, Biacore)

Sensor Chip NTA (BR-1000-34, Biacore)

NSB reducer (BR-1006-91, Biacore)

Mouse antibody capture kit (BR-1008-38, Biacore)

### *13.1.5 Crystallization materials*

24 well VDX™ plates (Hampton Research, HR3-172)

72 well microbatch plates (Hampton Research, HR3-122)

96 Well IMP@CT™ plates (Greiner Bio-One, 673 170)

AxyGem™ 96-well plates (Axygen Biosciences, CP-AxyGem-96-50)

Greiner CrystalQuick 96-well plates (Sigma, Z666130)

Siliconized cover slides (Hampton Research. HR3-215)

Micro-bridges™ (Hampton Research, HR3-342)

Silicon (Hampton Research, HR3-415)

Paraffin oil (Hampton Research, HR3-411)

Al's oil (Hampton Research, HR3-413)

Glycerol anhydrous (Fluka, 49767)

PEG 3350 (Hampton Research, HR2-591)

PEG 400 (Hampton Research, HR2-603)

QuikOptimize™ (Hampton Research, HR2-576)

Seed Bead™ (Hampton Research, HR2-320)

<u>Commercial crystallization screens</u>

JBScreen Membrane 1-3 (Jena Biosciences, CS-306L)

MembFac™ (Hampton Research, HR2-114)

PEG/Ion Screen™ (Hampton Research, HR2-126)

MemStart™ (Molecular Dimensions, MD1-21)

Structure Screen 1 (Molecular Dimensions, MD1-01)

Structure Screen 2 (Molecular Dimensions, MD1-02)

Crystal Screen™ (Hampton Research, HR2-110)

Crystal Screen 2™ (Hampton Research, HR2-112)

NexTal MbClass Suite I (Qiagen, 130711)

NexTal MbClass Suite II (Qiagen, 130712)

Crystallization Kit for Membrane Proteins (Fluka, 73513-1KT-F)

Additive Screen™ (Hampton Research, HR2-428)

StockOptions™ (Hampton Research, HR2-245)

### *13.1.6 Monoclonal antibodies*

Mouse hybridoma clones used in this work (Table 13.1) were provided by Dr. Volker Zickermann.

| Antibodies | Subtype | Binding epitope |
|---|---|---|
| 1F5 | G2a | NESM |
| 31A8 | G1 | conformation specific |
| 44G10 | G1 | conformation specific |

Table 13.1 Cell lines used in the project

## *13.2 HYBRIDOMA CELL CULTURE TECHNIQUES*

### *13.2.1 General aspects*

Cell lines used in this work were grown according to standard suspension cell culture techniques. Use of growth enhancing factors was dependent on the clone. Monoclonal antibodies were produced at low concentrations of fetal calf serum (1%) to minimize amount of immuneglobulins of external origin. It was possible to cultivate the clones in the absence of antibiotics.

<u>Medium composition</u>

PANSERIN 401 (Pan Biotech) or hybridoma express medium (PAA)

| | |
|---|---|
| 18-1% | fetal calf serum |
| 2 mM | L-glutamine |
| 100 U/ml | interleukin-6 |
| 1-2% | enhancing factor (optional) |
| 1% | D-(+)-glucose (below fetal calf serum concentration of 2%) |

### *13.2.2 Thawing of frozen stock cultures*

Frozen stock cultures were thawed fast in a 37°C water bath. Directly after thawing, the vial was briefly immersed in methanol before transfer to a laminar flow bench. Ice cold standard medium was added to thawed cells in a drop wise manner and transferred to a 15 ml tube. The cells were centrifuged for 5 minutes at 200 x *g*. The supernatant was removed, the sediment was resuspended gently and 37°C standard medium was added drop wise. Cells were cultured in 6 well plates.

### *13.2.3 Single cell cloning*

Single cell cloning by serial dilution in a 96 well plate was conducted for all of the clones. This was done according to standard technique. In short; 100µl of standard medium was added to all (except A1) of the wells in 96 well plate. 200µl of cell suspension was added to well A1. Using the same tip, 100µl from A1 were transferred to B1 and mixed. In the same manner serial dilution proceeded in direction of H1. Next, using an eight-channel pipettor, an additional 100µl of standard medium was added to every well in column 1 giving a final volume of 200µl. Then, using the same tips 100µl from the wells of first column were transferred to those in the second column (A2-H2). Such repetitions were carried out for the entire 96 well plate resulting in 100µl of cell suspension in each well. The wells were fed with an additional 100 µl of standard medium and the plate was incubated at 37°C in a humidified $CO_2$ incubator. After 7-10 days single cell colonies were selected by ELISA test and subsequently transferred to 24, and finally 6 well plates.

### *13.2.4 Cell vitality determination*

The trypan blue stain was used to determine the vitality of the cells [179]. Equal amounts of cell suspension and 0.5% Trypan blue were mixed and analyzed by means of a hemocytometer. The intact cell membrane of living cells remains impermeable for this diazo-dye. Dead cells in contrast absorb it and become dark blue. The ratio between blue and colorless cells is a measure for cell vitality.

### *13.2.5 Monoclonal antibody production*

The hybridoma cultivation was conducted according to a common strategy for all clones, first in 6 well plates and finally in 75 ml bottles in upright position (C. Hunte, personal communication). The fetal calf serum concentration was decreased, starting with 18%, followed by 9%, 4%, 2% and finally 1%. Clones 1F5 and 44G10 required growth enhancing factors at and be-

low fetal calf serum concentrations of 4%. At this point standard medium was supplemented with 1% glucose. At 1% fetal calf serum cells were transferred to standing bottles and diluted 1:2 with standard medium (1% fetal calf serum, 1% glucose). Dilution was repeated after 2 days and clones grew undisturbed for the following 10-14 days. Cell culture supernatant containing monoclonal antibodies was harvested, sterile filtered and stored at -80 $^{o}$C.

### *13.2.6 Freezing of cells*

Only vital cells were frozen for stock collection. 3 ml of cell suspension (one well of a six well plate) were sedimented at 200 x *g*. The pellet was resuspended in 1 ml of cold cryo medium in a drop wise manner. Cryovials were placed in a pre-cooled styrofoam box and stored for one hour in -20$^{o}$C. Afterwards the vials were moved to -80$^{o}$C to further cool down slowly. After one day, vials were frozen and stored in liquid nitrogen.

Cryo medium composition

PANSERIN 401 (Pan Biotech) or hybridoma express medium (PAA)
10% fetal calf serum
10% DMSO
100U/ml interleukin-6
2 mM L-glutamine
2% supplement (optional)

### *13.2.7 ELISA*

Functionality of the produced monoclonal antibodies was verified by ELISA. Each of the wells in a 96-well plate was coated with 100µl complex I (10 µg/ml in 0.2M $Na_2CO_3$ buffer). After one hour, the plate was washed three times with 200 µl of wash buffer (0.9% NaCl/0.1% Tween 20). Blocking was done with 200 µl of blocking buffer (150 mM NaCl, 1% BSA, 50 mM TrisCl, pH 7.5) for 15 minutes. The plate was washed as before. Non-diluted cell culture supernatant (50-100 µl) was added to each well and incubated for 60 minutes. A wash step was carried out to remove any unbound material. Secondary antibodies, anti-mouse alkaline phosphatase conjugate (1:1000 in 150 mM NaCl, 0.5% BSA, 0.05% Tween, 50 mM Tris-Cl, pH 7.5) were incubated with primary antibodies for an hour. The plate was washed thoroughly. 100 µl of substrate solution (10% diethanolamine pH 9.8, 0.5 mM $MgCl_2$, 1

mg/ml pNPP) was applied to the wells. After 30 minutes, the results were analyzed in a microplate reader at 405/450 nm.

### *13.2.8 Native ELISA*

Adsorption of the antigen on a plastic surface can result in its denaturation. To assure native conditions, Ni-NTA HisSorb Stripes (Qiagen) were used to immobilize Complex I by means of the His-Tag. Coating was done with 100µl complex I 15µg/ml in coating buffer (50mM potassium phosphate, pH 7.5, 300 mM NaCl, 0.1% N-dodecyl-β-maltoside). After an hour the plate was washed three times with 200 µl wash buffer (20 mM Tris-Cl, pH 7.5, 300 mM NaCl, 0.03% N-Dodecyl-β-maltoside, 0.2% BSA). 100 µl of cell culture supernatant was applied to the plate after it was mixed 9:1 with dilution buffer (2 M Tris-Cl, pH 8.0, 10% N-Dodecyl-β-maltoside). The plate was washed after an hour. Goat anti-mouse alkaline phosphatase conjugate antibodies (1:1000 in wash buffer) were incubated with the supernatant for 60 minutes. The plate was thoroughly washed to remove unbound material. Then, 100 µl of the alkaline phosphatase substrate solution (10% diethanolamine pH 9.8, 0.5 mM $MgCl_2$, 1 mg/ml pNPP) was applied to the plate and incubated for 30 minutes. Next, the results were analyzed in a microplate reader at wavelength of 405/450 nm.

### *13.2.9 Cell culture sterility*

Mouse hybridoma cell lines were cultivated without use of antibiotics. The plates were inspected using a light microscope in regular time intervals. The presence of mycoplasma, was excluded using the commercial detection assay MycoAlert ™ (Cambrex).

## *13.3 PURIFICATION OF MONOCLONAL ANTIBODIES*

Monoclonal antibodies were purified via one step affinity chromatography using a protein G column connected to a low pressure liquid chromatography system (BioLogic ™ BIORAD). Protein G is a bacterial cell wall protein from *Streptococci* group G. To reduce unspecific binding, the albumin and cell surface binding sites were eliminated in recombinant protein G, which is commonly expressed in *E.coli.* The Fc region binds most mammalian antibodies, in the same manner as Protein A. In this project, protein G immobilized by the CNBr method to Sepharose 4 Fast Flow was used (GE Healthcare).

Isolation of immunoglobulins from cell culture supernatants was carried out as follows. A 5 ml column was pre-equilibrated with four column volumes of 20 mM sodium phosphate buffer, pH 7.0 at a flow rate of 1 ml/min. The cell culture supernatant was applied to the col-

umn according to its binding capacity (6 mg IgG/ml drained medium). Loading was usually done over night at 4°C because the flow rate was limited to 0.5 ml/min. Then, the column was washed with 15 milliliters 20 mM sodium phosphate buffer, pH 7.0. Antibodies were eluted with 6 column volumes of 0.1 M glycine buffer, pH 3.0 directly afterwards. In order to avoid possible denaturation of IgGs at low pH, 28 µl of 1 M Tris-Cl, pH 9.0 buffer were placed in the collection tubes just before the program was started. The peak fractions were loaded on a 10% SDS-PAGE to verify the presence and purity of the antibodies. Concentration was performed in VivaSpin™ concentrators (Sartorius) MWCO 100000, along with buffer exchange for 0.01 M PBS, pH 7.2. The purified antibodies were shock frozen in aliquots and stored in liquid nitrogen. Repeated thawing and freezing was avoided.

The protein G column was regenerated with 2 column volumes of 0.1 M glycine buffer, pH 3.0, and re-equilibrated with 4 column volumes of 20 mM sodium-phosphate buffer, pH 7.0. Next, it was washed with 15 ml water and stored in 15% ethanol, 10 mM Tris-Cl, pH 7.2 at 4 °C.

## *13.4 AFFINITY MEASUREMENTS OF MONOCLONAL ANTI-BODIES AND Fab FRAGMENTS USING SURFACE PLASMON RESONANCE (BIACORE)*

The affinities of the monoclonal antibodies 1F5, 31A8 and 44G10 towards complex I were measured by surface plasmon resonance and were carried out on a Biacore X100™ System. The experiments were performed following two approaches. In the first protocol monoclonal antibodies (ligand) were immobilized on CM5 sensor chip via anti-mouse antibodies (Mouse antibody capture kit, Biacore), which in turn, were covalently attached to the chip by amine coupling. The final concentration of the ligand was 3 µg/ml. The running buffer was 150 mM NaCl, 20 mM Tris-Cl, 1mM EDTA, pH 7.4 supplemented with 0.025 % DDM. Complex I (analyte) was probed on the antibody coated chips at increasing final concentrations (0.1, 0.2, 0.5, 1, 2, 5, 10, 20 nM) depending on the antibody. Regeneration of the sensor chip was performed using 0.1 M glycine buffer pH 1.7. In the second approach, complex I (ligand) was immobilized on the nickel coated NTA sensor chip via the His-tag. The final concentration of complex I was 5 nM, which allowed ultra-low density surface measurements. Monoclonal antibodies (analyte) were probed on the complex I-derivatized chip with increasing concentrations (0.5, 1, 2, 5, 10 nM). 350 mM EDTA in the running buffer was used to regenerate the chip. The affinity of Fab fragments was assessed only by the second approach.

In order to evaluate the effect of NADPH on antibody binding, complex I was pre-incubated with increasing concentrations of NADPH (0.1, 1, 5, 10 µM). A null concentration of NADPH (complex I alone) was included in the first cycle of the experiment as a control. The incubation took place for at least 30 minutes on ice. The sample was probed on an antibody-coated chip and the relative response at the end of each binding event was recorded. The relative response was plotted against the NADPH concentration to assess the influence of NADPH on antibody binding to complex I.

## *13.5 PRODUCTION OF PROTEOLYTIC Fab FRAGMENTS*

### *13.5.1 Digestion of immunoglobulins*

Three different methods for production of proteolytic antibody fragments were employed in this project. Immobilized papain digestion was chosen as a standard procedure.

#### 13.5.1.1 Immobilized ficin (Pierce)

Monoclonal antibodies were fragmented using immobilized ficin pre-packed columns (Pierce) according to the supplier's procedure.

#### 13.5.1.2 Crystalline papain (Roche Diagnostics)

Fragmentation of immunoglobulins with crystalline papain was based on a protocol by Adamczyk *et al.*, [115]. Purified antibodies (1-2 mg/ml) were dialyzed against sample buffer (1 mM EDTA, 50 mM sodium phosphate, pH 7.0). Papain (10 µl, 10 mg/ml suspension) was mixed with 90 µl freshly prepared activation buffer (1 mM EDTA, 10 mM cysteine, 50 mM sodium phosphate, pH 7.0) and was activated for 10 minutes at 37 $^{o}$C. Digestion was carried out at different papain/antibody ratios (0.2, 0.5, 1.0, 2.0, 5.0, 15.0 w/w %) in order to find optimal digestion conditions. The mixtures were incubated at 37$^{o}$C for 2 hours. The reaction was terminated by addition of N-ethylmaleimide (NEM) to a final concentration of 30 mM. Results were analyzed on 10 % SDS-PAGE. The reaction time, amount of cysteine and NEM were optimized in additional experiments.

#### 13.5.1.3 Immobilized papain (Pierce)

Digestion of monoclonal antibodies with immobilized papain was performed according to the supplier's suggestions (Pierce). 0.5 ml of concentrated IgGs (10-20 mg/ml in sample buffer 20 mM sodium phosphate, 10 mM EDTA, pH 7.0) were diluted with an equal amount of digestion buffer (20 mM sodium phosphate, 20 mM cysteine HCl, 10 mM EDTA, pH 7.0). Using

a cut pipette tip, 0.5 ml of the immobilized papain slurry was transferred to a 15 ml test tube. Papain was activated by two fold washing with 4 ml of freshly prepared digestion buffer. Both washes were discarded. The gel was separated from the buffer by centrifugation and resuspended in 0.5 ml of digestion buffer. 1 ml of antibody solution was added to 1 ml of activated papain suspension and the test tube was placed in a thermo-shaker. The reaction was carried out at 37$^{o}$C, 750 rpm for 14-16 hours. The reaction was stopped by addition of 1.5 ml of 10 mM Tris-Cl, pH 7.5 to the digest. Next, the sample was centrifuged to separate the supernatant containing IgG fragments from immobilized papain.

### *13.5.2 Purification of proteolytic Fab fragments*

#### 13.5.2.1 Anion exchange – Mono Q column (GE Health Care)

The immobilized papain digest was dialyzed into 50 mM NaCl, 25 mM Tris-Cl, pH 8.0, and applied to the Mono Q column (1 ml, GE Health Care) pre-equilibrated with the same buffer. The separation was achieved by means of a linear gradient (10 column volumes) with 400 mM NaCl as a target concentration. In order to increase resolution, the final concentration of the gradient was decreased to 250 mM NaCl. The column was prepared in 25 mM NaCl, 25 mM Tris-Cl, pH 8.0 buffer. The column was regenerated with 1 ml 1 M NaCl, 25mM Tris-Cl, pH 8.0. After re-equilibrating with the start buffer, the column was washed with water and stored in ethanol at 4 $^{o}$C. The peak fractions were analyzed by 10 % SDS-PAGE.

#### 13.5.2.2 Cation exchange – S Hyper D column (Bio Sepra)

The column was pre-equilibrated with 50 mM sodium-acetate buffer, pH 5.0. The digestion mixture was prepared in the start buffer and loaded on the column. Fractions were eluted using a salt gradient (10 column volumes) with a final concentration of 400 mM NaCl in 50 mM sodium acetate buffer, pH 5.0. 1 ml of 1 M NaCl, 50 mM sodium acetate buffer, pH 5.0 was used to regenerate the column. Finally, the column was re-equilibrated with the start buffer, washed with water and stored in ethanol at 4 $^{o}$C. Eluted fractions were analyzed by 10% SDS-PAGE.

#### 13.5.2.3 Immobilized protein G magnetic beads (Dynabeads®Protein G)

Separation of the antibody fragments was done for three volumes of magnetic beads: 14, 30 and 100 µl. The beads were washed three times with 0.5 ml of sodium acetate buffer, pH 5.0. 100 µl of 0.5 mg/ml immobilized papain digestion mixture was added to each of the three reaction tubes and incubated at room temperature for 60 minutes under gentle shaking. Start-

ing at time zero, samples for analysis were taken every 20 minutes (in total 4 samples per each reaction tube). After washing, the beads were treated twice with 30 µl 0.1 M citrate buffer, pH 3.0 to elute the bound IgGs and their fragments. For reuse, magnetic beads were brought to neutral pH directly after elution and stored in buffer supplemented with 0.05% Tween 20®.

#### 13.5.2.4 Immobilized protein G columns – NAb™ Protein G Spin Columns (Pierce)

The separation of antibody fragments was performed according to the suppliers' protocols. Briefly, a 1 ml column was pre-equilibrated with binding buffer (20 mM sodium-phosphate, buffer, pH 7.0). 2 ml of the IgG digest was applied to the column and incubated at room temperature with end-over-end mixing for 10 minutes. The unbound fractions were separated by centrifugation at 1,000 x *g*. The column was washed three times with the binding buffer. 0.1 M glycin buffer, pH 3.0 was used for elution of the bound sample. Fractions were analyzed by 10% SDS-PAGE, as well as by Western Blot. The column was regenerated with the low pH buffer, re-equilibrated with PBS buffer (0.1 M phosphate, 0.15 M sodium chloride, pH 7.2) and stored in 0.02% sodium azide in PBS at 4 $^{o}$C.

#### 13.5.2.5 Size exclusion chromatography – HiLoad 16/60 Superdex (GE Health Care)

Purification of Fab fragments was done with a SEC column connected to an HPLC system. The column was pre-equilibrated with 150 mM NaCl, 50 mM sodium-phosphate, pH 7.2 buffer. The peak fractions were analyzed by 10% SDS-PAGE and pooled according to purity. The column was washed with water and stored in 15% ethanol, 10 mM Tris-Cl, pH 7.2 buffer at 4$^{o}$C.

### *13.5.3 Storage of purified Fab fragments*

The Fab fragments were sterile filtered directly after concentrating them and were stored in 20 mM sodium phosphate, 10 mM EDTA, pH 7.0 buffer at 4$^{o}$C for 2-3 weeks.

## *13.6 GENERAL PROTEIN CHEMISTRY METHODS*

### *13.6.1 Growth of Yarrowia lipolytica*

A *Yarrowia lipolytica* strain lacking sulfur-transferase [180] was used in this project. Colonies were grown on YPD plates. For pre-cultures 30 ml YPD medium were inoculated with a sin-

gle colony and grown in 300 ml shaking flasks at 28°C for 16-18 hours. The pre-culture was used to start a 400 ml culture that was grown in 2 L shaking flasks at 28°C for 8 hours. This culture was used to initiate fermentation in a 10 L fermenter (Biostat). After 16-18 hours fermentation yielded 45-55 g cells/L (wet weight). The cells were shock frozen and stored at -80°C.

| YPD medium | YPD agar plates |
|---|---|
| 10% Bacto™ Yeast Extract | 1L YPD medium |
| 20% Bacto™ Peptone | 15 g agar |
| 2,5% D-glucose | |

### *13.6.2 Preparation of mitochondrial membranes*

200 g of cells were resuspended in 500 ml buffer (600 mM sucrose, 1 mM EDTA, 20 mM MOPS, pH 7.2). The cell walls were broken in a cooled cell disintegrator (Bernd Euler Biotechnologie, Frankfurt) filled with 0.5 mm glass beads for 2 hours in the presence of 2 mM PMSF (protease inhibitor). The cell debris was separated from the supernatant containing the mitochondrial membranes by a 30 minute centrifugation at 2000 x *g*. The supernatant was ultracentrifuged for an hour at 100,000 x *g*. The pellet (mitochondrial membranes) was homogenized in a glass-ceramic Dounce homogenisator and resuspended in the same buffer as before, without EDTA. The ultracentrifugation step was repeated and the mitochondrial membranes were shock frozen and stored at -80°C.

The quality of the membranes was characterized using specific NADH:HAR oxidoreductase and dNADH:DBQ oxidoreductase activity tests (see 1.5.6 Activity measurements).

### *13.6.3 Purification of complex I*

His–tagged complex I was purified form isolated mitochondrial membranes by affinity chromatography according to a modified protocol [105]. The membranes were solubilized with 0.8 g/g N-dodecyl-β-maltoside. The $Ni^{2+}$-NTA column was pre-equilibrated with buffer containing 400 mM NaCl, 20 mM sodium phosphate, 55 mM imidazol, pH 7.2 and 0.025 % N-dodecyl-β-maltoside. The detergent was exchanged for $C_{12}E_9$ during wash step on the $Ni^{2+}$-NTA column (wash buffer: 400 mM NaCl, 20 mM sodium phosphate, 55 mM imidazol, pH 7.2 with 0.015% $C_{12}E_9$). Elution was performed using 140 mM imidazol in the wash buffer. Next, the sample was loaded on a size exclusion column, equilibrated with 100 mM NaCl, 20

mM Tris, 1 mM EDTA, pH 7.3 with 0.02 % $C_{12}E_9$. The purified complex I was concentrated in VivaSpin™ concentrators (Sartorius) MWCO 100,000 and sterile filtered. The quality of the isolated enzyme was assayed using specific NADH:HAR oxidoreductase and dNADH:DBQ oxidoreductase activity tests (13.6.6). The purity and subunit composition was checked by Tricine-SDS-PAGE [181] and dSDS-PAGE [170]

### *13.6.4 Protein quantification*

Protein concentration was determined according to the modified protocol of Lowry et al., [182].

### *13.6.5 Doubled SDS-Polyacrylamide Gel Electrophoresis*

Subunits of isolated complex I were resolved using Tricine dSDS-PAGE [170]. In short, lanes cut out from the first dimension gels (10% polyacrylamide, 6 M urea) were incubated in low pH buffer (100 mM Tris, 150 mM HCl, pH 2) for 30 minutes and subsequently analyzed by second dimension SDS-PAGE (16% polyacrylamide).

### *13.6.6 Activity measurements*

#### 13.6.6.1 NADH:HAR oxidoreductase activity

The measure of detergent- and inhibitor-insensitive NADH:HAR (hexa-ammine-ruthenium(III)-chloride) oxidoreductase activity was the NADH oxidation rate ($E_{340}$-$E_{400}$) in the presence of 200 µM NADH and 2 mM HAR in 20 mM HEPES, 250 mM sucrose, 0.2 mM EDTA, 2 mM $NaN_3$, pH 8.0 [183] . In this assay HAR serves as an artificial electron acceptor. The reaction was started by addition of either mitochondrial membranes or purified complex I and was monitored using a Shimadzu UV 300 spectrophotometer. The NADH:HAR oxidoreductase activity is specific for complex I [183] and depends on the presence of FMN [184]

#### 13.6.6.2 dNADH:DBQ oxidoreductase activity

For determination of complex I catalytic activity, dNADH oxidation ($E_{340}$-$E_{400}$) was measured in the presence of the ubiquinone analogue DBQ (electron acceptor). The assay was performed in 30$^{o}$C buffer (20 mM Na-MOPS, 50 mM NaCl, 2 mM KCN, pH 7.2) supplemented with 100 µM dNADH and 80 µM DBQ. The reaction was started by addition of decylubiquinone and was followed on Shimadzu UV 300 spectrophotometer. Since, NADH serves also as a substrate for the alternative NADH-dehydrogenase, dNADH is used to differentiate between complex I and alternative NADH-dehydrogenase activities [185].

### *13.6.7 Western blotting*

Proteins separated by PAGE were blotted onto polyvinylidene fluoride (PVDF) membrane (Immobilion P, Millipore) in a semidry mode. Blotting cartoons were soaked in blotting buffers (cathode buffer: 300 mM 6-aminocaproic acid, 30 mM Tris, pH 9.2; anode buffer: 300 mM Tris, 100 mM Tricine, pH 8.7). The PVDF membrane was rinsed with methanol. Gels were blotted overnight at 50 mA and 20 V. Blotted membranes were stained for 5 minutes with 0.02% SBG, 25 % methanol and 10 % acetic acid. De-staining was done 3 times for 10 minutes using 25% methanol and 10 % acetic acid.

### *13.6.8 Immunodetection*

#### 13.6.8.1 Chemiluminescent detection

The blotted membranes were blocked for 45 minutes with 0.5% Tween 20® in PBS. Next, the membranes were washed once for 15 minutes and twice for 5 minutes with PBS buffer containing 0.1% Tween 20®. Primary antibodies (anti *S. cerevisiae* Ugp1p produced in rabbit), diluted 1:5,000 were incubated with the membranes for 3 hours at room temperature. The blots were washed as before. Secondary antibodies, (goat anti-rabbit IgG horse radish peroxidase conjugate in case of Ugp1p detection and anti-mouse HRP conjugate for Fab detection) were diluted 1:20,000 in PBS buffer and incubated with the membranes for one hour at room temperature. The washed membranes were incubated in a 1:1 mixture of ECL-1 solution (2.5 mM Luminol, 450 µM p-coumaric acid) and ECL-2 (0.03% hydrogen peroxide). Chemiluminescence of the Luminol oxidation by the peroxidase could be detected on X-ray film.

#### 13.6.8.2 Chromogenic detection

Except for the last step, the procedure was identical to the chemiluminescent detection (13.6.8.1). Anti-mouse IgG (Fc specific) alkaline phosphatase conjugate, as well as Fab specific immunoglobulins were used as secondary antibodies. The detection was performed using SigmaFast™BCIP®/NBT tablets. The BCIP/NBT reaction leads to formation of formazan, which is an intensely blue, insoluble dye. The membranes were incubated in BCIP/NBT solution until the color appeared. The reaction was stopped with water.

### *13.6.9 Determination of lipid phosphorus by malachite green assay*

The lipid content in purified complex I and complex I/Fab co-complex was determined indirectly using the malachite green assay as described in [186]. Briefly, an 11 point standard

curve was prepared (0-40 nmol potassium phosphate). 200 µl of 70% perchloric acid was added to the protein sample (glass reaction tube) and standard solutions. The protein sample (as double determination) was incubated at 180°C for 30-60 minutes. After cooling, 200 µl of water was added. Next, 2 ml of malachite green/phosphomolybdenum mixture was added to each of the reaction tubes, including standards. Following 30 minutes incubation time at room temperature, the absorbance at 660 nm was measured using a UV-160A Shimadzu spectrophotometer.

## *13.7 PREPARATION OF COMPLEX I Fab CO-COMPLEXES*

The initial steps in complex I preparation were as described in 1.5.3. After elution from the $Ni^{2+}$-NTA column, the sample was concentrated in Centriprep YM-50 concentrators (Millipore). Complex I was mixed with purified Fab fragments in a molar ratio of 1:2-3 respectively. The binding reaction was performed either at analytical (< 1 ml) or preparative scale (≤ 5 ml). At the preparative scale, Fab solution was added to complex I and the mixture was stirred gently in a 10 ml cylinder at 4°C for at least 30 minutes. After that, the sample was sterile filtered and loaded on a size exclusion chromatography column (TSK G4000sw, TOSOH Bioscience) to verify the stability of the co-complex and remove the unbound excess of Fab molecules. Gel chromatography was performed in 100 mM NaCl, 1 mM EDTA, 20 mM Tris-Cl, pH 7.2 with 0.02% $C_{12}E_9$ on a column connected to an Äkta FPLC system (GE Health Care). For analytical scale experiments, a TSK G300swxl column was used (TOSOH, Bioscience). Peak fractions were analyzed by SDS-PAGE and Western Blot.

## *13.8 PURIFICATION OF UGP1P FROM YARROWIA LIPOLYTICA*

UDP glucose pyrophosphorylase displays affinity to $Ni^{2+}$-NTA and was co-purified with complex I. Size exclusion chromatography fractions containing Ugp1p were pooled and concentrated. After buffer exchange with 50 mM NaCl, 1mM EDTA, 20 mM TrisCl, pH 7.5 the sample was applied to a Mono Q column, which was pre-equilibrated with the same buffer. The separation was performed using a linear salt gradient with a NaCl target concentration of 350 mM. The peak fractions were analyzed by 10% SDS PAGE as well as by Western blotting using *S. cerevisiae* anti-Ugp1p antibodies (courtesy of Prof. Jared Rutter, University of Utah School of Medicine). Purified Ugp1p was frozen in liquid nitrogen or used directly for crystallization.

## *13.9 CRYSTALLIZATION TECHNIQUES*

### *13.9.1 Preparation of the CI/Fab crystallization sample*

The final detergent concentration in the CI/Fab solution was 0.02 % $C_{12}E_9$. The crystallization sample was prepared in a buffer containing the same amount of the primary detergent in addition to other detergents and additives. Most commonly phosphocholine/Cymal 4™ or DQA (2-decyl-4-quinazolinyl amine) were used in the dilution buffer and crystallization solution. Whereas, $C_{12}E_9$ was always present in the crystallization buffer, the secondary detergents varied. When the amount of endogenous lipids was higher than ~130 nmol phosphocholine/mg complex I, no additional lipids were used in the dilution and crystallization buffers.

### *13.9.2 Vapor diffusion*

Crystallization experiments were carried out at 4, 10 and 18$^{o}$C.

#### 13.9.2.1 Hanging drop

The hanging drop method was performed using 24-well VDX™ plates (Hampton Research). Typically, drops between 1-5 µl were placed on siliconized glass cover slides (Hampton Research) over 1 ml well solution.

#### 13.9.2.2 Sitting drop

Sitting drop experiments were performed using polypropylene Micro-Bridges® (Hampton Research). Drop volumes between 1 and 5 µl were used. The well solution volume was 1 ml.

#### 13.9.2.3 pH fine tuning of the crystallization conditions

In order to find optimal conditions for crystal growth a fine tuning of the pH of the crystallization buffers was performed as follows: buffer A (for example: 6% PEG 3350, 12% glycerol, 40 mM calcium acetate, pH 6.0) was mixed with buffer B (for example: 6% PEG 3350, 12% glycerol, 40 mM calcium acetate, pH 7.0) in the wells at variable ratios: 100 µl A + 900 µl B, 200 µl A + 800 µl B, 300 µl A + 700 µl B etc. The reservoir volume was 1 ml.

#### 13.9.2.4 pH/PEG fine tuning of the crystallization conditions

In this experiment, not only the influence of pH of the buffers was tested in minute value intervals, but also the PEG concentration was altered in small steps. The protein was mixed 1:1 with crystallization buffers of increasing PEG concentrations (4, 5, 6, 7 and finally 8% PEG,

10% glycerol 100 mM sodium potassium phosphate, pH 5.2) and placed over reservoir solution (8% PEG 3350, 10% glycerol 100 mM sodium potassium phosphate, pH 4.5).

#### 13.9.2.5 pH gradient vapor diffusion

The pH gradient in vapor diffusion experiments (hanging and sitting drop) was achieved by adjusting the reservoir solution one or two pH units below the pH value of the drop solution. Example, reservoir solution: 8% PEG 3350, 10% glycerol 100 mM sodium-potassium-phosphate, pH 4.3 versus drop solution: 8% PEG 3350, 10% glycerol 100 mM sodium-potassium-phosphate, pH 5.2.

#### 13.9.2.6 Vapor diffusion with oil barrier

An oil barrier was introduced into vapor diffusion experiments (hanging and sitting drop) to slow down the supersaturation process. The oil layer thickness was varied in the screening procedure. Silicon, paraffin oil and Al's oil (50% silicon:50% paraffin oil) as well as their mixtures were tested. The experiments were carried out at 18 $^{o}$C.

### *13.9.3 Dehydration of the co-complex crystals*

The purpose of the dehydration experiments was to improve the diffraction range of the co-complex crystals. The dehydration solution withdraws water molecules from the crystals, which can lead to tighter packing and at the same time increase the order of the crystal packing. The dehydration experiments were carried out by transfer of the cover slide with the protein drop containing crystals over a well with 1 ml dehydration solution (50% PEG 400, 20% glycerol, 40 mM calcium acetate, pH 7.3 or 100 mM sodium potassium phosphate, pH 5.2). After 1-3 hours the crystals were frozen by plunging in liquid nitrogen without use of additional cryoprotectant. The experiments were performed at 10 $^{o}$C.

### *13.9.4 Soaking of the co-complex crystals in $Ta_6Br_{12}^{2+}$*

The compound $Ta_6Br_{12}^{2+}$ (dodecabromohexatantalum cation) was reported in literature as a promising derivatization agent. Additionally, the cluster, having a roundish structure may incorporate into the crystal structure providing more ordered packing of the crystals in some cases [187]. Moreover, the green color of $Ta_6Br_{12}^{2+}$ allows easy control of the soaking process. For the soaking experiments, 10 mM water solution of $Ta_6Br_{12}^{2+}$ was prepared. The compound was kindly provided by Prof. Grzegorz Bujacz (Institute of Technical Biochemistry,Technical University of Lodz, Poland). The crystals were fished from the original drops and transferred to fresh drops with reservoir solution of the same volume, where the $Ta_6Br_{12}^{2+}$

end concentration was 0.01, 0.02, 0.05 and 0.1 mM. After 24 hours the crystals displayed green color, which was gone from the drops. Alternatively, few crumbs of $Ta_6Br_{12}^{2+}$ were added directly to the drop containing crystal of interest. No damage to the crystals was observed for either of the methods. The crystals were cryoprotected according to standard procedure (described in 13.9.8.1).

### *13.9.5 Microbatch*

Crystallization under oil was performed using 72-well microbatch plates (Hampton Research) or in 96 Well IMP@CT™ plates (Greiner Bio-One). Silicon, paraffin oil and Al's oil as well as their mixtures were tested in different volumes. Plates were covered with an oil layer. Protein drops were laid on the bottom of the wells and precipitant solution was added subsequently. Drop volumes were usually 1-2 µl. The experiments were carried out at 18 $^{o}$C.

### *13.9.6 Seeding*

Seed stock was prepared using 4-6 crystals, which were transferred to a stabilizing solution (of 4% higher PEG 3350 concentration with respect to the well of the crystal's origin) and crushed using the Seed Bead™ kit (Hampton Research). Serial dilutions were prepared from the stock seed by 10-fold dilution in the range from 1 x $10^0$ to 1 x $10^{-7}$. Three seeding techniques were applied:

1) Direct seeding, where 0.5 µl of seed from each dilution was added to 2 µl non-pre-equilibrated drop (1:1 diluted with reservoir solution).

2) Streak seeding, with use of a cat whisker on a non-pre-equilibrated drop.

3) Streak seeding, with use of a cat whisker on a pre-equilibrated drop.

### *13.9.7 Screening for optimal conditions*

#### 13.9.7.1 'Traditional' screening

Screening was performed in 24 well plates using either specifically designed solutions or commercial screens (Hampton Research, Qiagen, Molecular Dimensions, Fluka, Jena Biosciences). The protein drops were usually 1-4 µl and the well solution was 1 ml. This method was more time- and material-consuming, but avoided problems associated with up-scaling of the crystallization conditions.

#### 13.9.7.2 Automated screening and monitoring

Two types of crystallization robots were used for automated screening in this project: Cartesian MicroSys™ (Genomic Solutions, UK) and Mosquito™ (TTP Labtech, UK). Experiments were carried out in 96 well plates (see 'Materials' section). Commercial, as well as self-prepared solutions were used for testing. The drop volume working range 25 nL – 120 µl allowed extensive screening with sparse material. The crystallization experiments were monitored at 18$^{o}$C using Crystal Farm 400 and at 4$^{o}$C, using Crystal Farm 150 (Bruker).

### *13.9.8 Cryoprotection and freezing*

The cryoprotection method was optimized according to the crystal type and its growth conditions.

#### 13.9.8.1 Complex I/Fab co-complex crystals

Co-complex crystals grown from PEG 3350 were cryoprotected using two methods. The crystals were sequentially immersed in a cryosolution with PEG 3350 at a concentration 1-3% higher than the mother liquor and with increasing concentrations of glycerol. 5 µl of solution A (20% glycerol) was added to increase the volume of the drop and avoid drying of the crystals while fishing. Next crystals were transferred to a 5 µl drop of pure solution A. After 10 minutes, 2,5 µl of solution A was replaced by 2.5 µl of solution B (25% glycerol) and the step was repeated to ensure uniform concentration of glycerol. After another 10 minutes, 2.5 µl of solution B was replaced by 2.5 µl of solution C (30% glycerol) and the step was done again. According to the second method, crystals were soaked for 1-10 minutes in solution containing 50% PEG 400 instead of PEG 3350. The crystals were fished using a nylon loop and frozen by plunging into liquid nitrogen or cold propane.

#### 13.9.8.2 Ugp1p crystals

24% PEG 400 in the growth buffer was used for cryoprotection of the Ugp1p crystals. The crystals were fished with a nylon loop and frozen by plunging into liquid nitrogen.

# 14 AUSFÜHRLICHE DEUTSCHSPRACHIGE ZUSAMMENFASSUNG

## *14.1 NADH:UBICHINON OXIDOREDUKTASE (KOMPLEX I)*

Die NADH:Ubichinon Oxidoreduktase (Komplex I, EC 1.6.5.3) ist der größte, komplizierteste aber am wenigsten bekannte Enzykomplex der Atmungskette [1]. Das Enzym koppelt den Transfer von zwei Elektronen von NADH auf Ubichinon an die Translokation von vier Protonen über die innere mitochondriale Membran oder die Plasmamembran von vielen Bakterien. Der erzeugte elektrochemische Protonengradient wird von der ATP-Synthase zur Produktion von ATP genutzt. Elektronenmikroskopische Aufnahmen zeigen eine L-förmige Struktur des Komplex I mit einem membranständigen und einem zur Matrixseite orientierten peripheren Arm [3-7]. Fehlfunktionen der NADH:Ubichinon Oxidoreduktase wurden bei zahlreichen neurodegenerativen Erkrankungen identifiziert, darunter dem Leigh-Syndrom und der hereditären Leberschen Optikusneuropathie (LHON) [11]. Neben dem Cytochrom $bc_1$ Komplex, ist der Komplex I eine wichtige Quelle von toxischen Sauerstoffradikalen, für die eine Beteiligung am biologischen Alterungsprozess diskutiert wird [12;14].

Der eukaryotische Komplex I besteht aus mehr als 40 Untereinheiten und hat eine molekular Masse von circa 1 MDa [15-18]. Die 14 zentralen Untereinheiten sind zwischen Prokaryoten und Eukaryoten konserviert und bilden die Minimalform von Komplex I [19]. Sieben dieser Untereinheiten (75-kDa, 51-kDa, 49-kDa, 30-kDa, 24-kDa, TYKY, PSST) bilden den peripheren Teil, sind kernkodiert und enthalten alle bekannten Redoxgruppen (ein FMN und bis zu neun Eisen-Schwefel-Zentren [20;21]). Die übrigen sieben Polypeptide (ND1 bis ND6 und ND4L) befinden sich im Membranarm, sind stark hydrophob und werden bei den meisten Eukaryoten von der mitochondrialen DNA kodiert. Zusätzlich zu den 14 zentralen besitzt der eukaryotische Komplex I sogenannte akzessorische Untereinheiten deren Funktion bis jetzt unklar ist.

Komplex I ist die letzte Komponente der Atmungskette deren atomare Struktur unbekannt ist. Vor kurzem wurde die Röntgentruktur des hydrophilen Arms des Komplex I aus *Thermus thermophilus* gelöst [37]. Diese Teilstruktur (PDB 2fug) beinhaltet acht Untereinheiten Nqo1-6, Nqo9, und Nqo15, sowie neun Eisen-Schwefel-Zentren. Die Struktur des Komplex I aus *Yarrowia lipolytica* wurde bis jetzt mit Elektronmikroskopie untersucht und lieferte das derzeit beste Strukturmodell des eukaryotischen Enzyms [6]. Dennoch ist eine Röntgenstruk-

tur des Holoenzym erforderlich, um den Zusammenhang zwischen der Redoxchemie im peripheren Arm und der Protonentranslokation im Membranarm zu verstehen.

## *14.2 KRISTALLISATION VON MEMBRANPROTEINKOMPLEXEN MIT HILFE VON ANTIKÖRPERFRAGMENTEN*

Membranproteine sind an vielen zellulären Prozessen wie z.B. dem Stoffwechsel, dem Transport von Ionen und anderen Stoffen, der Atmung, der Umsetzung von Energie und der Signaltransduktion beteiligt. Außerdem sind Membranproteine wichtige Angriffspunkte für Medikamente. Für das Verständnis der Funktion eines Enzyms ist die Aufklärung seiner 3D Struktur mit atomarer Auflösung von großer Bedeutung. Im Gegensatz zu 49000 bekannten Strukturen von löslichen Proteinen gibt es nur 171 von Membranproteinen, die bis heute in der Protein Daten Bank (PDB) deponiert wurden. Die Schwierigkeit dreidimensionale Kristalle von Membranproteinen herzustellen, liegt vor allem in der amphiphilen Natur ihrer Oberfläche. Mit Hilfe von Detergenzien werden die Membranproteine möglichst in der nativen Konformation aus biologischen Membranen solubilisiert und gereinigt. Die Protein-Detergenz Komplexe dienen dann als Ausgangmaterial für die Kristallisation. Die Röntgenkristallographie erfordert dreidimensionale Kristalle, bei denen die spezifischen Kristallkontakte primär von den polaren Teilen der Proteine vermittelt sind. Leider ist dieser Anteil in vielen Fällen nicht groß genug, um ausreichende Kristallkontakte ausbilden zu können. Eine Möglichkeit die polare Oberfläche zu vergrößern, ist die Verwendung von Antikörperfragmenten [87]. Zusätzlich können Fragmente von Immunglobulinen bestimmte Proteinkonformationen stabilisieren und dadurch die Kristallisation fördern. Fv und Fab Antikörperfragmente wurden mit Erfolg zur Kristallisation von integralen Membranproteinen verwendet. Cytochrom *c* oxidase aus *Paracoccus denitrificans* wurde als erstes mittels Fv Fragmenten kristallisiert [61;68]. Danach wurde die Struktur eines Fv Co-Komplexes des Cytochrom $bc_1$ Komplexes aus *Saccharomyces cerevisiae* gelöst [60]. Die erste Fab-vermittelte Kristallisation wurde für den Kalium Kanal KcsA aus *Streptomyces lividans* berichtet. Außer zur Vergrößerung der hydrophilen Domäne, wurden die Antikörperfragmente auch zur Phasenbestimmung verwendet [85]. Das jüngste Beispiel für die erfolgreiche Kristallisation eines Fab-Membranprotein Co-Komplexes ist der humane Adrenorezeptor $\beta_2$AR [67].

In Anlehnung an die beschriebenen erfolgreichen Versuche zur Kristallisation von verschiedenen Membranproteinen mit Antikörperfragmenten, wird in der vorliegenden Arbeit die Kristallisation von Komplex I mit Hilfe von proteolytischen Fab Fragmenten beschrieben.

## *14.3 HERSTELLUNG UND REINIGUNG VON Fab FRAGMENTEN*

### *14.3.1 Reinigung monoklonaler Antikörper*

Die in dem Projekt verwendeten monoklonalen Antikörper (1F5, 31A8 und 44G10) wurden nach Standardtechniken für die Kultur von Hybridomazellen ohne Zusatz von Antibiotika gezüchtet. Typische Ausbeuten waren: 55 mg/L Zellkultur für 31A8, 35 mg/L Zellkultur für 1F5 und 30 mg/L Zellkultur für 44G10. Die monoklonalen Antikörper wurden aus dem Zellkulturüberstand mittels Protein G Affinitätschromatographie gereinigt. Polyacrylamidgelelektrophorese zeigte einen hohen Reinheitsgrad der isolierten Immunglobuline. Deren Funktionalität wurde sowohl in nativen ELISA Tests als auch in Bindungsexperimenten mit dem nativen Komplex I geprüft. Bindungskonstanten im nanomolaren Bereich wurden für die Antikörper und die entsprechenden Fab Fragmente gefunden.

### *14.3.2 Einfluss der Komplex I Konformation auf die Bindung von monoklonalen Antikörpern*

Die monoklonalen Antikörper 31A8 und 44G10 sind Western Blot negativ und binden nur an Komplex I im nativen Zustand. Der Antikörper 1F5 hingegen erkennt ein lineares Epitop des Komplexes. Es wurde gezeigt, dass NADPH die Sensitivität von verschiedenen Untereinheiten bei der limitierten Proteolyse von Komplex I beeinflusst [96;97]. Oberflächenplasmonresonanz-Experimente zeigten, dass NADPH keinen Einfluss auf die Bindung der Antikörper 31A8 und 44G10 an Komplex I aus *Y. lipolytica* hat. Eine signifikante Abnahme in den Oberflächenplasmonresonanzsignalen wurde überraschenderweise für den Antikörper 1F5 beobachtet, der im distalen Teil des Membranarms bindet.

### *14.3.3 Herstellung von Fab Fragmenten*

Die Herstellung von reinen Fab Fragmenten, die für die für Co-Kristallisations Experimente geeignet waren, war eines der wichtigsten Ziele des Projekts. Um ein optimales Protokoll für die proteolytische Spaltung zu entwickeln, wurden mehrere Proteasen (immobilisiertes Papain, immobilisiertes Ficin, kristallines Papain und Trypsin) und unterschiedliche Reaktionsbedinungen, wie verschiedene pH und Cysteinkonzentration getestet. Da der Verdau mit Papain sehr gute Ausbeute zeigte, und die Durchführung einfach und zuverlässig war, wurde diese Protease für weitere Experimente benutzt. Fab Fragmente wurden aus dem Proteolyseansatz gereinigt. Die Fc Teile enthaltenden Fragmente wurden durch Protein G Affinitätschromatographie entfernt. Anschließend wurde die Probe mittels Gelfiltration gereinigt. Die

Bindung der Fab Fragmente an den nativen Komplex I wurde mit analytischer Gelfiltration und Oberflächenplasmonresonanz geprüft. Die Fab Fragmente 1F5 und 44G10 zeigten hohe Affinität zum Komplex I und konnten in Western Blot Experimenten nachgewiesen werden. Die Bindungskonstanten lagen im nanomolaren Bereich. Demgegenüber konnte keine Bindung des Fab 31A8 an Komplex I gezeigt werden. Daraus wurde geschlossen, dass der Verdau mit Papain die Antigenbindungsstelle von 31A8 Antikörper beschädigt.

## *14.4 HERSTELLUNG VON Fab-KOMPLEX I CO-KOMPLEXEN*

Reine Fab Fragmente wurden in 1.5 fachem molaren Überschuss zu Komplex I eingesetzt. Die ungebundenen Fragmente wurden durch Gelfiltration entfernt. Es wurde gezeigt, dass die Bindung der Fab Fragmente die spezifische Aktivität von Komplex I (NADH:HAR Oxidoreduktase und dNADH:DBQ Oxidoreduktase) nicht verändern. Der Phospholipidgehalt des isolierten Ko-Komplexes war vergleichbar mit Komplex I Präparation ohne Fab Zusatz. Wegen beeinträchtigter Affinität des Fab 31A8, konnten keine funktionalen Untersuchungen mit diesen Antikörperfragment durchgeführt werden.

## *14.5 KRISTALLISATION VON KOMPLEX I-Fab CO-KOMPLEXEN*

Zur Kristallisation von Komplex I-Fab Co-Komplexen wurden bekannte Verfahren nach dem Prinzip der Dampfdiffusion (hängende Tropfen und sitzende Tropfen) eingesetzt. Kristallisationsroboter (Max-Planck-Institut für Biophysik, Frankfurt am Main) wurden für die Asuwahl von Initialbedinungen verwendet, wobei auch verschiedene kommerzielle „*sparse matrix kits*“ getestet wurden. Die ersten Kristalle von Komplex I-Fab 44G10 wuchsen in Ansätzen im Nanomaßstab, ließen sich aber nicht im größeren Maßstab reproduzieren. Daraus wurde geschlossen, dass Fab-Fragmente von 44G10 eine unvorteilhafte Kristallpackung bewirken und die Bildung von Kristallen eher verhindern.

Die initialen Kristalle des Co-Komplexes mit dem Fab-Fragment von 1F5 wuchsen unter ähnlichen Bedinungen wie der native Komplex I. Die Kristallqualität war jedoch limitiert und es konnten nur Reflexe bis 18 Å an der ID14 des ESRF in Frankreich beobachtet werden. Um die Qualität zu verbessern, wurden verschiedene Methoden angewendet, wie *seeding*, pH Gradient und unkontrollierte Dehydratation. Zusätzlich wurden konsequent die Kristallisationsbedingungen, wie Salztyp, Temperatur, Proteinkonzentration und Zusätze variiert. Es wurde gezeigt dass der Lipidgehalt eine sehr wichtige Rolle für die Kristallqualität spielte. Die verbesserten Kristalle zeigten Röntgenbeugung von bis zu 7 Å an der ID14-2 des ESRF in

Frankreich. Die vorläufigen Auswertung der Datensätze zeigt eine kubische Einheitzelle mit folgenden Dimensionen: a = 471 Å, b = 471 Å, c = 472 Å, α = 90˚, β = 90˚, γ = 90˚.

Die weitere Verbesserung der Kristallqualität ist die Grundvoraussetzung für die strukturelle Charakterisierung der Co-Komplexe. Als erstes müßten die Bedingungen für das Einfrieren optimiert werden. Die Anwendung von flüssigem Propan zeigte beim nativen Komplex I Vorteile gegenüber der Anwendung von flüssigem Stickstoff. Zweitens könnte eine weitere Vergrößerung der hydrophilen Domäne z.B. durch Bindung von Protein L an das Fab Fragment hilfreich sein [188;189]. Diese Methode birgt allerdings das Risiko größerer struktureller Flexibilität. Drittens scheint die Anwendung einer Humiditätskammer, die die kontrollierte Dehydratation von Proteinkristallen erlaubt, eine aussichtsreiche Methode für die Optimierung der Kristallqualität zu sein [98].

Die vorliegende Arbeit repräsentiert die erste erfolgreiche Kristallisation von Komplex I (NADH:Ubichinon Oxidoreduktase) aus *Y. lipolytica* mit gebundenen Fab Fragmenten. Durch konsequente Optimierung wurden die Beugungseigenschaften der Kristalle deutlich verbessert. Die initiale Datenanalyse deutet auf eine andere kristallographische Raumgruppe als die der Kristalle des nativen Enzyms hin. Die Aufklärung der Struktur von Komplex I-Fab Komplexen wird eine wichtige Informationsquelle für die strukturelle Charakterisierung der NADH:Ubichinon Oxidoreduktase (Komplex I) sein. Überdies könnten Antikörperfragmente als wichtiges Hilfsmittel für die Kristallisation von Komplex I Subkomplexen oder auch einzelnen Untereinheiten dienen.

## *14.6 UDP-GLUCOSE PYROPHOSPHORYLASE*

UDP-Glucose Pyrophosphorylase (UGP1, Ugp1p, UTP:α-D-Glukose-1-Phosphat uridylyltransferase, UDPGP, EC 2.7.7.9) katalysiert die $Mg^{2+}$-abhängige Bildung von UDP-Glucose und Pyrophosphat aus Glucose-1-Phosphat und UTP [126]. UDP-Glucose ist der wichtigste Glykosyl-Donor im Stoffwechsel und dient als aktivierte Vorstufe für viele Glykosylierungsreaktionen. In *S. cerevisiae* wird die UDP-Glucose zur Synthese der *β*-Glukane (1,6-*β*-Glukan and 1,3-*β*- Glukan) der Zellwand benutzt [133]. Die *β*-Glukane repräsentieren über 55% der Zellwandkohlenhydrate und sind wichtig für die Morphologie und osmotische Integrität der Hefezellen. Die Deletion des Gens für UDP-Glucose Pyrophosphorylase (UGP1) in *S. cerevisiae* war letal für die Zellen [134]. In tierischen Zellen werden die UDP-Glucose Einheiten für den Aufbau des Speicherpolysaccharids Glykogen verwendet.

UDP-Glucose Pyrophosphorylase gehört zu den sogenannten UGPasen, für die eine SGC-Domäne mit dem Signaturmotif LXXGXGTXXXXXXPK im aktiven Zentrum charakteris-

tisch ist [156]. Für die pflanzliche UGPase wurde eine Regulation der Enzymaktivität über den Oligomerisierungszustand des Enzyms vorgeschlagen, wobei die aktive Form ausschließlich das Monomer ist [190]. In Hefezellen spielen möglicherweise die PAS-Kinasen eine wichtige Rolle bei der Regulation der Enzymaktivität [191]. In der Bäckerhefe wurden aktive Enzyme nur als Oktamere gefunden [161]. Bis heute wurden Röntgenstrukturen von UGPasen aus folgenden Organismen gelöst: *A. thaliana* [166], *Leishmania major* [167], *Corynebacterium glutamicum* [192], *Escherichia coli* [168] *und S. cerevisiae* [161].

UDP-Glucose Pyrophosphorylase aus *Y. lipolytica* wurde bis jetzt noch nicht charakterisiert. Das Enzym zeigt 70% und 52% Sequenzidentität zu den Enzymen aus *S. cerevisiae* und *A. thaliana*. UDP-Glucose Pyrophosphorylase aus *Y. lipolytica* weist Affinität zu $Ni^{2+}$-NTA auf, weshalb es während der His-tag Affinitätsreinigung von Komplex I zusammen mit diesem aufgereinigt wurde. Die mit Ionenaustausch-Chromatographie weiter gereinigte Protein konnte mit einem Antikörper gegen das Enzym aus *S. cerevisiae* in einem Western Blot nachgewiesen werden. LILBID (laser-induced liquid bead ion desorption) Massenspektrometrie wurde zur Bestimmung des Oligomerisierungszustandes verwendet und zeigte dass, das Enzym aus *Y. lipolytica*, ähnlich wie aus *S. cerevisiae* als Oktamer mit einer molekularen Masse von ~ 450 kDa vorkommt.

Die bekannte Struktur des pflanzlichen Enzyms wurde für die Konstruktion eines Strukturmodells des Enzyms aus *Y. lipolytica* verwendet. Das Modell zeigt die typische Architektur von Pyrophosphorylasen mit einer zentralen SGC Domäne.

Die erste Kristalle wuchsen als sehr dünne Nadeln aus einem Ansatz mit PEG 400 als Fällungsmittel und zeigten ein Beugungsmuster mit einer Auflösung von 4 Å (gemessen an der PX II, SLS, Schweiz). Anwendung der *microbatch* Technik ergab größere Kristalle, die bis 3.2 Å beugten. Die Raumgruppe war *I*4 und die Einheitszelledimensionen waren wie folgt: a = 295 Å, b = 295 Å, c = 110 Å, $\alpha = 90^{\circ}$, $\beta = 90^{\circ}$, $\gamma = 90^{\circ}$. Die Struktur soll nun durch *molekular replacement* anhand der bekannten Struktur der *S. cerevisiae* UDP-Glucose Pyrophosphorylase gelöst werden (Zusammenarbeit mit Carola Hunte, Universität Leeds).

# 15 ABBREVIATIONS

| | |
|---|---|
| µM | micromolar |
| ADP | adenosine-5'-diphosphate |
| AGPase | ADP- glucose pyrophosphorylase |
| ATP | adenosine-5'-triphosphate |
| BSA | bovine serum albumin |
| $C_{12}E_9$ | dodecyl nonaethylene glycol ether |
| CI | complex I |
| CMC | critical micelle concentration |
| COX | cytochrome *c* oxidase |
| DBQ | n-decylubiquinone |
| dNADH | deaminodihydronicotinamide adenine dinucleotide |
| DQA | 2-decyl-4-quinazolinyl amine |
| EDTA | ethylenediaminetetraacetic acid |
| EPR | electron paramagnetic resonance |
| Fab | antigen binding fragment |
| Fc | crystallizable fragment |
| FMN | flavine mononucleotide |
| Fv | variable fragment |
| GPCR | G protein coupled receptor |
| HAR | hexa-ammine-ruthenium III-chloride |
| HEPES | N-2-hydroxyethylpiperazine-N-2-ethanesulfonic acid |
| IgG | immunoglobulin G |
| IPD | immobilized papain digest |
| kDa | kilo Dalton |
| LILBID | laser-induced liquid bead ion desorption |
| Mab | monoclonal antibody |
| mM | milimolar |
| NAD | nicotinamide adenine dinucleotide |
| NADH | nicotinamide adenine dinucleotide, reduced |
| NADP | nicotinamide adenine dinucleotide phosphate |
| NADPH | nicotinamide adenine dinucleotide phosphate, reduced |

| | |
|---|---|
| PAGE | polyacrylamide gel electrophoresis |
| PC | phosphatidyl-choline |
| PDI | protein disulphide isomerase |
| PEG | polyethylene glycol |
| PRM | protein – ribosome – mRNA – complex |
| QCR | cytochrome $bc_1$ complex |
| scFv | single chain variable fragment |
| SDS | sodium dodecylsulphate |
| $Ta_6Br_{12}^{2+}$ | dodecabromohexatantalum cation |
| Tris | tris(hydroxymethyl)aminomethane |
| UDP | uridine-5'-diphosphate |
| Ugp1p | uridylyl diphosphate glucose pyrophosphorylase |
| UGPase | UDP-glucose pyrophosphorylase |
| UTP | uridine-5'-triphosphate |

# 16 INDEX OF FIGURES

# 17 INDEX OF TABLES

# 18 REFERENCE LIST

[1] U.Brandt. Energy converting NADH : Quinone oxidoreductase (Complex I), Annu.Rev.Biochem. 75 (2006) 69-92.

[2] Y.Hatefi, A.G.Haavik, D.E.Griffiths. Studies on the electron transfer system. XL. Preparation and properties of mitochondrial DPNH-coenzyme Q reductase, J.Biol.Chem. 237 (1962) 1676-1680.

[3] V.Guenebaut, A.Schlitt, H.Weiss, K.Leonard, T.Friedrich. Consistent structure between bacterial and mitochondrial NADH:ubiquinone oxidoreductase (complex I), J.Mol.Biol. 276 (1998) 105-112.

[4] G.Peng, G.Fritzsch, V.Zickermann, H.Schägger, R.Mentele, F.Lottspeich, M.Bostina, M.Radermacher, R.Huber, K.O.Stetter, H.Michel. Isolation, characterization and electron microscopic single particle analysis of the NADH:ubiquinone oxidoreductase (complex I) from the hyperthermophilic eubacterium *Aquifex aeolicus*, Biochem. 42 (2003) 3032-3039.

[5] N.Grigorieff. Three-dimensional structure of bovine NADH:ubiquinone oxidoreductase (complex I) at 22 Å in ice, J.Mol.Biol. 277 (1998) 1033-1046.

[6] M.Radermacher, T.Ruiz, T.Clason, S.Benjamin, U.Brandt, V.Zickermann. The three-dimensional structure of complex I from *Yarrowia lipolytica*: A highly dynamic enzyme, J.Struct.Biol. 154 (2006) 269-279.

[7] K.Leonard, H.Haiker, H.Weiss. Three-dimensional structure of NADH:ubiquinone reductase (complex I) from *Neurospora* mitochondria determined by electron microscopy of membrane crystals, J.Mol.Biol. 194 (1987) 277-286.

[8] R.Acin-Perez, M.P.Bayona-Bafaluy, P.Fernandez-Silva, R.Moreno-Loshuertos, A.Perez-Martos, C.Bruno, C.T.Moraes, J.A.Enriquez. Respiratory complex III is required to maintain complex I in mammalian mitochondria, Molecular Cell 13 (2004) 805-815.

[9] H.Schägger, K.Pfeiffer. Supercomplexes in the respiratory chains of yeast and mammalian mitochondria, EMBO J. 19 (2000) 1777-1783.

[10] H.Schägger, R.de Coo, M.F.Bauer, S.Hofmann, C.Godinot, U.Brandt. Significance of respirasomes for the assembly/stability of human respiratory chain complex I, J.Biol.Chem. 279 (2004) 36349-36353.

[11] J.Smeitink, L.Van den Heuvel. Human mitochondrial complex I in health and disease, Am.J.Hum.Genet. 64 (1999) 1505-1510.

[12] J.Smeitink, L.Van den Heuvel, S.DiMauro. The genetics and pathology of oxidative phosphorylation, Nat.Rev.Genet. 2 (2001) 342-352.

[13] G.Lenaz. Role of mitochondria in oxidative stress and ageing, Biochim.Biophys.Acta Mol.Basis Dis. 1366 (1997) 53-67.

[14] S.Dröse, U.Brandt. The mechanism of mitochondrial superoxide production by the cytochrome $bc_1$ complex, J.Biol.Chem. 283 (2008) 21649-21654.

[15] N.Morgner, V.Zickermann, S.Kerscher, I.Wittig, A.Abdrakhmanova, H.D.Barth, B.Brutschy, U.Brandt. Subunit mass fingerprinting of mitochondrial complex I, Biochimica et Biophysica Acta-Bioenergetics 1777 (2008) 1384-1391.

[16] J.Carroll, I.M.Fearnley, J.M.Skehel, R.J.Shannon, J.Hirst, J.E.Walker. Bovine complex I is a complex of 45 different subunits, J.Biol.Chem. 281 (2006) 32724-32727.

[17] A.Abdrakhmanova, V.Zickermann, M.Bostina, M.Radermacher, H.Schägger, S.Kerscher, U.Brandt. Subunit composition of mitochondrial complex I from the yeast *Yarrowia lipolytica*, Biochim.Biophys.Acta 1658 (2004) 148-156.

[18] U.Brandt, A.Abdrakhmanova, V.Zickermann, A.Galkin, S.Dröse, K.Zwicker, S.Kerscher. Structure–function relationships in mitochondrial complex I of the strictly aerobic yeast *Yarrowia lipolytica*, Biochem.Soc.Trans. 33 (2005) 840-844.

[19] I.M.Fearnley, J.E.Walker. Conservation of sequences of subunits of mitochondrial complex I and their relationships with other proteins. [Review], Biochim.Biophys.Acta 1140 (1992) 105-134.

[20] T.Ohnishi. Iron-sulfur clusters semiquinones in complex I, Biochim.Biophys.Acta 1364 (1998) 186-206.

[21] P.Hinchliffe, L.A.Sazanov. Organization of iron-sulfur clusters in respiratory complex I, Science 309 (2005) 771-774.

[22] C.Mathiesen, C.Hägerhall. Transmembrane topology of the NuoL, M and N subunits of NADH : quinone oxidoreductase and their homologues among membrane- bound hydrogenases and bona fide antiporters, Biochimica et Biophysica Acta-Bioenergetics 1556 (2002) 121-132.

[23] R.Roth, C.Hägerhall. Transmembrane orientation and topology of the NADH:quinone oxidoreductase putative quinone binding subunit NuoH, Biochim.Biophys.Acta - Bioenerg. 1504 (2001) 352-362.

[24] J.Hirst, J.Carroll, I.M.Fearnley, R.J.Shannon, J.E.Walker. The nuclear encoded subunits of complex I from bovine heart mitochondria, Biochim.Biophys.Acta 1604 (2003) 135-150.

[25] M.Finel, J.M.Skehel, S.P.J.Albracht, I.M.Fearnley, J.E.Walker. Resolution of NADH:ubiquinone oxidoreductase from bovine heart mitochondria into two subcomplexes, one of which contains the redox centers of the enzyme, Biochem. 31 (1992) 11425-11434.

[26] L.A.Sazanov, S.Y.Peak-Chew, I.M.Fearnley, J.E.Walker. Resolution of the membrane domain of bovine complex I into subcomplexes: implications for the structural organization of the enzyme, Biochem. 39 (2000) 7229-7235.

[27] Y.M.Galante, Y.Hatefi. Purification and molecular and enzymatic properties of mitochondrial NADH dehydrogenase, Arch.Biochem.Biophys. 192 (1979) 559-568.

[28] Y.M.Galante, Y.Hatefi. Resolution of complex I and isolation of NADH dehydrogenase and an iron-sulfur protein, Methods Enzymol. 53 (1978) 15-21.

[29] C.I.Ragan, Y.M.Galante, Y.Hatefi, T.Ohnishi. Resolution of mitochondrial NADH dehydrogenase and isolation of two iron-sulfur proteins, Biochem. 21 (1982) 590-594.

[30] J.E.Walker. The NADH:ubiquinone oxidoreductase (complex I) of respiratory chains, Q.Rev.Biophys. 25 (1992) 253-324.

[31] J.Carroll, R.J.Shannon, I.M.Fearnley, J.E.Walker, J.Hirst. Definition of the nuclear encoded protein composition of bovine heart mitochondrial complex I - Identification of two new subunits, J.Biol.Chem. 277 (2002) 50311-50317.

[32] J.Carroll, I.M.Fearnley, R.J.Shannon, J.Hirst, J.E.Walker. Analysis of the subunit composition of complex I from bovine heart mitochondria, Mol.Cell.Proteomics 2 (2003) 117-126.

[33] M.Finel. Organization and evolution of structural elements within complex I, Biochim.Biophys.Acta 1364 (1998) 112-121.

[34] T.Friedrich, H.Weiss. Modular evolution of the respiratory NADH:ubiquinone oxidoreductase and the origin of its modules, J.theor.Biol. 187 (1997) 529-540.

[35] A.Tran-Betcke, U.Warnecke, C.Böcker, C.Zaborosch, B.Friedrich. Cloning and nucleotide sequences of the genes for the subunits of NAD-reducing hydrogenase of *Alcaligenes eutrophus* H16, J.Bacteriol. 172 (1990) 2920-2929.

[36] E.Nakamaru-Ogiso, T.Yano, T.Ohnishi. Characterization of the iron-sulfur cluster N7 (N1c) in the subunit NuoG of the proton-translocating NADH-quinone oxidoreductase from *Escherichia coli*, J.Biol.Chem. 280 (2005) 301-307.

[37] L.A.Sazanov, P.Hinchliffe. Structure of the hydrophilic domain of respiratory complex I from *Thermus thermophilus*, Science 311 (2006) 1430-1436.

[38] T.Ohnishi, E.Nakamaru-Ogiso. Were there any "misassignments" among iron-sulfur clusters N4, N5 and N6b in NADH-quinone oxidoreductase (complex I)?, Biochimica.et Biophysica.Acta (BBA.) - Bioenergetics. 1777 (2008) 703-710.

[39] G.Yakovlev, T.Reda, J.Hirst. Reevaluating the relationship between EPR spectra and enzyme structure for the iron-sulfur clusters in NADH: quinone oxidoreductase, Proceedings of the National Academy of Sciences of the United States of America 104 (2007) 12720-12725.

[40] R.Böhm, M.Sauter, A.Böck. Nucleotide sequence and expression of an operon in Escherichia coli coding for formate hydrogenlyase components, Mol.Microbiol. 4 (1990) 231-243.

[41] S.P.J.Albracht. Intimate relationships of the large and the small subunits of all nickel hydrogenases with two nuclear-encoded subunits of mitochondrial NADH:ubiquinone oxidoreductase, Biochim.Biophys.Acta 1144 (1993) 221-224.

[42] T.Friedrich. The NADH:ubiquinone oxidoreductase (complex I) from *Escherichia coli*, Biochim.Biophys.Acta 1364 (1998) 134-146.

[43] A.Garofano, K.Zwicker, S.Kerscher, P.Okun, U.Brandt. Two aspartic acid residues in the PSST-homologous NUKM subunit of complex I from *Yarrowia lipolytica* are essential for catalytic activity, J.Biol.Chem. 278 (2003) 42435-42440.

[44] M.Duarte, H.Populo, A.Videira, T.Friedrich, U.Schulte. Disruption of iron-sulphur cluster N2 from NADH:ubiquinone oxidoreductase by site-directed mutagenesis, Biochem.J. 364 (2002) 833-839.

[45] W.J.Ingledew, T.Ohnishi. An analysis of some thermodynamic properties of iron-sulfur centres in site I of mitochondria, Biochem.J. 186 (1980) 111-117.

[46] S.Magnitsky, L.Toulokhonova, T.Yano, V.D.Sled, C.Hägerhall, V.G.Grivennikova, D.S.Burbaev, A.D.Vinogradov, T.Ohnishi. EPR characterization of ubisemiquinones and iron-sulfur cluster N2, central components of the energy coupling in the NADH-ubiquinone oxidoreductase (complex I) in situ, J.Bioenerg.Biomembr. 34 (2002) 193-208.

[47] C.Mathiesen, C.Hägerhall. The 'antiporter module' of respiratory chain Complex I includes the MrpC/NuoK subunit - a revision of the modular evolution scheme, FEBS Lett. 549 (2003) 7-13.

[48] T.Clason, V.Zickermann, T.Ruiz, U.Brandt, M.Radermacher. Direct localization of the 51 and 24 kDa subunits of mitochondrial complex I by three-dimensional difference imaging, J.Struct.Biol. 159 (2007) 433-442.

[49] P.Hinchliffe, J.Carroll, L.A.Sazanov. Purification, characterisation and crystallisation of the hydrophilic domain of respiratory complex I from *Thermus thermophilus*, Biochimica et Biophysica Acta-Bioenergetics (2006) 175.

[50] V.Zickermann, M.Bostina, C.Hunte, T.Ruiz, M.Radermacher, U.Brandt. Functional implications from an unexpected position of the 49 kDa subunit of complex I, J.Biol.Chem. 278 (2003) 29072-29078.

[51] V.Guenebaut, R.Vincentelli, D.Mills, H.Weiss, K.Leonard. Three-dimensional structure of NADH-dehydrogenase from *Neurospora crassa* by electron microscopy and conical tilt reconstruction, J.Mol.Biol. 265 (1997) 409-418.

[52] V.Zickermann, S.Dröse, M.A.Tocilescu, K.Zwicker, S.Kerscher, U.Brandt. Challenges in elucidating structure and mechanism of proton pumping NADH:ubiquinone oxidoreductase (complex I), J Bioenerg Biomembr. 40 (2008) 475-483.

[53] J.Deisenhofer, H.Michel. The photosynthetic reaction centre from the purple bacterium *Rhodopseudomonas viridis*, Science 245 (1989) 1463-1473.

[54] J.V.Moller, M.Lemaire. Detergent binding as a measure of hydrophobic surface area of integral membrane proteins, J.Biol.Chem. 268 (1993) 18659-18672.

[55] R.M.Garavito, S.Ferguson-Miller. Detergents as tools in membrane biochemistry, J.Biol.Chem. 276 (2001) 32403-32406.

[56] H.Michel. Crystallization of membrane proteins, Trends Biochem.Sci. 8 (1983) 56-59.

[57] R.G.Laughlin. The aqueous phase behavior of surfactants, Academic Press, London, 1994.

[58] M.Zulauf. Physical chemistry of detergents. 1984. Ref Type: Unpublished Work

[59] C.Hunte, G.von Jagow, H.Schägger. Membrane protein purification and crystallization. A practical guide., Academic Press, London, 2004.

[60] C.Hunte, J.Koepke, C.Lange, H.Michel. Structure at 2.3 Å resolution of the cytochrome $bc_1$ complex from the yeast *Saccharomyces cerevisiae* co-crystallized with an antibody Fv fragment, Structure 8 (2000) 669-684.

[61] C.Ostermeier, A.Harrenga, U.Ermler, H.Michel. Structure at 2.7 Å resolution of the *Paracoccus denitrificans* two- subunit cytochrome c oxidase complexed with an antibody Fv fragment, Proc.Natl.Acad.Sci.USA 94 (1997) 10547-10553.

[62] W.Kuhlbrandt. 2-Dimensional crystallization of membrane proteins, Quart.Rev.Biophys. 25 (1992) 1-49.

[63] E.M.Landau, J.P.Rosenbusch. Lipidic cubic phases: A novel concept for the crystallization of membrane proteins, Proceedings of the National Academy of Sciences of the United States of America 93 (1996) 14532-14535.

[64] M.Kolbe, H.Besir, L.O.Essen, D.Oesterhelt. Structure of the light-driven chloride pump halorhodopsin at 1.8 Å resolution, Science 288 (2000) 1390-1396.

[65] H.Luecke, B.Schobert, J.K.Lanyi, E.N.Spudich, J.L.Spudich. Crystal structure of sensory rhodopsin II at 2.4 angstroms: Insights into color tuning and transducer interaction, Science 293 (2001) 1499-1503.

[66] A.Royant, P.Nollert, K.Edman, R.Neutze, E.M.Landau, E.Pebay-Peyroula, J.Navarro. X-ray structure of sensory rhodopsin II at 2.1 angstrom resolution, Proceedings of the National Academy of Sciences of the United States of America 98 (2001) 10131-10136.

[67] S.G.F.Rasmussen, H.J.Choi, D.M.Rosenbaum, T.S.Kobilka, F.S.Thian, P.C.Edwards, M.Burghammer, V.R.P.Ratnala, R.Sanishvili, R.F.Fischetti, G.F.X.Schertler, W.I.Weis, B.K.Kobilka. Crystal structure of the human $\beta_2$ adrenergic G protein-coupled receptor, Nature 450 (2007) 383-3U4.

[68] C.Ostermeier, S.Iwata, B.Ludwig, H.Michel. Fv fragment mediated crystallization of the membrane protein bacterial cytochrome *c* oxidase, Nature Structural Biology 2 (1995) 842-846.

[69] G.Koehler, C.Milstein. Continuous cultures of fused cells secreting antibody of predefined specificity, Nature 256 (1975) 495-497.

[70] D.Peer, J.M.Karp, S.Hong, O.C.FaroKHzad, R.Margalit, R.Langer. Nanocarriers as an emerging platform for cancer therapy, Nature Nanotechnology 2 (2007) 751-760.

[71] M.B.Dainiak, V.I.Muronetz, V.A.Izumrudov, I.Y.Galaev, B.Mattiasson. Production of Fab fragments of monoclonal antibodies using polyelectrolyte complexes, Anal.Biochem. 277 (2000) 58-66.

[72] J.S.Huston, J.McCartney, M.S.Tai, C.Mottola-Hartshorn, D.Jin, F.Warren, P.Keck, H.Oppermann. Medical applications of single-chain antibodies, International Review of Immunology 10 (1993) 195-217.

[73] R.E.Bird, K.D.Hardman, J.W.Jacobson, S.Johnson, B.M.Kaufman, S.M.Lee, T.Lee, S.H.Pope, G.S.Riordan, M.Whitlow. Single-chain antigen-binding proteins, Science 242 (1988) 423-426.

[74] F.Viti, F.Nilsson, S.Demartis, A.Huber, D.Neri. Design and use of phage display libraries for the selection of antibodies and enzymes, Applications of Chimeric Genes and Hybrid Proteins, Pt A 326 (2000) 480-505.

[75] D.Rothlisberger, K.M.Pos, A.Pluckthun. An antibody library for stabilizing and crystallizing membrane proteins - selecting binders to the citrate carrier CitS, FEBS Lett. 564 (2004) 340-348.

[76] N.A.Watkins, W.H.Ouwehand. Introduction to antibody engineering and phage display, Vox Sanguinis 78 (2000) 72-79.

[77] J.Hanes, L.Jermutus, A.Pluckthun. Selecting and evolving functional proteins in vitro by ribosome display, Applications of Chimeric Genes and Hybrid Proteins, Pt C 328 (2000) 404-430.

[78] G.Kleymann, C.Ostermeier, K.Heitmann, W.Haase, H.Michel. Use of antibody fragments (Fv) in immunocytochemistry, J Histochem.Cytochem. 43 (1995) 607-614.

[79] G.Kleymann, C.Ostermeier, B.Ludwig, A.Skerra, H.Michel. Engineered Fv fragments as tools for the one-step purification of integral multisubunit membrane protein complexes, Bio/Technology 13 (1995) 155-160.

[80] C.Ostermeier, H.Michel. Improved cloning of antibody variable regions from hybridomas by an antisense-directed RNase H digestion of the P3-X63-Ag8.653 derived pseudogene mRNA, Nucleic Acids Res. 24 (1996) 1979-1980.

[81] M.Venturi, C.Seifert, C.Hunte. High level production of functional antibody Fab fragments in an oxidizing bacterial cytoplasm, J.Mol.Biol. 315 (2002) 1-8.

[82] X.P.Jiang, Y.Ookubo, I.Fujii, H.Nakano, T.Yamane. Expression of Fab fragment of catalytic antibody 6D9 in an *Escherichia coli* in vitro coupled transcription/translation system, FEBS Lett. 514 (2002) 290-294.

[83] X.P.Jiang, K.Oohira, Y.Iwasaki, H.Nakano, S.Ichihara, T.Yamane. Reduction of protein degradation by use of protease-deficient mutants in cell-free protein synthesis system of *Escherichia coli*, Journal of Bioscience and Bioengineering 93 (2002) 151-156.

[84] L.A.Ryabova, D.Desplancq, A.S.Spirin, A.Pluckthun. Functional antibody production using cell-free translation: Effects of protein disulfide isomerase and chaperones, Nature Biotechnology 15 (1997) 79-84.

[85] Y.F.Zhou, J.H.Morais-Cabral, A.Kaufman, R.MacKinnon. Chemistry of ion coordination and hydration revealed by a $K^+$ channel-Fab complex at 2.0 angstrom resolution, Nature 414 (2001) 43-48.

[86] C.Ostermeier, L.O.Essen, H.Michel. Crystals of an antibody Fv fragment against an integral membrane protein diffracting to 1.28 A resolution, Proteins 21 (1995) 74-77.

[87] C.Hunte, Michel H. Crystallisation of membrane proteins mediated by antibody fragments., Curr Opin.Struct.Biol 12 (4) (2002) 503-508.

[88] C.Lange, C.Hunte. Crystal structure of the yeast cytochrome $bc_1$ complex with its bound substrate cytochorme *c*, Proc.Natl.Acad.Sci.USA 99 (2002) 2800-2805.

[89] D.A.Doyle, J.M.Cabral, R.A.Pfuetzner, A.L.Kuo, J.M.Gulbis, S.L.Cohen, B.T.Chait, R.MacKinnon. The structure of the potassium channel: Molecular basis of K+ conduction and selectivity, Science 280 (1998) 69-77.

[90] A.Skerra. Engineered protein scaffolds for molecular recognition, Journal of Molecular Recognition 13 (2000) 167-187.

[91] K.Nord, E.Gunneriusson, J.Ringdahl, S.Stahl, M.Uhlen, P.A.Nygren. Binding proteins selected from combinatorial libraries of an alpha-helical bacterial receptor domain, Nature Biotechnology 15 (1997) 772-777.

[92] J.Abramson, G.Larsson, B.Byrne, A.Puustinen, A.Garcia-Horsman, S.Iwata. Purification, crystallization and preliminary crystallographic studies of an integral membrane protein, cytochrome bo(3) ubiquinol oxidase from *Escherichia coli*, Acta Crystallographica Section D-Biological Crystallography 56 (2000) 1076-1078.

[93] B.Byrne, J.Abramson, M.Jansson, E.Holmgren, S.Iwata. Fusion protein approach to improve the crystal quality of cytochrome bo(3) ubiquinol oxidase from *Escherichia coli*, Biochimica et Biophysica Acta-Bioenergetics 1459 (2000) 449-455.

[94] G.G.Prive, H.R.Kaback. Engineering the lac permease for purification and crystallization, J.Bioenerg.Biomembr. 28 (1996) 29-34.

[95] J.P.Zhuang, G.G.Prive, G.E.Werner, P.Ringler, H.R.Kaback, A.Engel. Two-dimensional crystallization of *Escherichia coli* lactose permease, J.Struct.Biol. 125 (1999) 63-75.

[96] Mamedova A.A., P.J.Holt, J.Carroll, L.A.Sazanov. Substrate-induced conformational change in bacterial complex I, J.Biol.Chem. 279 (2004) 23830-23836.

[97] G.Belogrudov, Y.Hatefi. Catalytic sector of complex I (NADH:Ubiquinone oxidoreductase): subunit stoichiometry and substrate-induced conformation changes., Biochem. 33 (1994) 4571-4576.

[98] R.Kiefersauer, M.E.Than, H.Dobbek, L.Gremer, M.Melero, S.Strobl, J.M.Dias, T.Soulimane, R.Huber. A novel free-mounting system for protein crystals: transformation and improvement of diffraction power by accurately controlled humidity changes, Journal of Applied Crystallography 33 (2000) 1223-1230.

[99] A.Korostelev, S.Trakhanov, M.Laurberg, H.F.Noller. Crystal structure of a 70S ribosome-tRNA complex reveals functional interactions and rearrangements, Cell 126 (2006) 1065-1077.

[100] B.Böttcher, D.Scheide, M.Hesterberg, L.Nagel-Steger, T.Friedrich. A novel, enzymatically active conformation of the *Escherichia coli* NADH:ubiquinone oxidoreductase (complex I), J.Biol.Chem. 277 (2002) 17970-17977.

[101] E.A.Baranova, D.J.Morgan, L.A.Sazanov. Single particle analysis confirms distal location of subunits NuoL and NuoM in *Escherichia coli* complex I, J.Struct.Biol. 159 (2007) 238-242.

[102] D.J.Morgan, L.A.Sazanov. Three-dimensional structure of respiratory complex I from *Escherichia coli* in ice in the presence of nucleotides, Biochimica et Biophysica Acta-Bioenergetics 1777 (2008) 711-718.

[103] M.A.Tocilescu, U.Fendel, K.Zwicker, S.Kerscher, U.Brandt. Exploring the ubiquinone binding cavity of respiratory complex I, J.Biol.Chem. 282 (2007) 29514-29520.

[104] V.Zickermann, K.Zwicker, M.A.Tocilescu, S.Kerscher, U.Brandt. Characterization of a subcomplex of mitochondrial NADH:ubiquinone oxidoreductase (complex I) lacking the flavoprotein part of the N-module, Biochim.Biophys.Acta 1767 (2007) 393-400.

[105] N.Kashani-Poor, S.Kerscher, V.Zickermann, U.Brandt. Efficient large scale purification of his-tagged proton translocating NADH : ubiquinone oxidoreductase (complex I) from the strictly aerobic yeast *Yarrowia lipolytica*, Biochimica et Biophysica Acta-Bioenergetics 1504 (2001) 363-370.

[106] R.R.Porter. Hydrolysis of rabbit gamma-globulin and antibodies with crystalline papain, Biochem.J. 73 (1959) 119-126.

[107] P.Parham. On the fragmentation of monoclonal IgG1, IgG2A, and IgG2B from balb-c mice, Journal of Immunology 131 (1983) 2895-2902.

[108] E.Lamoyi. Preparation of F(ab')2 fragments from mouse IgG of various subclasses, Methods Enzymol. 121 (1986) 652-663.

[109] G.Boulot, V.Guillon, R.A.Mariuzza, R.J.Poljak, M.M.Riottot, H.Souchon, S.Spinelli, D.Tello. Crystallization of antibody fragments and their complexes with antigen, Journal of Crystal Growth 90 (1988) 213-221.

[110] L.J.Harris, E.Skaletsky, A.McPherson. Crystallographic structure of an intact IgG1 monoclonal antibody, J.Mol.Biol. 275 (1998) 861-872.

[111] L.J.Harris, S.B.Larson, K.W.Hasel, J.Day, A.Greenwood, A.McPherson. The 3-dimensional structure of an intact monoclonal-antibody for canine lymphoma, Nature 360 (1992) 369-372.

[112] L.J.Harris, S.B.Larson, E.Skaletsky, A.McPherson. Comparison of the conformations of two intact monoclonal antibodies with hinges, Immunological Reviews 163 (1998) 35-43.

[113] G.Gorini, G.A.Medgyesi, G.Doria. Heterogeneity of mouse myeloma gamma G globulins as revealed by enzymatic proteolysis, Journal of Immunology 103 (1969) 1132-&.

[114] Y.Yamaguchi, H.Kim, K.Kato, K.Masuda, I.Shimada, Y.Arata. Proteolytic fragmentation with high specificity of mouse immunoglobulin G mapping of proteolytic cleavage sites in the hinge region, J.Immunol.Methods 181 (1995) 259-267.

[115] M.Adamczyk, J.C.Gebler, J.Wu. Papain digestion of different mouse IgG subclasses as studied by electrospray mass spectrometry, J.Immunol.Methods 237 (2000) 95-104.

[116] J.Werner. Heterologe Expression von Antikörperfragmenten zur Kristallisation von Membranproteinen. 2006. Institut für Biochemie I, Molekulare Bioenergeitk am Gustav-Embden-Zentrum der Biologischen Chemie. Ref Type: Thesis/Dissertation

[117] E.A.Stura, M.Graille, J.B.Charbonnier. Crystallization of macromolecular complexes: Combinatorial complex crystallization, Journal of Crystal Growth 232 (2001) 573-579.

[118] E.A.Stura, M.Graille, M.J.Taussig, B.Sutton, M.G.Gore, G.J.Silverman, J.B.Charbonnier. Crystallization of macromolecular complexes: stoichiometric variation screening, Journal of Crystal Growth 232 (2001) 580-590.

[119] E.Padan, Venturi M., Michel H., C.Hunte. Production and characterization of monoclonal antibodies directed against native epitopes of NhaA, the Na+/H+ antiporter of Escherichi coli, FEBS Lett. 441 (1998) 53-58.

[120] Venturi M., Rimon A., Gerchman Y., C.Hunte, E.Padan, Michel H. The monoclonal antibody 1F6 identifies a pH-dependent conformational change in the hydrophilic $NH_2$ terminus of NhaA $Na^+/H^+$ antiporter of *Escherichia coli*, J.Biol.Chem. 275 (2002) 4734-4742.

[121] R.Wyatt, P.D.Kwong, E.Desjardins, R.W.Sweet, J.Robinson, W.A.Hendrickson, J.G.Sodroski. The antigenic structure of the HIV gp120 envelope glycoprotein, Nature 393 (1998) 705-711.

[122] P.D.Kwong, R.Wyatt, J.Robinson, R.W.Sweet, J.Sodroski, W.A.Hendrickson. Structure of an HIV gp120 envelope glycoprotein in complex with the CD4 receptor and a neutralizing human antibody, Nature 393 (1998) 648-659.

[123] Y.X.Jiang, A.Lee, J.Y.Chen, V.Ruta, M.Cadene, B.T.Chait, R.MacKinnon. X-ray structure of a voltage-dependent K+ channel, Nature 423 (2003) 33-41.

[124] Y.X.Jiang, V.Ruta, J.Y.Chen, A.Lee, R.MacKinnon. The principle of gating charge movement in a voltage-dependent K+ channel, Nature 423 (2003) 42-48.

[125] Q.X.Jiang, D.N.Wang, R.MacKinnon. Electron microscopic analysis of KvAP voltage-dependent $K^+$ channels in an open conformation, Nature 430 (2004) 806-810.

[126] R.Turnquist, Hansen RG. Part A, Nucleotidy transfer, nucleosidyl transfer. Uridine diphosphoryl glucose pyrophosphorylase, in: PD.Boyer (Ed.), Academic Press, New York, 1973, pp. 51-71.

[127] A.C.Lamerz, T.Haselhorst, A.K.Bergfeld, M.von Itzstein, R.Gerardy-Schahn. Molecular cloning of the Leishmania major UDP-glucose pyrophosphorylase, functional characterization, and ligand binding analyses using NMR spectroscopy, J.Biol.Chem. 281 (2006) 16314-16322.

[128] K.K.Tsuboi, K.Fukunaga, Petricci, JC. Purification and specific kinetic properties of erythrocyte uridine diphosphate glucose pyrophosphorylase, J.Biol.Chem. 244 (1969) 1008-&.

[129] K.F.R.Sheu, P.A.Frey. UDP-Glucose Pyrophosphorylase - stereochemical course of reaction of glucose-1-phosphate with uridine-5'[1-thiotriphosphate], J.Biol.Chem. 253 (1978) 3378-3380.

[130] L.J.Wong, P.A.Frey. Galactose-1-P uridylyltransferase - kinetic and radiochemical evidence for a double displacement pathway and a uridylyl-enzyme intermediate, Fed.Proc. 33 (1974) 1243.

[131] L.J.Wong, P.A.Frey. Galactose-1-phosphate uridylyltransferase - rate studies confirming a uridylyl-enzyme intermediate on catalytic pathway, Biochem. 13 (1974) 3889-3894.

[132] L.J.Wong, P.A.Frey. Galactose 1-phosphate uridylytransferase - isolation of a uridylyl-enzyme intermediate, J.Biol.Chem. 249 (1974) 2322-2324.

[133] F.M.Klis, A.Boorsma, P.W.J.De Groot. Cell wall construction in *Saccharomyces cerevisiae*, Yeast 23 (2006) 185-202.

[134] J.M.Daran, N.Dallies, D.Thinessempoux, V.Paquet, J.Francois. Genetic and biochemical-characterization of the Ugp1 gene encoding the UDP-glucose pyrophosphorylase from *Saccharomyces cerevisiae*, Eur.J.Biochem. 233 (1995) 520-530.

[135] R.Kornfeld, D.H.Brown. Activity of some enzymes of glycogen metabolism in fetal and neonatal guinea pig liver, J.Biol.Chem. 238 (1963) 1604-&.

[136] S.C.Huber, J.L.Huber. Role of sucrose-phosphate synthase in sucrose metabolism in leaves, Plant Physiol. 99 (1992) 1275-1278.

[137] L.A.Kleczkowski, M.Geisler, I.Ciereszko, H.Johansson. UDP-Glucose pyrophosphorylase. An old protein with new tricks, Plant Physiol. 134 (2004) 912-918.

[138] L.A.Kleczkowski. Back to the drawing board: Redefining starch synthesis in cereals, Trends in Plant Science 1 (1996) 363-364.

[139] Y.-Z.Jin, H.-L.Tang, S.-L.Li, C.-L.Tsou. The triphasic reduction of cytochrome b in the succinate-cytochrome c reductase, Biochim.Biophys.Acta 637 (1981) 551-554.

[140] J.R.Cupp-Vickery, R.Y.Igarashi, M.Perez, M.Poland, C.R.Meyer. Structural analysis of ADP-glucose pyrophosphorylase from the bacterium *Agrobacterium tumefaciens*, Biochem. 47 (2008) 4439-4451.

[141] S.Teheesen, L.Lehle, A.Weissmann, M.Aebi. Isolation of the Alg5 Locus Encoding the Udp-Glucose-Dolichyl-Phosphate Glucosyltransferase from *Saccharomyces cerevisiae*, Eur.J.Biochem. 224 (1994) 71-79.

[142] A.Herscovics, P.Orlean. Glycoprotein biosynthesis in Yeast, FASEB J. 7 (1993) 540-550.

[143] R.C.Montijn, J.Vanrinsum, F.A.Vanschagen, F.M.Klis. Glucomannoproteins in the cell wall of *Saccharomyces cerevisiae* contain a novel type of carbohydrate side-chain, J.Biol.Chem. 269 (1994) 19338-19342.

[144] J.E.Silbert, G.Sugumaran. Intracellular membranes in the synthesis, transport, and metabolism of proteoglycans, Biochimica et Biophysica Acta-Reviews on Biomembranes 1241 (1995) 371-384.

[145] L.Bonofiglio, E.Garcia, M.Mollerach. Biochemical characterization of the pneumococcal glucose 1-phosphate uridylyltransferase (GalU) essential for capsule biosynthesis, Current Microbiology 51 (2005) 217-221.

[146] Goppert F. Galaktosurie nach Milchzuckergabe bei angeborenem, familiärem chronischem Leberleiden., Klinische Wochenschrift 54 (1917) 473-477.

[147] K.Lai, L.J.Elsas. Overexpression of human UDP-glucose pyrophosphorylase rescues galactose-1-phosphate uridyltransferase-deficient yeast, Biochemical and Biophysical Research Communications 271 (2000) 392-400.

[148] J.A.Dobbie, J.B.Holton, J.R.Clamp. Defective galactosylation of proteins in cultured skin fibroblasts from galactosaemic patients, Annals of Clinical Biochemistry 27 (1990) 274-275.

[149] J.B.Holton. Galactose disorders - an overview, J.Inherited Metab.Dis. 13 (1990) 476-486.

[150] A.Alano, S.Almashanu, J.M.Chinsky, P.Costeas, M.G.Blitzer, E.A.Wulfsberg, T.M.Cowan. Molecular characterization of a unique patient with epimerase-deficiency galactosaemia, J.Inherited Metab.Dis. 21 (1998) 341-350.

[151] A.Munchpetersen, H.M.Kalckar, E.Cutolo, E.E.B.Smith. Enzymic production of uridine triphosphate - uridine diphosphoglucose pyrophosphorolysis, Nature 172 (1953) 1036-1037.

[152] G.J.Albrecht, S.T.Bass, L.L.Seifert, R.G.Hansen. Crystallization and properties of uridine diphosphate glucose pyrophosphorylase from liver, J.Biol.Chem. 241 (1966) 2868-&.

[153] P.C.Newell, M.Sussman. Regulation of enzyme synthesis by slime mold cell assemblies embarked upon alternative developmental programs, J.Mol.Biol. 49 (1970) 627-&.

[154] V.N.Nigam, MACDONAL.HL, A.Cantero. Limiting factors for glycogen storage in tumors. Limiting Enzymes, Cancer Res. 22 (1962) 131-&.

[155] C.Villarpalasi, J.Larner. Levels of activity of the enzymes of the glycogen cycle in rat tissues, Arch.Biochem.Biophys. 86 (1960) 270-273.

[156] U.M.Unligil, S.H.Zhou, S.Yuwaraj, M.Sarkar, H.Schachter, J.M.Rini. X-ray crystal structure of rabbit N-acetylglucosaminyltransferase I: catalytic mechanism and a new protein superfamily, EMBO J. 19 (2000) 5269-5280.

[157] J.M.Rini, N.Sharon. Carbohydrates and glycoconjugates glycosyltransferases, sugar nucleotide transporters and bacterial surface lectins - at the cutting edge of glycobiology, Current Opinion in Structural Biology 10 (2000) 507-509.

[158] E.Garcia, D.Llull, R.Munoz, M.Mollerach, R.Lopez. Current trends in capsular polysaccharide biosynthesis of *Streptococcus pneumoniae*, Research in Microbiology 151 (2000) 429-435.

[159] M.Johnston, S.Andrews, R.Brinkman, J.Cooper, H.Ding, J.Dover, Z.Du, A.Favello, L.Fulton, S.Gattung, C.Geisel, J.Kirsten, T.Kucaba, L.Hillier, M.Jier, L.Johnston, Y.Langston, P.Latreille, E.J.Louis, C.Macri, E.Mardis, S.Menezes, L.Mouser, M.Nhan, L.Rifkin, L.Riles, H.Stpeter, E.Trevaskis, K.Vaughan, D.Vignati, L.Wilcox, P.Wohldman, R.Waterston, R.Wilson, M.Vaudin. Complete nucleotide sequence of *Saccharomyces cerevisiae* chromosome-Viii, Science 265 (1994) 2077-2082.

[160] A.C.Weissborn, Q.Y.Liu, M.K.Rumley, E.P.Kennedy. UTP-alpha-D-glucose-1-phosphate uridylyltransferase of *Escherichia coli* - Isolation and DNA sequence of the GalU gene and purification of the enzyme, J.Bacteriol. 176 (1994) 2611-2618.

[161] A.Roeben, J.M.Plitzko, R.Korner, U.M.K.Bottcher, K.Siegers, M.Hayer-Hartl, A.Bracher. Structural basis for subunit assembly in UDP-glucose pyrophosphorylase from *Saccharomyces cerevisiae*, J.Mol.Biol. 364 (2006) 551-560.

[162] F.Martz, M.Wilczynska, L.A.Kleczkowski. Oligomerization status, with the monomer as active species, defines catalytic efficiency of UDP-glucose pyrophosphorylase, Biochem.J. 367 (2002) 295-300.

[163] W.A.Wilson, A.V.Skurat, B.Probst, A.Paoli-Roach, P.J.Roach, J.Rutter. Control of mammalian glycogen synthase by PAS kinase, Proceedings of the National Academy of Sciences of the United States of America 102 (2005) 16596-16601.

[164] J.Rutter, B.L.Probst, S.L.McKnight. Coordinate regulation of sugar flux and translation by PAS kinase, Cell 111 (2002) 17-28.

[165] T.L.Smith, J.Rutter. Regulation of glucose partitioning by PAS kinase and Ugp1 phosphorylation, Molecular Cell 26 (2007) 491-499.

[166] J.G.Mccoy, E.Bitto, C.A.Bingman, G.E.Wesenberg, R.M.Bannen, D.A.Kondrashov, G.N.Phillips. Structure and dynamics of UDP-glucose pyrophosphorylase from *Arabidopsis thaliana* with bound UDP-glucose and UTP, J.Mol.Biol. 366 (2007) 830-841.

[167] T.Steiner, A.C.Lamerz, P.Hess, C.Breithaupt, S.Krapp, G.Bourenkov, R.Huber, R.Gerardy-Schahn, U.Jacob. Open and closed structures of the UDP-glucose pyrophosphorylase from *Leishmania major*, J.Biol.Chem. 282 (2007) 13003-13010.

[168] J.B.Thoden, H.M.Holden. Active site geometry of glucose-1-phosphate uridylyltransferase, Protein Science 16 (2007) 1379-1388.

[169] J.B.Thoden, H.M.Holden. The molecular architecture of glucose-1-phosphate uridylyltransferase, Protein Science 16 (2007) 432-440.

[170] I.Rais, M.Karas, H.Schägger. Two-dimensional electrophoresis for the isolation of integral membrane proteins and mass spectrometric identification., Proteomics 4 (2004) 2567-2571.

[171] U.K.Laemmli. Cleavage of structural proteins during the assembly of the head of bacteriophage T4, Nature 227 (1970) 680-685.

[172] K.Brown, F.Pompeo, S.Dixon, D.Mengin-Lecreulx, C.Cambillau, Y.Bourne. Crystal structure of the bifunctional N-acetylglucosamine 1-phosphate uridyltransferase from *Escherichia coli*: a paradigm for the related pyrophosphorylase superfamily, EMBO J. 18 (1999) 4096-4107.

[173] X.S.Jin, M.A.Ballicora, J.Preiss, J.H.Geiger. Crystal structure of potato tuber ADP-glucose pyrophosphorylase, EMBO J. 24 (2005) 694-704.

[174] C.Peneff, P.Ferrari, V.Charrier, Y.Taburet, C.Monnier, V.Zamboni, J.Winter, M.Harnois, F.Fassy, Y.Bourne. Crystal structures of two human pyrophosphorylase isoforms in complexes with UDPGlc(Gal)NAc: role of the alternatively spliced insert in the enzyme oligomeric assembly and active site architecture, EMBO J. 20 (2001) 6191-6202.

[175] T.Mio, T.Yabe, M.Arisawa, H.Yamada-Okabe. The eukaryotic UDP-N-acetylglucosamine pyrophosphorylases - gene cloning, protein expression, and catalytic mechanism, J.Biol.Chem. 273 (1998) 14392-14397.

[176] R.M.Bennett-Lovsey, A.D.Herbert, M.J.E.Sternberg, L.A.Kelley. Exploring the extremes of sequence/structure space with ensemble fold recognition in the program Phyre, Proteins-Structure Function and Bioinformatics 70 (2008) 611-625.

[177] E.Potterton, S.McNicholas, E.Krissinel, K.Cowtan, M.Noble. The CCP4 molecular-graphics project, Acta Crystallographica Section D-Biological Crystallography 58 (2002) 1955-1957.

[178] F.Martz, M.Wilczynska, L.A.Kleczkowski. Oligomerization status, with the monomer as active species, defines catalytic efficiency of UDP-glucose pyrophosphorylase, Biochem.J. 367 (2002) 295-300.

[179] R.I.Freshney. Culture of animal cells: A manual of basic technique, Alan R. Liss, Inc., New York, 1987.

[180] A.Abdrakhmanova, K.Dobrynin, K.Zwicker, S.Kerscher, U.Brandt. Functional sulfurtransferase is associated with mitochondrial complex I from *Yarrowia lipolytica*, but is not required for assembly of its iron-sulfur clusters, FEBS Lett. 579 (2005) 6781-6785.

[181] H.Schägger, G.von Jagow. Tricine-sodium dodecyl sulfate polyacrylamide gel electrophoresis for the separation of proteins in the range from 1-100 kDalton, Anal.Biochem. 166 (1987) 368-379.

[182] O.H.Lowry, N.R.Rosebrough, A.L.Farr, R.J.Randall. Protein measurement with the folin phenol reagent, J.Biol.Chem. 193 (1951) 265-275.

[183] V.D.Sled, A.D.Vinogradov. Reductive inactivation of the mitochondrial three subunit NADH dehydrogenase., Biochim.Biophys.Acta 1143 (1993) 199-203.

[184] E.V.Gavrikova, V.G.Grivennikova, V.D.Sled, T.Ohnishi, A.D.Vinogradov. Kinetics of the mitochondrial three-subunit NADH dehydrogenase interaction with hexammineruthenium(III), Biochim.Biophys.Acta 1230 (1995) 23-30.

[185] K.Matsushita, T.Ohnishi, H.R.Kaback. NADH-ubiquinone oxidoreductases of the *Escherichia coli* aerobic respiratory chain, Biochem. 26 (1987) 7732-7737.

[186] X.Zhou, G.Arthur. Improved procedures for the determination of lipid phosphorus by malachite green, J.Lip.Res. 33 (1992) 1233-1236.

[187] O.Pasternak, A.Bujacz, J.Biesiadka, G.Bujacz, M.Sikorski, M.Jaskolski. MAD phasing using the $Ta_6Br_{12}^{2+}$ cluster: a retrospective study, Acta Crystallographica Section D-Biological Crystallography 64 (2008) 595-606.

[188] E.A.Stura, M.Graille, M.J.Taussig, B.Sutton, M.G.Gore, G.J.Silverman, J.B.Charbonnier. Crystallization of macromolecular complexes: stoichiometric variation screening, Journal of Crystal Growth 232 (2001) 580-590.

[189] E.A.Stura, M.Graille, J.B.Charbonnier. Crystallization of macromolecular complexes: Combinatorial complex crystallization, Journal of Crystal Growth 232 (2001) 573-579.

[190] F.Martz, M.Wilczynska, L.A.Kleczkowski. Oligomerization status, with the monomer as active species, defines catalytic efficiency of UDP-glucose pyrophosphorylase, Biochem.J. 367 (2002) 295-300.

[191] J.Rutter, B.L.Probst, S.L.McKnight. Coordinate regulation of sugar flux and translation by PAS kinase, Cell 111 (2002) 17-28.

[192] J.B.Thoden, H.M.Holden. The molecular architecture of glucose-1-phosphate uridylyltransferase, Protein Science 16 (2007) 432-440.

# CURRICULUM VITAE
## Blanka Wrzesniewska

### Personal information

| | |
|---|---|
| Birthday/Place | 15th October 1980, Opole, Poland |
| Nationality | polish |
| Family status | single |

### Education

| | |
|---|---|
| 09/2004 - 01/2009 | **Goethe University, Frankfurt am Main**<br>PhD programme at the Biochemistry, Chemistry and Pharmacy Department<br>Expected completion: March 2009 |
| 10/1999 – 06/2004 | **Technical University of Lodz, International Faculty of Engineering, Poland**<br>Biochemistry and Technical Biotechnology Department<br>**Master of Science** in Biotechnology |
| 02/2003 – 06/2003 | **University of Natural Resources and Applied Life Sciences, Vienna**<br>Erasmus scholarship |
| 05/1999 | **Maria Konopnicka High School, Opole, Poland**<br>Secondary school certificate |

### Scientific works

| | |
|---|---|
| Ph.D. thesis | "Crystallization and structural characterization of protein complexes involved in the energy metabolism of *Yarrowia lipolytica.*"<br>Under supervision of Prof. Ulrich Brandt |
| Master thesis | "Cryoprotection of protein crystals by salts of organic acids. "<br>Under supervision of Prof. Grzegorz Bujacz |

Blanka Wrzesniewska

20th January 2009, Frankfurt am Main